PLACE IN RETURN BOX to remove this checkout from your record. TO AVOID FINES return on or before date due.

DATE DUE	DATE DUE	DATE DUE

MSU Is An Affirmative Action/Equal Opportunity Institution ctelrelatedus.pm3-p.1

# THE THEORY AND PRACTICE OF MEMBRANE EXTRACTIONS

By

Mark Anthony LaPack

### A DISSERTATION

Submitted to
Michigan State University
in partial fulfillment of the requirements
for the degree of

DOCTOR OF PHILOSOPHY

Department of Chemistry

1994

### ABSTRACT

## THE THEORY AND PRACTICE OF MEMBRANE EXTRACTIONS

By

### Mark Anthony LaPack

The selection of a membrane for a given separation of a mixture is generally based upon the "like-dissolves-like" rule, which often times is an inadequate guide. In this work, membrane extractions have been studied using silicone membranes and mass spectrometry. Aqueous and gas samples were exposed to one side of the membrane while the contents on the other side were analyzed by mass spectrometry. Predictive permeation models have been developed. Good correlations are observed between the permeation data, chromatographic data, a solubility parameter model, and a model based on the boiling points of the analytes. The effects of experimental parameters on membrane extractions have also been examined. The effects of the configuration of the membrane extractor, membrane dimensions, temperature, sample flow rate, and other parameters are presented in the context of optimizing the separation technique. A membrane extraction mass spectrometric technique has been developed for on-line analysis of organic components of multiple liquid and gas streams, and applied in an aerobic biological wastewater treatment process. Mass balance determinations were performed by quantitatively measuring organic contaminants in influent and effluent water and air streams.

Copyright by

MARK ANTHONY LAPACK

1995

to my Pat

### **ACKNOWLEDGMENTS**

First, I thank my research advisors. I thank Chris Enke for sharing with me his wisdom, creativity, encouragement, and his patience. I also thank Jim Tou for his support and encouragement and for his keen attention to detail. I will always remember the pioneering spirit of these two men.

I thank Vicki McGuffin for her enthusiasm, inspiration, and technical guidance.

For their valuable combinations of critique and encouragement, I thank Dr. Jack Watson, Dr. James Harrison, Dr. Bill Reusch, and Bob Bredeweg.

For their complete support of this work, I thank the management of the Dow Chemical Company, especially Mel Koch, Jim Havel, Foppe Dupuis, Marylu Gibbs, Wes Westover, Don Calvin, Paul Dean, Jackie Kelyman, and Irv Snyder.

To my friends at MSU and in Midland, for their friendship and encouragement, especially Jane Tou, Jim Shao, Mike DesJardin, Bruce Bell, Mark Cole, Paul O'Connor, Mark Dittenhafer, Steve Humphrey, the Enke Group and the Special Analysis Group.

For helping me to keep my priorities in check, I thank my beautiful children, Makenzie and Daniel.

I am very grateful for the love of my two families in Indianapolis - especially my mother, father, and siblings, who never missed a chance to remind me how long I have been in school.

For my wife, Patty, for standing by me, for taking on more than her share of keeping our home together, and for playing the role of the single parent.

Finally, I thank God with all my heart for bringing all of these wonderful people and opportunities into my life.

# TABLE OF CONTENTS

LIST OF TA	BLES	vi
LIST OF FI	GURES	ix
CHAPTER		
1	INTRODUCTION	1
	Background	
	Purpose of this work	
2	PERMEATION FUNDAMENTALS	12
	Steady state permeation	
	Non-steady state permeation	
	Organic enrichment	
3	THE CORRELATION OF PERMEABILITY TO HILDEBRAND SOLUBILITY PARAMETERS	35
	The solubility parameter	
	Development of the theory	
	Correlation of data to theory	
4	A MODEL FOR CHARACTERIZING AND PREDICTING MEMBRANE EXTRACTIONS BASED ON CHROMATOGRAPHIC RETENTION	79
	Retention and distribution equilibria	
	Band spreading and diffusivity	
	Efficiency and enrichment	

5	PRACTICAL ASPECTS OF MEMBRANE EXTRACTIONS	119
	Membrane dimension considerations	
	Temperature considerations	
	Sample flow rate considerations	
	Extractor configuration considerations	
	Effects of distance between the extractor and the analyzer	
6	THE APPLICATION OF MEMBRANE EXTRACTION MASS SPECTROMETRY TO THE ANALYSIS OF GAS AND LIQUID PROCESS STREAMS	154
	Experimental	
	Multiple gas and liquid stream analysis	
	Application to a biological wastewater treatment process	
	Conclusions	
APPENDIX		186
	Permeation measurements	

#### LIST OF TABLES

- Table 1.1. Membrane separation terms and some analogous terms used in analytical chemistry.
- Table 2.1. Effect of hollow fiber membrane radial dimensions on analytical response. The silicone hollow fibers were 2.5-cm long. Temperature =  $23 \, ^{\circ}$ C.
- Table 2.2. Survey of temperature effects on detection limits (S/N = 2) for organic compounds in air and water. The membrane is a 2.5-cm long, 0.0305-cm i.d., 0.0635-cm o.d. silicone hollow fiber.
  - Table 2.3. Effects of membrane thickness on response time for gas phase organic compounds. The membranes are 2.5-cm long silicone hollow fibers. Temperature = 23 °C.
  - Table 2.4. Survey of temperature effects on response time,  $t_{50}$ , for organic compounds in nitrogen. The membrane is a 2.5-cm long, 0.0305-cm i.d., 0.0635-cm o.d. silicone hollow fiber.
  - Table 2.5. Survey of temperature effects on the enrichment over the sample matrix for organic compounds in nitrogen and water.
  - Table 3.1. Molar volumes ( $v_i$ ) and Hildebrand solubility parameters ( $\delta_i$ ) from References 1, 12, and 28.
  - Table 3.2. Experimental permeation parameters for substances in a silicone elastomer membrane at 25 °C.
- Table 3.3. Experimental and theoretical distribution ratios for substances in a silicone elastomer membrane, at 25 °C.
  - Table 3.4. Experimental and theoretical distribution selectivities for substances relative to methane and to methanol in a silicone elastomer membrane at 25 °C.
  - Table 3.5. Partial molar volumes,  $v'_i$ , for surface-active functional groups from Reference 31.

- Table 3.6. Data for determining the active volume ratio,  $V_f/V_p$ , in a silicone elastomer membrane at 25 °C.
- Table 3.7. Experimental and theoretical diffusivities for substances in a silicone elastomer membrane at 25 °C.
- Table 3.8. Experimental and theoretical (D-k model, Equation 3.42) diffusivity selectivities for substances relative to methane and to methanol in a silicone elastomer membrane at 25 °C.
- Table 3.9. Enrichment factors for compounds relative to methane and to methanol in a silicone elastomer membrane at 25 °C. Theoretical values were obtained from the product of distribution (Equation 3.16) and diffusion selectivities (D-k model, Equations 3.36 and 3.42).
- Table 4.1. Molar volumes, Hildebrand solubility parameters (7, 8, 10), and boiling points (11) for the compounds used in this study.
- Table 4.2. Experimental distribution ratios, K<sub>i</sub>, determined by ME and GC at 25 °C.
- Table 4.3. Values for the heats of solution for selected compounds in the membrane and chromatographic stationary phases.
- Table 4.4. Distribution selectivities for compounds over nitrogen and heptane at 25 °C.  $T_b$  = predicted from the boiling points (Equation 4.7); SP = predicted from solubility parameter theory (Equation 4.3); ME = experimental from ME data; GC = experimental from GC data.
- Table 4.5. Mobile phase diffusivities,  $D_{i,m}$ , and chromatographic band spreading components used to calculate diffusivities in the stationary phase at 25 °C.
- Table 4.6. Diffusivities at 25 °C in the stationary phase for compounds of interest determined by membrane extraction experiments (ME), and gas chromatographic experiments (GC).
- Table 4.7. Values for the activation energies for diffusion for selected compounds in the membrane stationary phase.
- Table 4.8. Diffusion selectivities for compounds over nitrogen and over heptane at 25 °C.  $T_b$  = predicted from boiling point model (Equation 4.24); SP = predicted from solubility parameter theory (Equation 4.31); ME = experimental from ME data; GC = experimental from GC data.
- Table 4.9. Values for the activation energies for permeation for selected compounds in the membrane stationary phase.

- Table 4.10. Enrichment factors for compounds over nitrogen and heptane at 25 °C.  $T_b$  = predicted from the boiling point model (Equation 4.40); SP = predicted from solubility parameter theory (Equations 4.3 and 4.32); ME = experimental from ME data  $(P_i/P_j)$ ; GC = experimental from GC data (Equation 4.35).
- Table 5.1. Gas permeabilities and permeation rates/unit concentration (given per unit ppm by volume) through a 2.54-cm-long, 0.0305-cm-i.d., 0.0635-cm-o.d. silicone hollow fiber membrane.
- Table 5.2. Permeabilities and flow rates for gases through a 2.5-cm-long, 0.0305-cm-i.d., 0.0635-cm-o.d. silicone hollow fiber membrane.
- Table 5.3. The effects of interface tube length on response.
- Table 5.4. Comparisons between response time  $(t_{50}-t_0)$  and rise time  $(t_{90}-t_{10})$  for 1-butanol.
- Table 5.5. The effects of analyzer conductance on response time.
- Table 6.1. Spike sets with volume % in acetone, monitored ions, and standard response factors. Baseline response was 0.0005.
- Table 6.2. Spike concentrations (mg/L) in the influent wastewater.
- Table 6.3. Concentrations (mg/L) detected in the effluent water and the air streams in the reactive process. Styrene and chlorobenzene are not detected (N.D.) above the baseline in the effluent water.
- Table 6.4. Percent recoveries and standard deviations for the spiked organic compounds.
  - Table 6.5. Percent recoveries and standard deviations in the effluent water streams.
  - Table 6.6. Percent recoveries and standard deviations in the effluent air streams.
  - Table 6.7. Percent bio-uptake and standard deviations. Experimental values corrected for the recoveries in the analytical test reactor (reactor 2) are given in parentheses.
  - Table A.1. Mass spectrometric response factors, relative to toluene, used to determine permeation parameters.
  - Table A.2. Relative standard deviation for each known source of error and for each computed permeation parameter.

#### LIST OF FIGURES

- Figure 1.1. The components of a typical membrane extractor.
- Figure 1.2. A typical membrane permeation response curve.
- Figure 2.1. A cross-section view of the general components of the permeation process.
- Figure 2.2. The mass spectrometric response and pressure vs. concentration of toluene in the feed stream. Aqueous standard concentrations are reported on a grams/liter basis while gas standards are reported on a volume/volume basis. The portion of the toluene in air response curve labeled ¥ deviates from linearity due to excessive pressure in the ion source.
- Figure 2.3. The effects of temperature on permeability.
- Figure 2.4. A plot of solutions to non-steady state permeation (Equation 2.12), calculated from  $t_{50}$  values, and permeation response data for chloroform at 26 °C and 85 °C.
- Figure 2.5. Normalized permeation response curves for 1,2,4-trichlorobenzene as a function of temperature.
- Figure 3.1. Thermodynamic interaction effects of a filler on diffusive transport.
- Figure 3.2. Hollow fiber membrane permeation cell.
- Figure 3.3. Correlation between distribution ratio and solubility parameter for substances in a silicone elastomer membrane at 25 °C.
- Figure 3.4. Correlation between diffusivity, corrected for tortuosity, and the molar volume for substances in a silicone elastomer membrane at 25 °C.
- Figure 3.5. Correlation between surface free energy,  $[RT/(N^{1/3} \circ v_i^{2/3})] \circ [ln(k'_i) ln(V_f/V_p)]$ , and cohesive energy density,  $\delta_i^2$ , for substances in a silicone elastomer membrane, at 25 °C. The line is fitted to the halogenated compound and alcohol data only.

- Figure 3.6. Correlation between experimental and theoretical selectivities for substances relative to methane in a silicone elastomer at 25 °C.
- Figure 3.7. Correlation between experimental and theoretical selectivities for substances relative to methanol in a silicone elastomer at 25 °C.
- Figure 4.1. The effect of temperature on the stationary phase/mobile phase distribution ratio,  $K_{l}$ , obtained by ME (a) and by GC (b).
- Figure 4.2. The correlation of the distribution ratio,  $K_i$ , with boiling point,  $T_{bi}$ , at 25 °C, obtained by ME (a) and by GC (b).
- Figure 4.3. The effect of temperature on diffusivity,  $D_{i,s}$ , in the ME stationary phase.
- Figure 4.4. The correlation of diffusivity,  $D_{i,s}$ , with boiling point,  $T_{bi}$ , at 25 °C, obtained by ME (a) and by GC (b).
- Figure 4.5. The effect of temperature on permeability,  $P_i$ , in the ME stationary phase.
- Figure 4.6. The correlation of the enrichment factor (over nitrogen),  $\mathcal{E}_{1/N2}$ , with boiling point,  $T_{bi}$ , for the data obtained by ME at 25 °C.
- Figure 4.7. The correlation of GC retention times with ME permeation parameters at 25 °C.
- Figure 5.1. Flow-over hollow fiber membrane extractor.
- Figure 5.2. Flow-through hollow fiber membrane configuration.
- Figure 5.3. A cross-section view of the effect of boundary layers on the permeation process.
- Figure 5.4. Response for toluene vs. sample flow rate through a 2.5-cm-long, 0.0305-cm i.d., 0.0635-cm o.d. hollow fiber.
- Figure 5.5. The response curves for m/z 92 following a step change in the concentration of toluene in a gas sample with different lengths of ME-MS interface tube lengths.
- Figure 5.6. Response time vs. ME-MS interface tube length for various volatile compounds.
- Figure 5.7. The response curves for 1-butanol (m/z 56) with different lengths of ME-MS interface tube.

- Figure 5.8. Comparison of response vs. concentration plots for the flow-over and the flow-through membrane extractor configurations.
- Figure 5.9. Relative organic/water response ratios for the flow-over vs. flow-through inlets obtained at comparable sample linear velocities.
- Figure 5.10. Exploded view of the hollow fiber membrane extractor valve.
- · Figure 5.11. Exploded view of the sheet membrane extractor valve.
  - Figure 5.12. A membrane extraction valve coupled to a direct insertion probe.
  - Figure 5.13. A configuration of ME valve where the lower section of the valve is expanded so that the process is carried out in direct contact with the membrane.
  - Figure 6.1. A configuration for the influent and effluent analysis by ME-MS of a multi-stream, multi-phase process.
  - Figure 6.2. A diagram of the wastewater treatment bioreactor.
  - Figure 6.3. The syringe and mixing jar configuration for spiking organic compounds into liquid streams.
  - Figure 6.4. A process flow diagram illustrating the spiking and on-line sampling of three wastewater treatment bioreactors.
- Figure 6.5. Mass flow rate plots for carbon tetrachloride in A, reactor 3 (reactive, not spiked), B, reactor 2 (non-reactive, spiked), and C, reactor 1 (reactive, spiked). The spike was begun at the 8-hour mark.
- Figure 6.6. Mass flow rate plots for benzene in A, reactor 3 (reactive, not spiked), B, reactor 2 (non-reactive, spiked), and C, reactor 1 (reactive, spiked). The spike was begun at the 8-hour mark.
- Figure A.1. Experimental determination of permeation parameters.

# CHAPTER 1

# Introduction

The need for real-time trace analysis of air and water streams has increased in recent years. Methods are being sought for on-line analysis of process streams for process optimization and control. The challenge of environmental monitoring of air and wastewater emissions grows with increasingly stringent government regulations. In many cases, the extraction, concentration, desorption, and analysis of organic compounds from air or water streams can be accomplished in a single step using a membrane extraction device.

### **BACKGROUND**

Membranes have long been used in industry and medicine for processes requiring purification or enrichment of a gas or liquid stream (1, 2). These membrane processes include separation of hydrocarbons, separation of the components of air, purification of water, and detoxification of blood. The same membranes used in these industrial and medical processes also may be utilized on a smaller scale in analytical separations. Terms that are commonly used by membrane technologists (3) and the analogous terms that may be used by analytical chemists are summarized in Table 1.1. These terms may be used interchangeably in this work.

Table 1.1. Membrane separation terms and some analogous terms used in analytical chemistry.

membrane technology termalternate termsmembranestationary phase

feed sample stream, mobile phase reject waste stream, vent stream

permeate extract stream

permselectivity enrichment factor, concentration

factor

diffusivity diffusion coefficient
permeability permeation coefficient
solubility Henry's law coefficient,

distribution ratio

In general, membrane processes are comprised of the membrane, the feed stream (sample), the reject stream (waste or vent), and the permeate stream (sample extract) as shown in Figure 1.1. The permeate stream is enriched in analytes due to the selective permeation properties of the membrane. The permeation of an

 selective partitioning of the analyte from the sample into the membrane polymer matrix,

analyte through a membrane is defined by three processes;

- 2) selective diffusion of the analyte through the membrane, and
- desorption of the analyte from the membrane into a vacuum or sweep gas.

Diffusion through the membrane is assumed to be the rate determining process, while partitioning at the sample surface and desorption from the permeate surface are considered to be

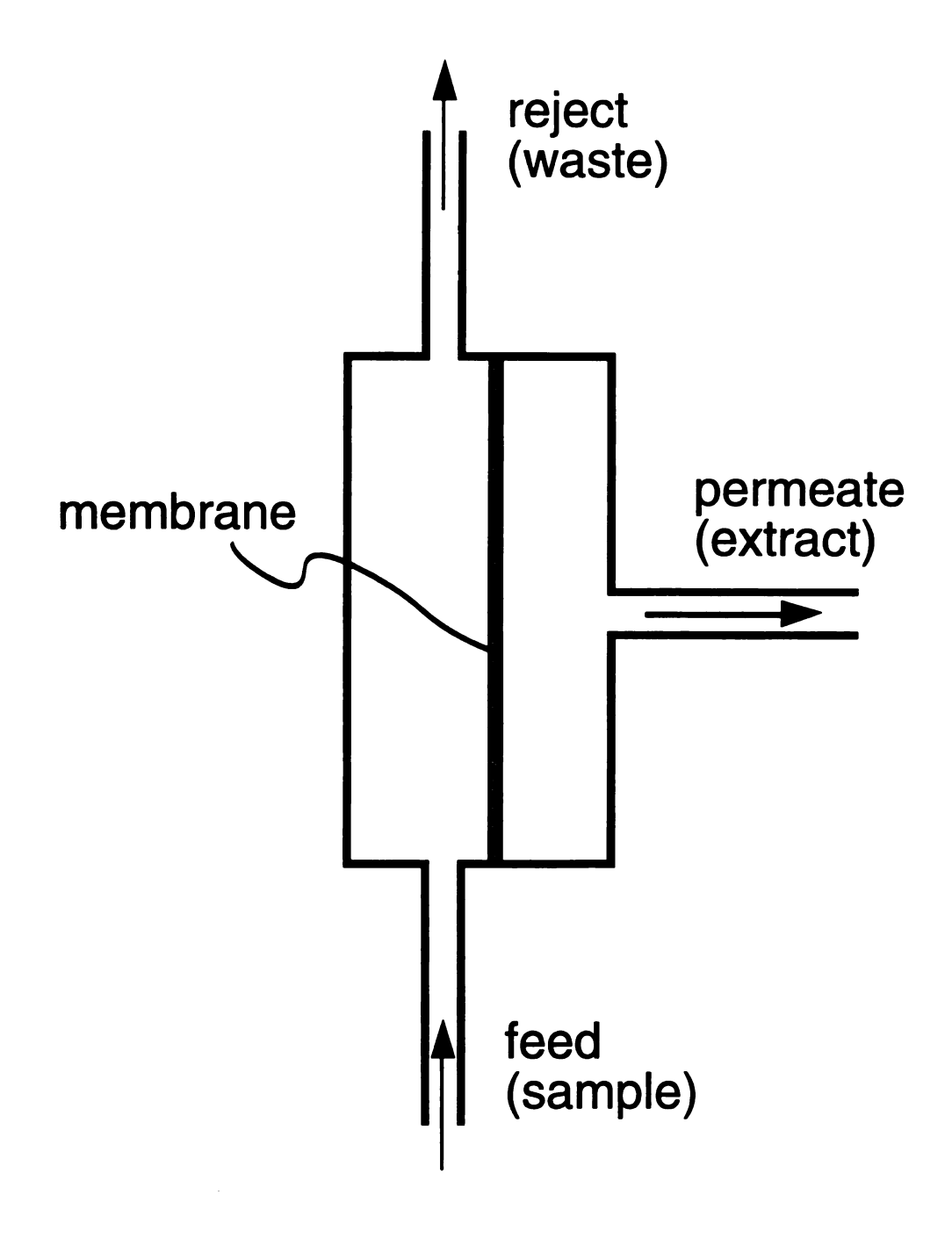


Figure 1.1. The components of a typical membrane extractor.

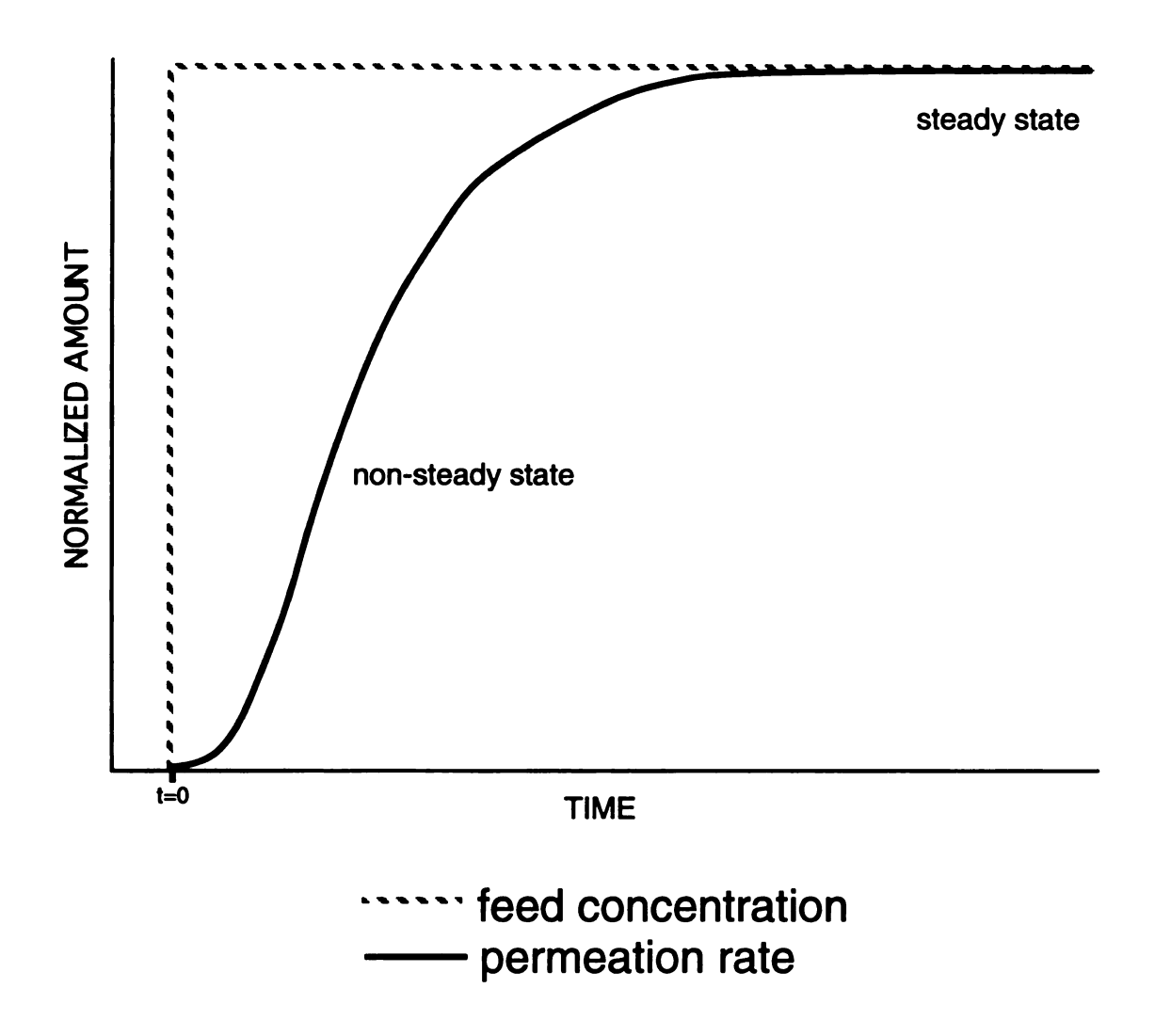


Figure 1.2. A typical membrane permeation response curve.

instantaneous. A step change in analyte concentration in the sample results in the typical permeation response curve shown in Figure 1.2. The sensitivity of a membrane separation technique is determined by the steady state permeation response, while the non-steady state permeation characteristics of the analyte in the membrane determine the response time. These processes will be discussed in detail in the following chapters.

The development of membrane extraction (ME) techniques have given birth to a family of powerful hyphenated analytical techniques, including ME-mass spectrometry (ME-MS) (4, 5), ME-gas chromatography (ME-GC) (6), ME-flow injection analysis (ME-FIA) (7), ME-liquid chromatography (8), ME-ion chromatography (9), and others, including GC-ME-MS (10, 11) and FIA-ME-MS (12, 13). The membrane extractor is much more than an inlet or sampling system for an analyzer. Membrane extractors have become indispensable for techniques that require high specificity, sensitivity, and speed, particularly for on-line analyses (14-16).

Although applicable to any analytical technique, the membrane studies and applications described in this work were performed with analyses of the permeate by mass spectrometry. Historically, membranes have been used as molecular separators in gas chromatography-mass spectrometry (GC-MS) to reduce the amount of helium carrier gas flowing into the mass spectrometer. Llewellen and Littlejohn (10) have used a flat silicone membrane that is selectively permeable to organic molecules relative to helium. The GC effluent

flows across one surface of the membrane, through which the organic molecules permeate into the analyzer while the helium is largely rejected. Lipsky, Horvath, and McMurray (11) used a heated Teflon tube to act as a molecular separator interface for GC-MS. In this case, helium preferentially permeates the porous Teflon membrane, resulting in an enrichment of the organic analytes flowing into the analyzer as the stream rejected by the membrane.

Westover, Tou, and Mark (5) evaluated various hollow fiber membrane materials for MS analysis of organic compounds in air and water without GC separations. The membrane was the direct interface between the sample and the analyzer, with the inside of the hollow fiber exposed to the MS vacuum and the outer surface exposed to the sample. This particular configuration will hereafter be termed the "flow-over" hollow fiber inlet. Cooks and co-workers (17) reversed the configuration such that sample flows through the inner volume of the hollow fiber while the outer surface is exposed to the MS vacuum. Hence, "flow-through" will be the terminology describing this configuration. The two configurations are contrasted and discussed in detail in Chapter 5. Except where specifically stated, all of the data reported in the present work were obtained with a flow-through hollow fiber membrane extractor. There are advantages to analyzing the sample directly without chromatographic separation. In cases where interferences between analytes are minimal or can be accounted for, the analysis or screening of batch samples can be shortened (12). In addition, transient processes can be much better studied by direct and continuous analysis (18, 19).

### **GOALS OF THIS WORK**

Much of the literature on the subject of sampling with membranes is devoted to useful applications. Relatively little emphasis has been placed on the development of practical models (a) for predicting the capacity of a membrane to separate two components in a sample or (b) for choosing the appropriate material for performing a desired membrane separation. A goal of the present work was to provide useful models and experimental guidelines for performing membrane extractions so that the versatility of the technique may be better exploited.

In Chapter 2, generalized forms of the permeation rate equation for analytical applications to both air and water samples are developed. Results and discussion of the effects of various experimental parameters on permeation rates are presented with their theoretical bases. A mass spectrometric method for determining the permeation parameters, including enrichment factors, permeabilities, diffusivities, and distribution ratios, will be presented. Many of the results in this chapter have been published (20, 21).

In Chapter 3, a permeation model is developed based on regular solution theory. Equilibrium partitioning of substances between the membrane and feed phases results in two phases that may modeled utilizing Hildebrand solubility parameters. In addition, the effect on diffusive transport of partitioning a diffusing substance between a filler and polymer phase in a composite membrane also may

be correlated to solubility parameters. Finally, experimental and theoretical enrichment factors for a composite membrane are correlated in the solution-diffusion model. The information presented in this chapter has been published (22).

Chapter 4 is a practical extension of the principles developed in Chapter 3. In Chapter 4, chromatographic separation principles and data are applied to membrane extractions. Since both techniques are governed by the same thermodynamic and kinetic factors, a model is described utilizing well known chromatographic principles. Very good experimental agreement is observed in correlations made between the selectivities obtained by membrane extractions and by gas chromatography. Such correlations become more complicated for strong hydrogen bonding compounds because the membrane contains a finely dispersed silica filler to provide it with strength and elasticity. This silica filler affects both the thermodynamic and the transport rate properties of the material. Comparisons are made between a simple boiling point model and the solubility parameter model described in Chapter 3. The information presented in this chapter has been submitted for publication (23).

In Chapter 5, guidelines for the construction and use of simple membrane inlets are presented. Experimental parameters are discussed in the context of analytical sensitivity and response time. These experimental parameters include analyte concentration, sample flow rate, temperature, membrane thickness and surface area, membrane extractor configuration, and distance of the membrane

extractor from the analyzer and the sample. Portions of this chapter have been previously published (20, 21). Much of the additional information has been submitted for publication (24).

In Chapter 6, the application of an ME-MS technique that was developed for on-line analysis of organic components of multiple liquid and gas streams is presented. The silicone membranes are shown to allow for extraction of organic chemicals from complex and dirty matrices with no sample preparation. Multiple streams of both air and water were analyzed on-line with a single analyzer. This method has been applied in an aerobic biological wastewater treatment process. Mass balance determinations were performed by quantitatively measuring the organic contaminants in the influent wastewater stream, in the effluent water stream, and in the effluent air stream. The information presented in this chapter has been published (25).

#### REFERENCES

- (1) Bier, M., Ed. <u>Membrane Processes in Industry and Biomedicine</u>; Plenum Press: New York, NY; 1971.
- (2) Hwang, S.-T.; Kammermeyer, K. <u>Membranes in Separations</u>; Robert E. Krieger Publishing: Malabar, FL; 1984.
- (3) Gekas, V. Desalination 1988, 68, 77.
- (4) Hoch, G.; Kok, B. Arch. Biochem. Biophys. **1963**, 101, 160.
- (5) Westover, L.B.; Tou, J. C.; Mark, J. H. Anal. Chem. 1974, 46, 568.
- (6) Bredeweg, R. A.; Langhorst, M. L.; Dittenhafer, D. R.; Strandjord, A. J.; Willis, R. S. 16th Annual Meeting of the Federation of Analytical Chemistry and Spectroscopy Societies, Chicago, IL, 1989.
- (7) Melcher, R. G. Anal. Chim. Acta 1988, 214, 299.
- (8) Melcher, R. G.; Bouyoucos, S. A. *Process Control and Quality* **1990**, 1, 63.
- (9) Stevens, T. S.; Jewett, G. L.; Bredeweg, R. A. Anal. Chem. **1982**, 54, 1206.
- (10) Llewellen, P. M.; Littlejohn, D. P. U.S. Patent 3,429,105, February, 1969.
- (11) Lipsky, S. R.; Horvath, C. G.; McMurray, W. J. Anal. Chem. **1966**, 38, 1585.
- (12) Langvardt, P. W.; Brzak, K. A.; Kastl, P. E. 34th ASMS Conference on Mass Spectrometry and Allied Topics, Cincinnati, OH, 1986.

- (13) Hayward, M. J.; Kotiaho, T.; Lister, A. K.; Cooks, R. G.; Austin, G. D.; Narayan, R.; Tsao, G. T. *Anal. Chem.* **1990**, 62, 1798.
- (14) Kallos, G. J.; Tou, J. C. Environ. Sci. Technol. 1977, 11, 1101.
- (15) Heinzle, E.; Reuss, M. <u>Mass Spectrometry in</u>
  <u>Biotechnological Process Analysis and Control;</u> Plenum Press:
  New York, NY; 1987.
- (16) Savickas, P. J.; LaPack, M. A.; Tou, J. C. Anal. Chem. 1989, 61, 2332.
- (17) (a) Bier, M. E.; Cooks, R. G.; Tou, J. C.; Westover, L. B. U.S. Patent 4,791,292, 1989.
  (b) Bier, M. E.; Cooks, R. G. Anal. Chem. 1987, 59, 597.
- (18) Tou, J. C.; Westover, L. B.; Sonnabend, L. F. J. Phys. Chem. **1974**. 78. 1096.
- (19) Calvo K. C.; Weisenberger, L. B.; Anderson, L. B.; Klapper, M. H. *Anal. Chem.* **1981**, 53, 981.
- (20) LaPack, M. A.; Tou, J. C.; Enke, C. G. 37th ASMS Conference on Mass Spectrometry and Allied Topics, 1989, Miami Beach, FL.
- (21) LaPack, M. A.; Tou, J.C.; Enke, C.G. Anal. Chem. 1990, 62, 1265.
- (22) LaPack, M. A.; Tou, J. C.; McGuffin, V.L.; Enke, C. G. J. Membrane Sci. 1994, 86, 263.
- (23) LaPack, M. A.; Tou, J. C.; McGuffin, V.L.; Enke, C. G. Anal. Chem. submitted for publication.
- (24) LaPack, M. A.; Tou, J. C.; Cole, M. J.; Enke, C. G. Anal. Chem. submitted for publication.
- (25) LaPack, M.A.; Tou, J.C.; Enke, C. G. Anal. Chem. 1991, 63, 1631.

# CHAPTER 2

# Permeation Fundamentals

Permeation is a broad term that describes a variety of processes involving transport of substances across boundaries (1). Many of these processes have been given specific phenomenological names. For example, as opposed to gas permeation, the term pervaporation is often used to describe the penetration of a substance into a polymer from the liquid phase, diffusion of the substance through the polymer, and desorption from the polymer into the gas phase (2, 3). It has been suggested that the term sorption indicates the penetration into the polymer of a substance from the gas phase while absorption indicates the penetration from the liquid phase (4). Regarding the work described in the following pages, the more broadly descriptive terms, permeation and sorption, will be used in both gas and liquid applications. The term adsorption will be used in describing the assimilation of molecules from a gas or liquid phase by an impermeable surface. The term desorption describes the reverse process of sorption, absorption, and adsorption.

As introduced in Chapter 1, the permeation of a compound through an amorphous polymer is governed by sorption of the compound into the polymer, diffusive transport through the polymer matrix, and desorption from the downstream side of the polymer.

This description of the permeation process is generally known as the solution-diffusion model (5). Sorption and desorption are equilibrium processes that may be described by classical thermodynamics (6, 7) as will be discussed further in Chapters 3 and 4. Because it is such a rapid process, desorption of the permeating compound into a vacuum or carrier gas is commonly ignored when discussing the permeation of gases and volatile organic compounds. The diffusion process is driven by the concentration gradient across the thickness of the membrane. Quantitative treatments of diffusion in solids under various conditions have been presented (8, 9). In this chapter, sorption and diffusion are discussed in regards to the two regions of the permeation rate curve, steady state and non-steady state (see Figure 1.2), and to their importance to the selectivity of the permeation process.

### STEADY STATE PERMEATION

Steady state permeation is described by Fick's first law

$$F_{i} = -A \cdot D_{i,s} \cdot \partial c_{i,s} / \partial x$$
 (2.1)

where  $F_i$  is the flow rate (permeation rate) of substance i in the permeate (extract stream), A is the surface area of the membrane,  $D_{i,s}$  is the diffusivity of the substance in the membrane polymer (stationary phase), and  $\partial c_{i,s}/\partial x$  is the concentration gradient for substance i across the membrane thickness. For a sheet membrane, Fick's first law gives

$$F_i = A \cdot D_{i,s} \cdot (c_{i,s1} - c_{i,s2})/d$$
 (2.2)

and for a hollow fiber membrane,

$$F_{i} = 2 \cdot \pi \cdot L \cdot D_{i,s} \cdot (c_{i,s1} - c_{i,s2}) / \ln(o.d./i.d.)$$
(2.3)

where  $c_{i,s1}$  and  $c_{i,s2}$  are the concentrations of substance i in the feed surface and the permeate surface of the membrane, respectively, d is the thickness of the sheet membrane, L is the length of the hollow fiber, and o.d. and i.d. are the outer and inner radii of the hollow fiber, respectively. The general components of the permeation process are shown in Figure 2.1 (for a sheet membrane). If the permeate side of the membrane is exposed to the mass spectrometer vacuum or swept with a carrier gas, a concentration gradient is established and c<sub>s2i</sub> becomes very small relative to  $c_{i,s1}$  and can be ignored. This concentration gradient is the driving force for diffusion. The concentration c<sub>i,s1</sub> is established by the partitioning process and, for gas samples, is directly proportional to the partial pressure of component i, pi, in the sample by the Henry's law of solubility coefficient,  $S_i$ , such that  $c_{i,s1} = S_i \cdot p_i$ . However, since the desired measurement for most analytical methods is concentration and not partial pressure of a substance in the sample, Equations 2.2 and 2.3 can be rewritten for the sheet as

$$F_i = A \cdot D_{i,s} \cdot S_i \cdot p_t \cdot (p_i/p_t)/d$$
 (2.4)

and for the hollow fiber as

#### Permeation through a Membrane

- 1) Sorption into the membrane
- 2) Diffusion through the membrane
- 3) Desorption from the membrane

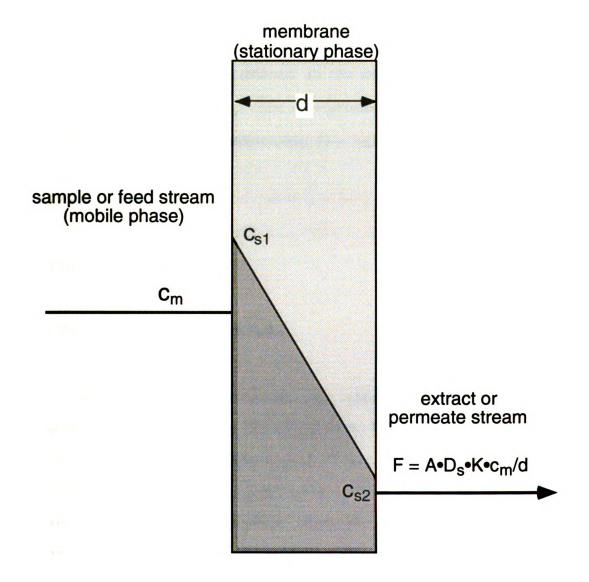


Figure 2.1. A cross-section view of the general components of the permeation process.

$$F_i = 2 \cdot \pi \cdot L \cdot D_{i,s} \cdot S_i \cdot p_t \cdot (p_i/p_t) / \ln(o.d./i.d.) . \qquad (2.5)$$

The substance i partial pressure/total sample pressure ratio,  $p_i/p_t$ , gives the molar concentration of the substance in the feed (mobile phase),  $c_{i,m}$ . The product,  $S_i \cdot p_t$ , can be rewritten to yield the ratio of the concentration in the membrane,  $c_{i,s1}$ , to the concentration in the feed,  $c_{i,m}$ , which is defined as the concentration distribution ratio, where  $K_i = c_{i,s1}/c_{i,m}$ . The distribution ratio provides a more generalized form of the permeation rate equation, where for the sheet

$$F_i = A \cdot D_{i,s} \cdot K_i \cdot c_{i,m} / d$$
 (2.6)

and for the hollow fiber

$$F_i = 2 \cdot \pi \cdot L \cdot D_{i,s} \cdot K_i \cdot c_{i,s} / \ln(o.d./i.d.)$$
(2.7)

This form of the permeation rate equation is also readily applied to aqueous samples where the membrane/water distribution ratio for the substance and the concentration of the substance in the aqueous sample are used (10). The product of diffusivity and distribution ratio is the permeability ( $P_i = D_{i,s} \cdot K_i$ ). Typically, membrane technologists utilize the Henry's Law coefficient ( $P_i = D_{i,s} \cdot S_i$ ) and the units  $cm^3 \cdot cm/[s \cdot cm^2 \cdot cm \cdot Hg]$  for gas permeabilities. Since the distribution ratio has no units, the units for permeability will be given as  $cm^2/[s \cdot c_{i,m}]$  where appropriate in the present work.

At a given temperature and pressure, the permeability and the dimension factor (A/d for the sheet,  $2 \pi L/\ln(o.d./i.d.)$  for the hollow fiber) are constants. The permeation rate and therefore the analytical signal,  $I_i$ , is directly proportional to the sample concentration, where

$$I_{i} = Q_{i} \cdot F_{i} = rf_{i} \cdot c_{i,m}$$
 (2.8)

where  $Q_i$  is the absolute instrumental response factor and  $rf_i$  is the analytical response factor for compound i. Depending upon the application, the sample concentration may, in fact, be expressed in any useful units to obtain an analytical working curve. For example, organic contaminants in aqueous samples are often expressed in units of mg/L, while organic contaminants in air may be expressed in units of L/L or mole/mole.

The linear relationship between permeation rate and sample concentration is exhibited over a wide dynamic range, as shown in Figure 2.2, in which the response is directly proportional to the permeation rate. The upper limit of this range is determined by the maximum amount of analyte that the analyzer will tolerate for linear response and/or the swelling of the membrane due to high sorption of organic analytes. Aqueous samples generally provide a wider dynamic range because the low end of the range is extended. The detection limits for aqueous samples are generally lower than for air samples.

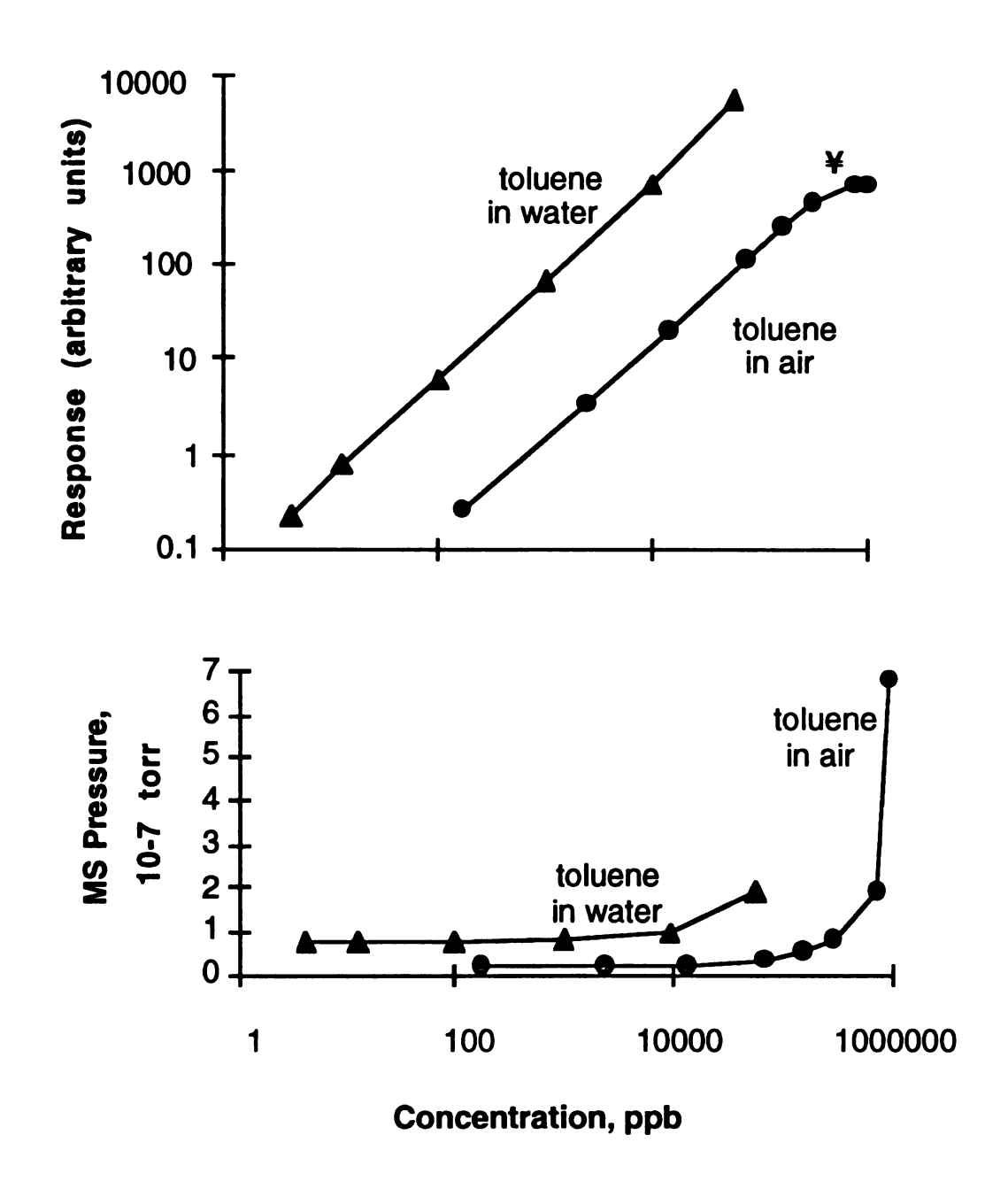


Figure 2.2. The mass spectrometric response and pressure vs. concentration of toluene in the feed stream. Aqueous standard concentrations are reported on a grams/liter basis while gas standards are reported on a volume/volume basis. The portion of the toluene in air response curve labeled ¥ deviates from linearity due to excessive pressure in the ion source.

### Effects of membrane dimensions

It is apparent from Equations 2.6 and 2.7 that increasing the surface area of the sheet and the length of the hollow fiber proportionally increases the permeation rate. Membrane thickness has an inverse effect on permeation. For a sheet membrane, the permeation rate is simply proportional to 1/d. For a given length of hollow fiber, the effect of hollow fiber radial dimensions on permeation is given by  $1/\ln(r_0/r_1)$ . A comparison of signals obtained from the analysis of organic compounds in air with two hollow fibers of approximately equal lengths, but different radial dimensions, is shown in Table 2.1. Experimental and theoretical response ratios show reasonably good agreement for individual components as well as for the total gas throughput indicated by the analyzer pressure.

Table 2.1. Effect of hollow fiber membrane radial dimensions on analytical response. The silicone hollow fibers were 2.5-cm long. Temperature = 23 °C.

	response, (ar	,		
	membrane 1	membrane 2	response	
	i.d.=0.0305 cm	i.d.=0.147 cm	ratio, $I_1/I_2$	
compound	o.d.=0.0635 cm	o.d.=0.196 cm	exp.	theor.
dichloromethane	2.8	5.5	2.0	2.5
1,1-dichloroethene	0.6	1.3	2.2	2.5
chlorobenzene	1.2	2.4	2.0	2.5
acetone	0.8	2.0	2.5	2.5
analyzer pressure (torr)	6.2x10 <sup>-8</sup>	1.4x10 <sup>-7</sup>	2.3	2.5
. •				

### Effects of temperature

Permeation is a temperature-dependent phenomenon obeying the Arrhenius relation:

$$P_i = P_{i,o} \cdot \exp[-E_{Pi} \cdot (1/RT - 1/RT_o)]$$
 (2.9)

where the initial permeability of substance i,  $P_{i,o}$ , is given at some initial temperature,  $T_o$ , the activation energy for permeation,  $E_{Pi}$ , is the sum of the activation energy for diffusion,  $E_{Di}$ , and the difference in heats of solution between the membrane and the sample matrix,  $\Delta H_{Si} = H_{Si} \text{(membrane)-} H_{Si} \text{(matrix) for substance i. Substituting}$   $D_{i,s} \cdot K_i = P_i \text{ into Equation 2.9 gives}$ 

$$D_{i,s} \circ K_i = D_{i,so} \circ K_{i,o} \circ \exp[-(E_{Di} + \Delta H_{Si}) \circ (1/RT - 1/RT_o)]$$
 (2.10)

The activation energy,  $E_{Di}$ , is greater than zero, while in general,  $\Delta H_{Si}$  is less than zero. The direction for the change in permeability with changing temperature is dependent upon whether the change in diffusivity or distribution ratio dominates, as determined by the relative magnitudes of  $E_{Di}$  and  $\Delta H_{Si}$ .

The relative trends for the permeabilities of air, water, and organic compounds with increasing temperature are shown in Figure 2.3. At higher temperatures, permeabilities of air and water increase because increasing diffusivities dominate their permeability-temperature relationship. Organic permeabilities from water samples also increase largely due to increasing diffusivities. In contrast to

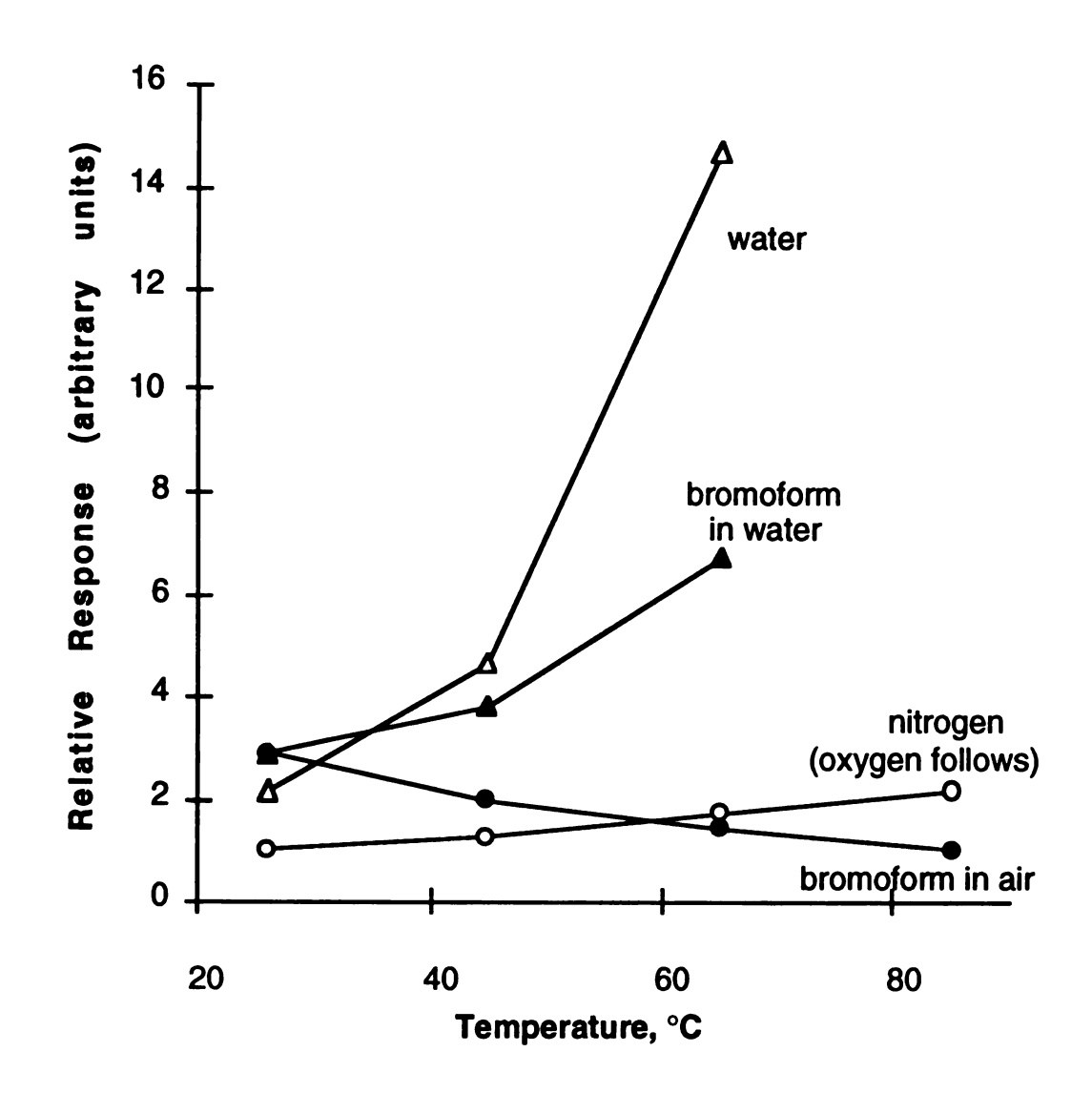


Figure 2.3. The effects of temperature on permeability.

Table 2.2. Survey of temperature effects on detection limits (S/N = 2) for organic compounds in air and water. The membrane is a 2.5-cm long, 0.0305-cm i.d., 0.0635-cm o.d. silicone hollow fiber.

	_	detection limit (ppb)			
		in air		in water	
compound	m/z	<u>26 °C</u>	<u>45 °C</u>	<u>26 °C</u>	45 °C
chloromethane	50	325	368	-	-
dichloromethane	84	669	742	6	5
chloroform	83	182	233	7	5
carbon tetrachloride	117	130	163	18	13
chloroethene	62	269	301	-	-
1,1-dichloroethene	61	101	125	6	5
trichloroethene	128	30	39	29	25
tetrachloroethene	166	29	34	32	25
dibromomethane	172	28	36	106	93
bromoform	171	14	21	62	34
benzene	78	42	54	3	2
toluene	91	31	38	2	2
ethylbenzene	106	45	57	6	5
chlorobenzene	112	12	14	8	7
1,3-dichlorobenzene	146	3	3	23	16
1,2,4-trichlorobenzene	180	3	5	51	29

aqueous samples, air samples show a decrease in permeabilities for organic compounds due to their reduced partitioning into the membrane at higher temperatures. This effect will be discussed further in the following chapters. Since, as shown in Table 2.2, organic permeabilities decrease for air samples with increasing temperatures, their detection limits increase. Because of the greater permeabilities of organic compounds from water at higher temperatures, their detection limits improve. However, organic enrichments decay at higher temperatures, as discussed below. Further observations on these temperature-related phenomena are presented below in the discussion on organic enrichment and their implications in chemical analyses are discussed in Chapter 5.

#### **NON-STEADY STATE PERMEATION**

Non-steady state permeation is governed by Fick's second law:

$$\partial c_{i,s}/\partial t = -D_{i,s} \cdot (\partial^2 c_{i,s}/\partial x^2). \tag{2.11}$$

The mathematical solution for diffusion through a membrane of thickness d following a step change in sample concentration is (11)

$$F_{i(t)} = F_{i(ss)} \cdot \{1 + [2 \cdot \Sigma(-1)^n \cdot \exp(-(n \cdot \pi/d)^2 D_{i,s} \cdot t)]\}.$$
 (2.12)

where  $F_{i(t)}$  and  $F_{i(ss)}$  indicate the permeation rate of substance i at time t and at steady state conditions, respectively. The permeation process exhibits an asymptotic approach to steady state, thus the time

required to achieve steady state, or even 95% steady state,  $t_{95}$ , may be difficult to determine. It is convenient, therefore, to relate response time to the time required to achieve 50% steady state permeation,  $t_{50}$ , which is more easily determined. The first order approximation at  $t_{50}$ , neglecting all but the first exponential term (n=1), can be used to determine the diffusion coefficient (12), where

$$D_{i.s} = 0.14 \cdot (d^2/t_{50}) \tag{2.13}$$

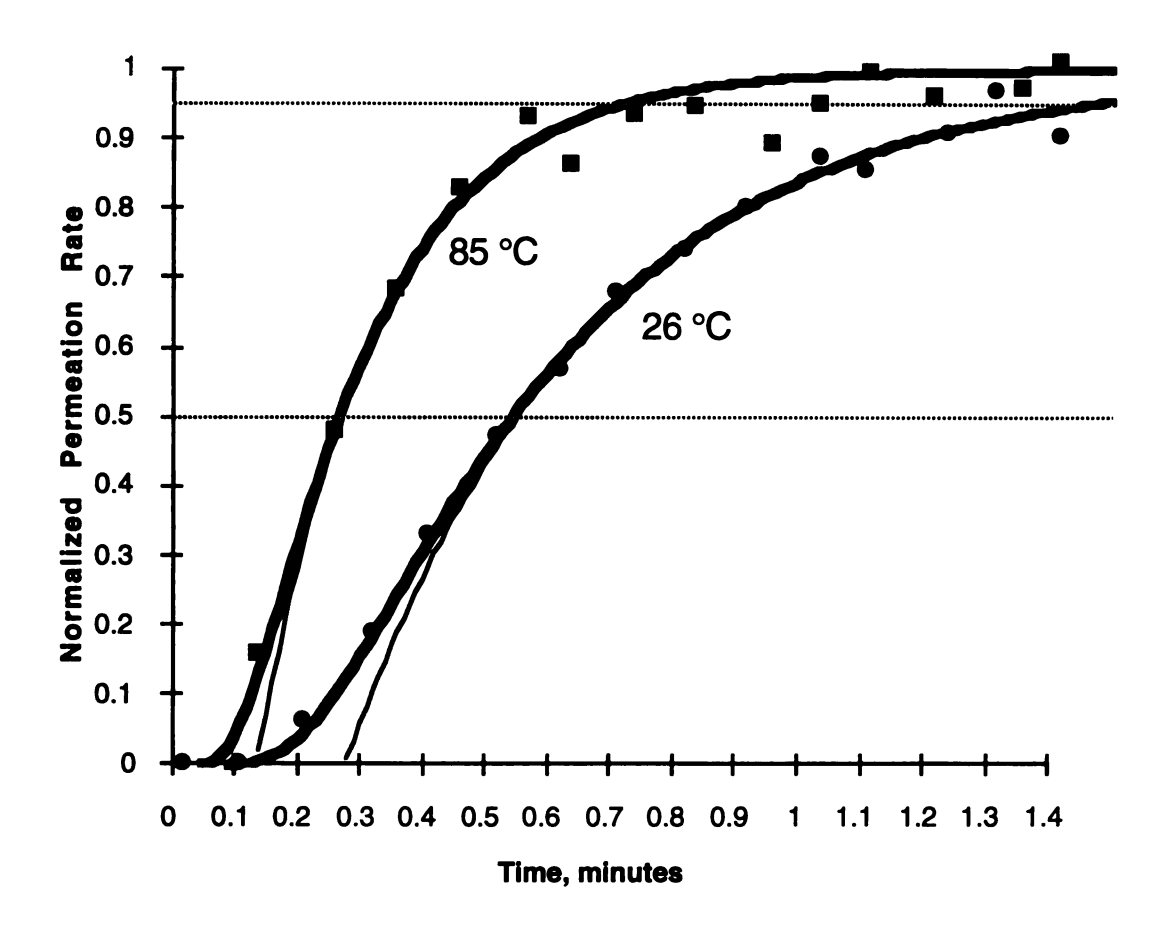
Further evaluation yields a  $t_{95}/t_{50}$  theoretical ratio of 2.7. Good agreement is obtained for times greater than  $t_{50}$  when the first approximation is applied to experimental response curves, as shown in Figure 2.4. Thus, the response time approximation  $t_{95} = 2.7 \cdot t_{50}$  is valid. For times less than  $t_{50}$ , additional terms in the polynomial are required for a good fit. Response times are reported in this work in terms of  $t_{50}$  measurements.

#### Effects of membrane dimensions

Since diffusivity is a constant for a given substance in a given polymer and at a given temperature, the response time-thickness relationship can be expressed as follows:

$$t_{(50)2}/t_{(50)1} = (d_2/d_1)^2. (2.14)$$

The increase in response times for organic gases permeating a hollow fiber membrane with a 0.0216-cm wall thickness compared with that for a 0.0165-cm wall thickness is shown in Table 2.3. As



## **Key:**Circles and squares = experimental data Thin lines = solutions using only the first term (n=1) of the polynomial Heavy lines = solutions using the first five terms (n=1-5)

Figure 2.4. A plot of solutions to non-steady state permeation (Equation 2.12), calculated from  $t_{50}$  values, and permeation response data for chloroform at 26 °C and 85 °C.

described in the Appendix, the experimental measurement of  $t_{50}$  is dependent upon errors in defining the steady state permeation response and in establishing the time when the sample makes initial contact with the membrane,  $t_0$ . Thinning of the membrane caused by the pressure difference between the inside and the outside of the hollow fiber also may result in the deviations between the experimental and theoretical response time ratios in Table 2.3.

Table 2.3. Effects of membrane thickness on response time for gas phase organic compounds. The membranes are 2.5-cm long silicone hollow fibers. Temperature = 23 °C.

	response tin	t <sub>(50)2</sub> /t <sub>(50)1</sub>		
compound	<u>d</u> <sub>1</sub> =0.0165 cm	<u>d<sub>2</sub>=0.0245 cm</u>	exp.	theor.
dichloromethane	0.38	0.60	1.6	2.2
1,1-dichloroethene	0.28	0.48	1.7	2.2
chlorobenzene	0.72	1.60	<b>2.2</b>	2.2
acetone	1.88	3.02	1.6	2.2

Effects of temperature

Diffusivity obeys the Arrhenius relation given by

$$D_{i,s} = D_{i,so} \cdot \exp[-E_{Di} \cdot (1/RT - 1/RT_o)]. \tag{2.15}$$

Higher temperatures result in increased diffusivities and therefore shorter response times. The permeation rate response curves for a step change in sample concentration at various temperatures are shown for 1,2,4-trichlorobenzene in Figure 2.5. The  $t_{50}$  values for

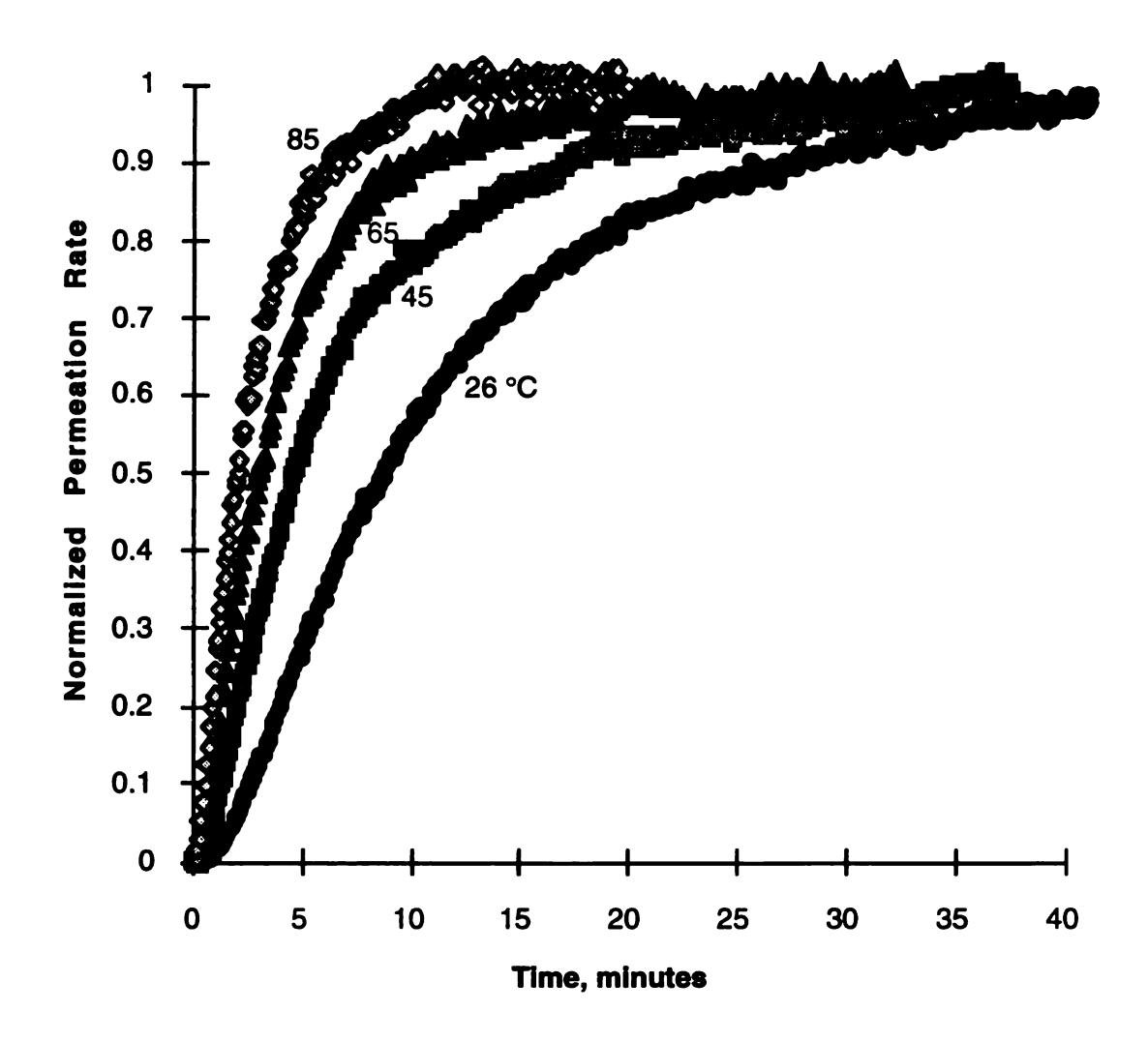


Figure 2.5. Normalized permeation response curves for 1,2,4-trichlorobenzene as a function of temperature.

Table 2.4. Survey of temperature effects on response time,  $t_{50}$ , for organic compounds in nitrogen. The membrane is a 2.5-cm long, 0.0305-cm i.d., 0.0635-cm o.d. silicone hollow fiber.

	response time, t <sub>50</sub> , (minutes)			
compound	<u>26 °C</u>	<u>45 °C</u>	<u>65 °C</u>	<u>85 °C</u>
chloromethane	0.23	0.19	0.18	0.17
dichloromethane	0.34	0.30	0.24	0.20
chloroform	0.42	0.36	0.30	0.24
carbon tetrachloride	0.52	0.38	0.32	0.27
chloroethene	0.25	0.20	0.18	0.16
1,1-dichloroethene	0.36	0.30	0.25	0.23
trichloroethene	0.41	0.35	0.28	0.21
tetrachloroethene	0.78	0.55	0.41	0.33
dibromomethane	0.57	0.40	0.33	0.25
bromoform	1.30	0.88	0.62	0.50
benzene	0.43	0.32	0.26	0.24
toluene	0.59	0.46	0.35	0.24
ethylbenzene	0.86	0.60	0.42	0.30
chlorobenzene	0.93	0.63	0.45	0.37
1,3-dichlorobenzene	4.40	1.70	1.00	0.95
1,2,4-trichlorobenzene	8.70	4.60	3.00	2.00

several gas phase organic compounds at different temperatures are given in Table 2.4. Aqueous sample response times mimic gas samples when the transport-rate through the sample is negligible, as discussed in detail in Chapter 5.

#### ORGANIC ENRICHMENT

The relative permeability through the membrane for one compound over another determines membrane selectivity. The enrichment factor,  $\mathcal{E}_{i/j}$ , of one component, i, over another, j, (e.g., an organic compound over the sample matrix) is defined by the ratio of their permeabilities;

$$\mathcal{E}_{i/j} = (D_{i,s} \bullet K_i) / (D_{j,s} \bullet K_j) = (F_i / c_{i,m}) / (F_j / c_{j,m})$$
(2.15)

Effects of membrane dimensions

The enrichment factor is independent of membrane dimensions, as seen in Equation 2.15. Increasing the length or number of the hollow fiber will increase permeation rates of all components proportionally, with no effect on observed organic enrichment, if  $c_{mi}$  does not change over the length of the hollow fiber. Typically, increasing the membrane surface area will be more efficiently accomplished by increasing the number, rather than the length, of hollow fibers exposed to the sample.

#### Effects of temperature

With increasing temperature, the enrichment factors for organic components are reduced because the permeabilities for air and water increase more than the permeabilities for most organic compounds studied, as shown in Figure 2.3. For trace level organic samples, the analyzer pressure follows the permeabilities of the air or water.

Based on steady state response data used to determine the detection limits in Table 2.2, permeabilities from aqueous samples increased an average 35% (range = 14-83%) when the temperature was increased from 26 °C to 45 °C for the compounds analyzed in water. Diffusivities through the membrane for these same organic compounds increased an average 46% (range = 13-159%) based upon the response time data in Table 2.4, where  $[D_s(45 \text{ °})-D_s(26 \text{ °})]/D_s(26 \text{ °}) = [1/t_{50}(45 \text{ °})-1/t_{50}(26 \text{ °})]/[1/t_{50}(26 \text{ °})]$ . Although the organic permeabilities increased, water permeability increased 130% for the same temperature change.

For air samples, organic responses decreased an average 20% (range = 10-33%) when the temperature was increased from 26 °C to 45 °C, even though diffusivities increased an average 43% (range = 13-159%). Therefore, the decrease in the membrane/air distribution ratio dominates the permeabilities for these compounds. While the organic permeabilities decreased, the nitrogen permeability increased 29%. Enrichment factors relative to nitrogen and water for several organic compounds are given in Table 2.5.

Table 2.5. Survey of temperature effects on the enrichment over the sample matrix for organic compounds in nitrogen and water.

<u>-</u>	enrichment factor				
	relative to	<u>nitrogen</u>	relative to water		
<u>compound</u>	<u>26°C</u>	<u>45°C</u>	<u>26°C</u>	<u>45°C</u>	
chloromethane	40	27	-	-	
dichloromethane	48	33	1900	1100	
chloroform	91	58	2100	1100	
carbon tetrachloride	110	74	1800	1100	
chloroethene	37	26	-	-	
1,1-dichloroethene	57	35	3300	1800	
trichloroethene	140	81	970	530	
tetrachloroethene	310	180	600	360	
dibromomethane	84	50	190	100	
bromoform	320	170	570	330	
benzene	170	110	2600	1400	
toluene	380	230	2300	1300	
ethylbenzene	450	280	2200	1200	
chlorobenzene	550	330	1300	730	
1,3-dichlorobenzene	520	350	470	300	
1,2,4-trichlorobenzene	780	400	450	390	

Most of the permeation parameters (permeability, diffusivity, solubility, and enrichment factors) reported in the literature are for simple gases such as hydrogen, nitrogen, oxygen, argon, and light hydrocarbons and alcohols (15-20). Very few studies have been performed to determine these parameters for the more complex organic compounds that are of interest to analytical chemists (21, 22). A mass spectrometric technique developed for obtaining the permeation parameters reported in this work is described in the Appendix.

#### REFERENCES

- (1) Hwang, S.-T.; Kammermeyer, K. <u>Membranes in Separations</u>, Robert E. Krieger Publishing Co., Inc.; Malabar, FL; 1984.
- (2) Frennesson, I.; Tragardh, G.; Hahn-Hagerdal, B. Chem. Eng. Commun. 1986, 45, 277.
- (3) Mulder, M. H. V.; Smolders, C. A. *J. Membrane Sci.* **1984**, 17, 289.
- (4) Conway, B. E. In <u>The Solid-Gas Interface</u>, Vol. 2, Flood, E. A., ed.; Marcel Dekker, Inc.: New York, NY; 1967.
- (5) Mears, P. In <u>Membrane Separation Processes</u>; Mears, P., Ed.; Elsevier: Amsterdam, Netherlands; 1976.
- (6) Ben-Naim, A. Solvation Thermodynamics; Plenum Press: New York, NY; 1987.
- (7) Karger, B. L.; Snyder, L. R.; Horvath, C. An Introduction to Separation Science; Wiley-Interscience: New York, NY; 1973.
- (8) Barrer, R. M. <u>Diffusion in and Through Solids</u>; Cambridge University Press: New York, NY; 1951.
- (9) Crank, J. <u>The Mathematics of Diffusion</u>, 2nd Ed.; Oxford University Press: New York, NY; 1975.
- (10) Lee, C. H. J. App. Polym. Sci. 1975, 19, 83.
- (11) Pasternak, R. A.; Schimscheimer, J. F.; Heller, J. J. Polym. Sci. **1970**, 8, 467.
- (12) Ziegel, K. D.; Frensdorff, H. K.; Blair, D. E. *J. Polym. Sci.* **1969**, 7, 809.

- (13) Bier, M. E.; Kotiaho, T.; Cooks, R. G. Anal. Chem. Acta 1990, 231, 175.
- (14) Lauritsen, F. R. Int. J. Mass Spectrom. Ion Proc. 1990, 95, 259.
- (15) Stern, S. A.; Shah, V. M.; Hardy, B. J. J. Polymer Sci.: Part B: Polymer Physics **1987**, 25, 1263.
- (16) Kammermeyer, K. Ind. Eng. Chem. 1957, 49, 1685.
- (17) Hodgson, M. E. Filtr. and Separ. 1973, July/August, 418.
- (18) Kim, T. H.; Koros, W. J.; O'Brien, K. C. *J. Membrane Sci.* **1988**, 37, 45.
- (19) Friedlander, H. Z.; Litz, L. M. In <u>Membrane Processes in Industry and Biomedicine</u>, Bier, M., Ed.; Plenum Press: New York, NY; 1971.
- (20) Bell, C.-M.; Gerner, F. J.; Strathman, H. J. Membrane Sci. 1988, 36, 315.
- (21) Ho, J. S.-Y.; Schlecht, P. C. Am. Ind. Hyg. Assoc. J. 1981, 42, 70.
- (22) Tou, J. C.; Rulf, D. C.; DeLassus, P. T. Anal. Chem. 1990, 62, 592.

#### CHAPTER 3

### The Correlation of Permeability with Hildebrand Solubility Parameters

In addition to guiding the selection of liquid extraction solvents, the "like-dissolves-like" rule is commonly used to guide the selection of membrane materials. For example, the extraction of non polar organic compounds from an aqueous matrix can be accomplished with a silicone membrane because of the tremendous selectivity this polymer exhibits for the permeation of the non polar materials (Table 2.5). However, this simple rule does not predict nor explain the fact that, in the gas phase, 1-propanol permeates this same silicone membrane nearly two times better than pentane and methanol permeates over forty times better than methane. In addition, membrane extractions are kinetic, as well as thermodynamic, processes such that the effects of selective diffusivities in the membrane become important, not only for the separation efficiency, but also for the analytical response time.

A fundamental understanding of the membrane extraction process, facilitated by a simple model, can help to generate more versatile separation techniques and perhaps a wider selection of membrane materials. In this chapter, a permeation model is developed based upon Hildebrand solubility parameters. A correlation

of this model is made to the partition selectivity, to the diffusion selectivity, and to the permselectivity or enrichment factor.

#### THE SOLUBILITY PARAMETER

As discussed in Chapter 2, the solution-diffusion permeation model assumes that a permeating substance is in equilibrium at the interface between the feed and membrane phases. This equilibrium, in combination with a vacuum or sweep fluid at the permeate side of the membrane, establishes a concentration gradient across the membrane that results in diffusive flow. For component i, the permeation coefficient,  $P_i$ , is given by the product of the diffusivity,  $D_{i,s}$ , and the Henry's law solubility coefficient,  $S_i$ ,

$$P_{i} = D_{i,s} \circ S_{i} \tag{3.1}$$

The permselectivity or enrichment factor,  $\mathcal{E}_{i/j}$ , of a membrane for one substance, i, relative to another, j, is defined as

$$\mathcal{E}_{i/j} = (D_{i,s}/D_{j,s}) \cdot (S_i/S_j)$$
(3.2)

By assuming that the sorption of a gas into a polymer phase may be modeled as a solution process, a correlation of solubility parameters to the solution-diffusion permeation model arises naturally. Hildebrand solubility parameters have been used in estimating the compatibility of polymers with solvents, additives, and coatings (1-6). The solubility parameter,  $\delta_i$ , (7, 8) for substance i is the square root of the cohesive energy density for the pure liquid substance, defined as

$$\delta_{i} = [\Delta E_{Vi}/v_{i}]^{1/2} = [(\Delta H_{Vi}-RT)/v_{i}]^{1/2}$$
(3.3)

where  $\Delta E_{Vi}$  is the molar energy of vaporization,  $v_i$  is the molar volume,  $\Delta H_{Vi}$  is the molar heat of vaporization, R is the gas constant and T is the absolute temperature. The relationship between the solubility parameter and the activity coefficient,  $\gamma_{i,s}$ , for some substance i in some phase m is given by the Flory-Huggins relationship (5)

$$\ln[\gamma_{i,s}] = \ln[\nu_i/\nu_s] + (1 - [\nu_i/\nu_s]) \cdot \Phi_s + \chi_{i,s} \cdot \Phi_s^2$$
(3.4)

where  $v_s$  and  $\Phi_s$  are the molar volume and the volume fraction of the phase m, respectively, and the binary interaction parameter,  $\chi_{i,s}$ , is

$$\chi_{i,s} = [v_i/(RT)] \cdot [\delta_i - \delta_s]^2$$
(3.5)

Application of the solubility parameter to separation processes has been most successful for solutions of similar materials where dispersion interaction forces predominate. The solubility parameter theory has been expanded (1, 9) to include other interaction forces such as dipole induction and orientation forces as well as hydrogen-bonding forces. In the present study, the single parameter treatment was found to give reasonably good correlations with experimental results for a membrane composed of poly(dimethylsiloxane) with a fumed-silica filler.

#### **DEVELOPMENT OF THE MODEL**

For the model described below, the following assumptions are made:

- 1) The feed or mobile phase is an ideal gas.
- 2) The permeating substance is at infinite dilution in both mobile (feed) and stationary (membrane) phases.
- 3) The distribution process can be described using the regular solution model as modified by Flory-Huggins [5], with all assumptions inherent therein. Specifically, no changes in phase volumes occur due to sorption.
- 4) The diffusion process obeys Fick's laws, with all assumptions inherent therein.

#### Distribution equilibrium

In the solution-diffusion model, an equilibrium is established at the feed-membrane interface for a permeating substance as described by Henry's law:

$$X_{i,s} = p_i/[p_i^{o \bullet} \gamma_{i,s}]$$
 (3.6)

where  $X_{i,s}$  is the mole fraction and  $\gamma_{i,s}$  is the activity coefficient of substance i in the membrane stationary phase, s, and  $p_i$  and  $p_i^o$  are the equilibrium and standard-state partial pressures, respectively, for the substance in the mobile phase. Equation 3.6 may be expressed in the natural logarithmic form and combined with Equation 3.4 and Equation 3.5 to yield

$$ln[X_{i,s}] = ln[p_i/p_i^o] - ln[v_i/v_s] - (1 - [v_i/v_s]) \bullet \Phi_s$$
$$- [v_i/(RT)] \bullet [\delta_i - \delta_s]^2 \bullet \Phi_s^2$$
(3.7)

In the case of a membrane consisting of two distinct phases, such as a polymer with a uniformly distributed filler, the molar volume is defined by

$$v_{s} = v_{p} \bullet X_{p,s} + v_{f} \bullet X_{f,s}$$
(3.8)

where  $v_p$  and  $v_f$  are the molar volumes and where  $X_{p,s}$  and  $X_{f,s}$  are the mole fractions of the polymer and the filler, respectively, in the stationary phase. These parameters need not be quantitatively specified in the treatment described below. Transport properties for a substance in a polymeric membrane containing a filler have also been modeled using the additive properties of the two phases in the membrane (10, 11). Similarly, the solubility parameter for the stationary phase based on regular solution theory is given by

$$\delta_{s} = \delta_{p} \bullet \Phi_{p} + \delta_{f} \bullet \Phi_{f} \tag{3.9}$$

where  $\delta_p$  and  $\delta_f$  are the solubility parameters for the polymer and filler phases, respectively, and  $\Phi_p$  and  $\Phi_f$  are the volume fractions of the polymer and the filler, respectively, in the membrane. Equation 3.7 is rearranged to give

$$\ln[X_{i,s} \bullet (v_i/v_s)] = \ln[p_i/p_i^o] - (1 - [v_i/v_s]) \bullet \Phi_s$$
$$- [v_i/(RT)] \bullet [\delta_i - \delta_s]^2 \bullet \Phi_s^2$$
(3.10)

At infinite dilution,  $X_{i,s} = n_{i,s}/n_s$ , where the ratio  $n_{i,s}/n_s$  is the number of moles of sorbed substance i per mole of stationary phase. Therefore, the volumetric concentration of the substance in the stationary phase,  $C_{i,s}$ , is given by

$$X_{i,s} \bullet [v_i/v_s] = V_{i,s}/V_s = C_{i,s}$$
 (3.11)

where  $V_{i,s}/V_s$  is the volume of the sorbed substance per unit volume of stationary phase. Similarly, the volumetric concentration of the substance in the gaseous mobile phase,  $C_{i,m}$ , is given by the ratio of the partial pressure to total feed pressure:

$$p_i/p_t = V_{i,m}/V_m = C_{i,m}$$
 (3.12)

Equation 3.10 can now be represented in terms of the concentration distribution ratio,  $C_{i,s}/C_{i,m} = K_i$ , where

$$\ln[K_{i}] = \ln[p_{t}/p_{i}^{0}] - (1 - [v_{i}/v_{s}]) \cdot \Phi_{s}$$
$$- [v_{i}/(RT)] \cdot [\delta_{i} - \delta_{s}]^{2} \cdot \Phi_{s}^{2}$$
(3.13)

Because substance i is assumed to be at infinite dilution,  $\Phi_s = 1$ . In addition, the molar volume of the stationary phase,  $v_s$ , is much greater than that of the sorbed substance,  $v_i$ . Therefore, Equation 3.13 reduces to

$$\ln[K_i] = \ln[p_t/p_i^{\circ}] - 1 - [v_i/(RT)] \cdot [\delta_i - \delta_s]^2$$
(3.14)

This relationship is consistent with gas chromatographic studies of dilute solutions of organic molecules in polymers (5). Hildebrand, Prausnitz, and Scott proposed a model for the solubility of a gas in a solvent in which the gas first condenses to a hypothetical pure liquid and then dissolves in the solvent (8). In the case of non polar gases at temperatures above their critical temperature, they have calculated fugacities of these hypothetical liquids to estimate solubilities. Solubility parameters have been calculated for such gases by Prausnitz and Shair (12). Giddings, et. al (13) have described an expression for determining the solubility parameters of compressed gases using their critical properties. In the present work, an attempt is made to develop a general model that provides predictions for the solubility of gases of varying polarities and critical temperatures, using a minimum of readily available parameters. This model utilizes the hypothetical and experimental solubility parameter values provided in the literature. In this model, the vapor pressure term in Equation 3.14 is related to the Hildebrand solubility parameter by Equation 3.3 and the Clausius-Clapeyron equation in the following manner:

$$ln[p_t/p_i^o] = [v_i/(RT)] \cdot (\delta_i - \alpha)^2$$
(3.15)

The experimentally determined constant,  $\alpha$ , corresponds to the solubility parameter for the hypothetical liquid feed matrix and corrects for deviations from Henry's law, Flory-Huggins, and regular solution theory. A correlation between the distribution ratio and solubility parameter is then given by the following equation:

$$\ln[K_i] = [v_i/(RT)] \cdot [(\delta_i - \alpha)^2 - (\delta_i - \delta_s)^2] - 1$$
 (3.16)

The distribution selectivity for substance i relative to substance j is calculated from

$$K_i/K_i = \exp\{[2 \cdot (\delta_s - \alpha) \cdot (\delta_i v_i - \delta_j v_i) + (\alpha^2 - \delta_s^2) \cdot (v_i - v_i)]/(RT)\}$$
(3.17)

#### Diffusion

According to the free volume theory of Brandt (14), the activation energy for diffusion,  $E_{Di}$ , in elastomers is dominated by intermolecular forces and may be related to the cohesive energy density of the polymer,  $\delta_p^2$ , as well as dimensions of the polymer chains and diffusing substance. The relationship is given by (10):

$$E_{Di} = 0.5 \cdot s_p \cdot \sigma_p \cdot \sigma_i \cdot \delta_p^2 \cdot N$$
(3.18)

where  $s_p$  is the polymer segment length associated with the free volume,  $\sigma_p$  is the average diameter of the polymer molecule,  $\sigma_i$  is the diameter of the diffusing substance, and N is Avogodro's number. Equation 3.18 may be expressed in terms of the molar volume of the diffusing substance:

$$E_{Di} = 0.62 \cdot N^{2/3} \cdot s_{p} \cdot \sigma_{p} \cdot \delta_{p}^{2} \cdot v_{i}^{1/3}$$
(3.19)

Although the free volume of some liquids may be significant, for many substances the liquid molar volume is consistent with the molecular volume (7). For the purpose of the present model, the liquid molar

volume of the diffusing substance is used rather than the molecular volume so that consistency with the solution model is maintained and so that the number of variable terms are minimized.

The constants and polymer-related terms in Equation 3.19 may be combined into a single constant parameter,  $\vartheta$ , so that the activation energy may be written to be proportional to the molar volume of the diffusing substance. The dependence of the diffusivity on the molar volume may then be described by

$$ln[D_{i,p}] = ln[D_{o,p}] - [\vartheta/(RT)] \cdot v_i^{1/3}$$
 (3.20)

where  $\vartheta$ , the polymer-related constant, and  $\ln[D_{0,p}]$ , the natural logarithm of the diffusivity of some hypothetical substance with v=0, are determined from the slope and the y-intercept, respectively, of a plot of  $\ln[D_{i,p}]$  vs.  $v_i^{1/3}$ .

Equation 3.20 does not account for the effects of a filler on diffusive transport in a polymer. Thermodynamic partitioning or adsorption of some substances may become significant in cases where the two phases of the filled membrane are quite different in polarity or hydrogen-bonding character. This inhibition of diffusive flow through a filled membrane is manifested as an apparent diffusivity that is lower than predicted from the molar volume of the substance. If it is assumed that migration of a substance through the membrane occurs only in the polymer phase, any delay in this migration time is due to partition into or adsorption onto the filler. The individual retention

processes of this transport mechanism is illustrated in Figure 3.1. The degree of retention by the filler in a composite membrane is determined by the molar partition or adsorption coefficient, k'<sub>i</sub>,

$$k'_{i} = n_{i,f}/n_{i,p} = (t_{i,s} - t_{i,p})/t_{i,p}$$
 (3.21)

where  $n_{i,f}$  and  $n_{i,p}$  are the number of moles of substance i in the filler and the polymer phases, respectively, at equilibrium,  $t_{i,p}$  is the time for diffusion of substance i through the polymer, and  $t_{i,s}$  is the time for diffusion of i through the filled membrane. Equation 3.21 may be rearranged to give

$$t_{i,s} = t_{i,p} \cdot (1 + k'_i)$$
 (3.22)

It is clear from Equation 3.22 that no retention is observed when the diffusing substance has no affinity for the filler (i.e.,  $k'_i = 0$ ). The diffusivity of substance i in the membrane may be determined experimentally from the sorption rate curves (15) using the following equation:

$$D_{i} = 0.14 \cdot d^{2}/t_{(50)}$$
 (3.23)

where d is the membrane thickness and  $t_{(50)}$  is the time required to attain one-half steady-state permeation following a step-change in the concentration of the substance in the mobile phase. By combining Equations 3.22 and 3.23, a relationship is obtained between the diffusivities with and without retention by the filler:

# Polymer Phase Polymer Phase Filler Phase Polymer Phase Polymer Phase Additional Phase Partition or adsorption coefficient, k', established at filler/polymer interface in membrane

PERMEATE

Figure 3.1. Thermodynamic interaction effects of a filler on diffusive transport.

$$D_{i,s} = D_{i,p}/(1 + k'_i)$$
 (3.24)

where  $D_{i,s}$  is the diffusivity of substance i in the filled polymer stationary phase and  $D_{i,p}$  is the diffusivity in the unfilled polymer. This relationship is consistent with that reported by Barrer and coworkers (16, 17). In addition, a reduction in mass transport rates is observed in a polymer containing impermeable particles or crystallites due to the tortuous path the diffusing substance must travel (18). These effects have been summarized by van Amerongen (19), where the diffusivity in a membrane containing a non-retentive spherical filler is related to that in the unfilled polymer by the volume fraction of the filler in the membrane,  $\Phi_f$ , such that:

$$D_{i,s} = D_{i,p}/[1 + (\Phi_f/2)]$$
 (3.25)

The retention and tortuosity terms are combined to yield the diffusion-partition (D-k) model given by the following equation:

$$D_{i,s} = D_{i,p} / \{ [1 + (\Phi_f/2)] \cdot [1 + k'_i] \}$$
(3.26)

To estimate the diffusivity of a substance in a membrane that contains a filler, Equations 3.20 and 3.26 are combined to give

$$D_{i,s} = D_{o,p} \cdot \exp\{-[\vartheta/(RT)] \cdot v_i^{1/3}\}$$

$$/\{[1 + (\Phi_f/2)] \cdot [1 + k'_i]\}$$
(3.27)

Whereas retention processes may play a large role, the tortuosity factor is independent of the nature of the permeating substance and is, therefore, not important for estimating selectivity.

Where retention arises from a thermodynamic partition process, the distribution coefficient may be estimated using solubility parameter theory. At equilibrium, if substance i is partitioned between the polymer and filler phases, then

$$X_{i,f}/X_{i,p} = \gamma_{i,p}/\gamma_{i,f}$$
 (3.28)

where the subscripts f and p designate the filler and polymer, respectively. Rearranging and combining Equation 3.28 with Equations 3.4 and 3.5 yields the following relation:

$$\begin{split} \ln[X_{i,f}/X_{i,p}] &= \ln[v_i/v_p] - \ln[v_i/v_f] + (1 - [v_i/v_p]) \bullet \Phi_p \\ &- (1 - [v_i/v_f]) \bullet \Phi_f + [v_i/(RT)] \bullet [\delta_i - \delta_p]^2 \bullet \Phi_p^2 \\ &- [v_i/(RT)] \bullet [\delta_i - \delta_f]^2 \bullet \Phi_f^2 \end{split} \tag{3.29}$$

Assuming infinite dilution for substance i in all phases and assuming the molar volume of substance i to be small relative to the molar volumes of the filler and polymer phases, Equation 3.29 is simplified to the following:

$$\ln[X_{i,f}/X_{i,p}] = \ln[(v_i/v_p)/(v_i/v_f)] + [v_i/(RT)] \cdot [(\delta_i - \delta_p)^2] - [v_i/(RT)] \cdot [(\delta_i - \delta_f)^2]$$
(3.30)

Following the substitution of Equation 3.11 into Equation 3.30, the distribution ratio for substance i partitioned between the filler and polymer is given by

$$ln[C_{i,f}/C_{i,p}] = ln[K'_{i}] = [v_{i}/(RT)] \cdot [(\delta_{i} - \delta_{p})^{2}]$$

$$- [v_{i}/(RT)] \cdot [(\delta_{i} - \delta_{f})^{2}]$$
(3.31)

Since the distribution ratio is the product of the molar partition coefficient and the volume phase ratio,  $K'_i = k'_i \cdot (V_p/V_f)$ , then Equation 3.31 can be rewritten as follows:

$$\ln[k'_{i}] = \ln[V_{f}/V_{p}] + [v_{i}/(RT)] \cdot [(\delta_{i} - \delta_{p})^{2}]$$

$$- [v_{i}/(RT)] \cdot [(\delta_{i} - \delta_{f})^{2}]$$
(3.32)

If retention arises from an adsorption process, the entire molecule may not participate in the interaction with the solid adsorbent surface. The energy of adsorption at the surface is typically described by the surface free energy,  $E_{Ai}/(N^{1/3} \cdot v_i^{2/3})$ , and involves only the molar area,  $N^{1/3} \cdot v_i^{2/3}$ , of the adsorbed molecules (7, 20, 21). Karger, Snyder, and Eon (9) have proposed a model of liquid-solid chromatography in which the adsorption energy is proportional to the product of the area of the adsorbed molecule and the cohesive energy density. This relationship is given in the present model as

$$E_{Ai} = (RT)\ln[K'_i] = v_i^{2/3} \cdot [A \cdot \delta_i^2 + B]$$
 (3.33)

where the proportionality constants, A and B, are determined experimentally. The molar adsorption coefficient is correlated to the Hildebrand solubility parameter and molar volume by the following equation:

$$\ln[k'_{i}] = \ln[V_{f}/V_{p}] + [v_{i}^{2/3}/(RT)] \cdot [A \cdot \delta_{i}^{2} + B]$$
(3.34)

This theoretical model may be compared with a model using a modification of Equation 3.32 to describe adsorption of substances on the filler phase. Since the entire molecule does not participate in the adsorption process, the partial molar volume,  $v_i$ , of the surface-active functional group may be substituted for the total molar volume,  $v_i$ , in Equation 3.32. In such cases, the molar adsorption coefficient may be estimated as follows:

$$\ln[k'_{i}] = \ln[V'_{f}/V_{p}] + [v_{i}/(RT)] \cdot [(\delta_{i} - \delta_{p})^{2}]$$

$$- [v'_{i}/(RT)] \cdot [(\delta_{i} - \delta_{f})^{2}]$$
(3.35)

where  $V_f$  is the interfacial layer volume and  $V_f/V_p$  is the active volume ratio, which is determined experimentally.

From Equation 3.27, the diffusion selectivity between substance i and j is given by

$$D_{i,s}/D_{j,s} = \{ [1 + k'_{j}]/[1 + k'_{i}] \}$$

$$\bullet \exp\{-[\vartheta/(RT)] \bullet [v_{i}^{1/3} - v_{j}^{1/3}] \}$$
(3.36)

where the molar adsorption coefficients, k'<sub>i</sub> and k'<sub>j</sub>, are obtained from the experimental solutions for Equation 3.34 or Equation 3.35.

The distribution and diffusion-retention models have been evaluated for a silicone elastomer membrane that contains a fumed-silica filler. The experimental membrane separation parameters and their correlations with the models are presented below.

#### CORRELATION OF DATA TO THE MODEL

#### Experimental conditions

The membrane used to investigate the correlation of solubility parameters with permeability was a silicone elastomer, composed by weight of 69% poly(dimethylsiloxane) and 31% fumed silica (0.011-µm diameter particles). The membrane was a Silastic<sup>TM</sup> silicone elastomer hollow fiber (2.5-cm length, 0.0305-cm i.d., 0.0635-cm o.d.) from Dow Corning Corporation. The hollow fiber was mounted in a stainless-steel tee as shown in Figure 3.2.

Gas-phase samples were prepared by injecting known amounts of the substances of interest into a nitrogen-filled 5-L Saran<sup>TM</sup> gas sampling bag (22, 23). The concentration of organic substances was sufficiently low to prevent swelling of the membrane (less than 0.1% by volume gas phase). The samples were analyzed immediately after preparation to minimize sorption into the bag. The gas-phase samples were pulled through the hollow fiber membrane at a rate of 100-cm<sup>3</sup>/minute with a gas pump from Metal Bellows Corporation.

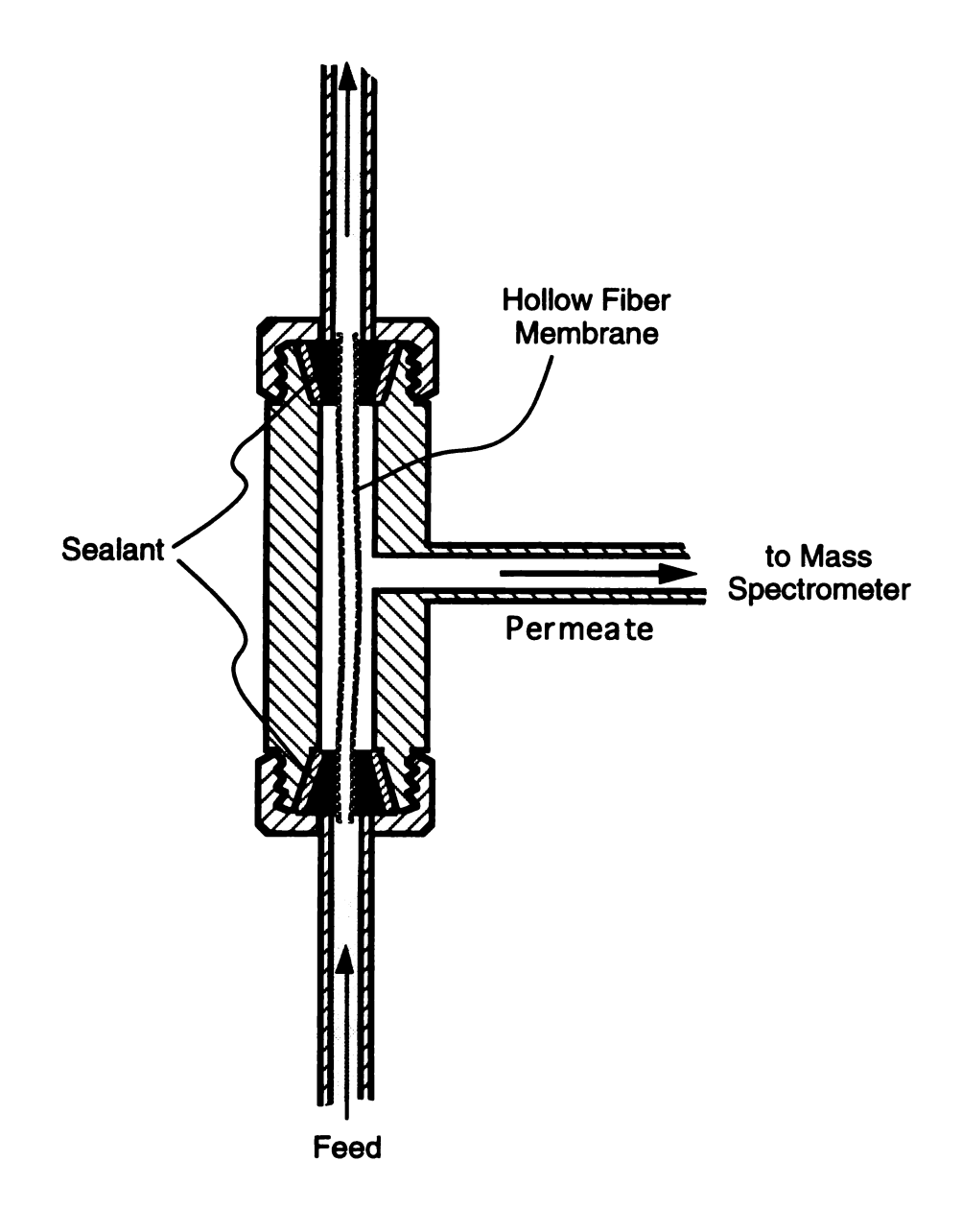


Figure 3.2. Hollow fiber membrane permeation cell.

Permeation measurements were obtained by mass spectrometry with a Hewlett-Packard 5971-A Mass Selective Detector modified for process analysis applications (24). All experiments were performed at 25 °C.

The membrane separation parameters including enrichment factor, E, permeability, P, diffusivity, D, and distribution ratio, K, were determined for the substances of interest from mass spectral data in combination with data from literature sources. The method for the determination of these parameters is described in Chapter 2 and in the Appendix of this work. The enrichment factor  $(\mathcal{E}_{i/N_2} = P_i/P_{N_2})$ values were determined from mass spectrometric response ratios and molar response factors (25), as described previously (26). The permeabilities were estimated from these experimentally determined enrichment factors and a literature value for  $P_{N_2}$  (26), where  $P_i$  =  $\mathcal{E}_{1/N_2}(\exp) \bullet P_{N_2}(\text{lit})$ . The diffusivities were determined using Equation 3.23 and the permeation rate curves generated from the mass spectrometric experiments (26). The distribution ratio,  $K_i$ , in this study replaces the Henry's law solubility coefficient  $(S_i = P_i/D_{i,s})$ traditionally used in gas permeation studies. The distribution ratio of the substance between the gaseous mobile phase and membrane stationary phase is simply the product of S<sub>i</sub> and the total feed pressure (26), where  $K_i = C_{i,s}/C_{i,m} = S_i \cdot 76$  cm Hg.

In order to provide a comprehensive test of the theoretical models, a wide variety of substances with differing size and chemical functionality was examined in this study. These substances include permanent gases, alkanes, chlorinated and brominated hydrocarbons,

Table 3.1. Molar volumes ( $v_i$ ) and Hildebrand solubility parameters ( $\delta_i$ ) from References 1, 12, and 28.

	molar volume	solubility parameter
<u>compound</u>	<u>cm<sup>3</sup>/mole</u>	$(J/cm^3)^{1/2}$
gases		
nitrogen	32.4	5.3
oxygen	33.0	8.2
argon	57.1	10.9
carbon dioxide	55.0	12.3
alkanes		
methane	<b>52.0</b>	11.6
ethane	70.0	13.5
propane	85.0	13.6
butane	101.4	13.9
pentane	116.2	14.3
hexane	131.6	14.9
heptane	147.4	15.1
aromatic hydrocarbons		
benzene	89.4	18.8
toluene	106.8	18.2
ethylbenzene	123.1	18.0
chloromethanes		
chloromethane	55.4	19.8
dichloromethane	63.9	19.8
chloroform	80.7	19.0
carbon tetrachloride	97.1	17.6
chloroethenes		
chloroethene	68.1	16.0
1,1-dichloroethene	79.0	18.6
trichloroethene	90.2	18.8
tetrachloroethene	101.1	19.0
bromomethanes		
bromomethane	56.1	19.6
dibromomethane	68.9	22.3
bromoform	87.5	21.8
alcohols		
methanol	40.7	29.7
ethanol	58.5	26.0
1-propanol	<b>75.2</b>	24.3
1-butanol	91.5	23.3

Table 3.2. Experimental permeation parameters for substances in a silicone elastomer membrane at 25 °C.

compound	P(X10 <sup>6</sup> )a	$\underline{\mathrm{D_s}(\mathrm{X}10^6)^b}$	<u>S</u> c
gases			
nitrogen	0.028	21	0.0013
oxygen	0.053	21	0.0025
argon	0.053	21	0.0025
carbon dioxide	0.33	13	0.026
alkanes			
methane	0.13	16	0.0079
ethane	0.33	11	0.030
propane	0.80	6.4	0.13
butane	1.0	6.3	0.16
pentane	6.9	4.5	1.5
hexane	8.8	3.5	2.5
heptane	22	3.2	7.0
aromatic hydrocarbons			
benzene	13	4.9	2.8
toluene	27	3.5	7.6
ethylbenzene	42	1.7	25
chloromethanes			
chloromethane	1.9	11	0.17
dichloromethane	9.7	9.1	1.2
chloroform	12	4.9	2.4
carbon tetrachloride	12	2.9	4.2
chloroethenes			
chloroethene	1.6	9.1	0.21
1,1-dichloroethene	8.0	5.8	1.4
trichloroethene	18	3.7	4.8
tetrachloroethene	45	2.4	19
bromomethanes	_		
bromomethane	1.9	9.1	0.21
dibromomethane	16	4.2	3.8
bromoform	67	1.3	<b>52</b>
alcohols			
methanol	5.3	0.42	13
ethanol	11	0.40	28
1-propanol	13	0.47	28
1-butanol	14	0.50	29

a Units for permeability are cm<sup>3</sup>(STP)•cm/[s•cm<sup>2</sup>•cmHg]
 b Units for diffusivity are cm<sup>2</sup>/s
 c Units for solubility are cm<sup>3</sup>(STP)/[cm<sup>3</sup> polymer•cmHg].

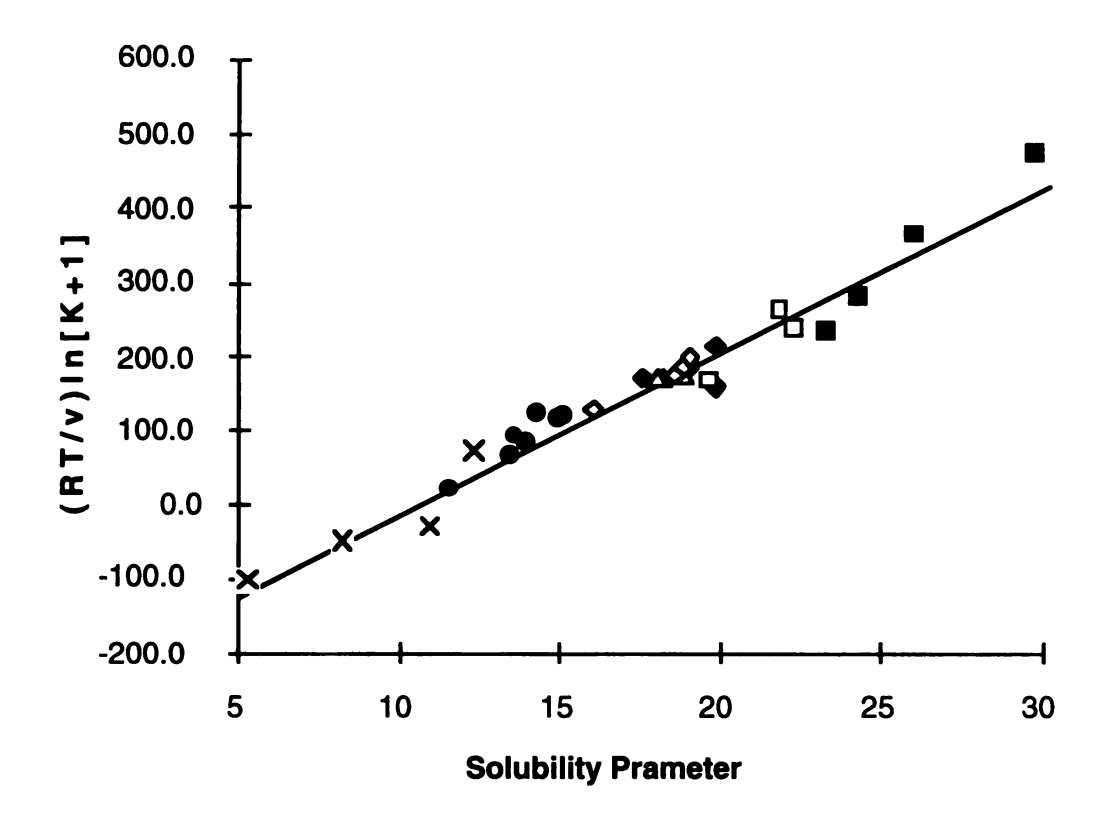
alcohols, and aromatic hydrocarbons. As shown in Table 3.1, the molar volumes of these substances vary from 32.4 to 147.4 cm<sup>3</sup>/mole and the solubility parameters vary from 5.3 to  $29.7 \, (J/cm^3)^{1/2} \, (2, 10, 10)^{1/2} \, (2, 10)^{$ 28). The values for the membrane separation parameters, Pi, Dis, and S<sub>i</sub> measured for these substances are summarized in Table 3.2. These data illustrate that permselectivity for these substances in the silicone elastomer membrane is determined predominantly by the relative solubilities. The solubilities vary by as much as four orders of magnitude whereas the diffusivities for most of the substances vary by less than a factor of ten. However, a comparison between the diffusivities of the alcohols and those of the alkanes illustrates the influence of the silica filler on the rate of mass transport. The diffusivities for the alcohols are very low and exhibit no apparent dependence upon molar volume. It is clear that retention by the highly polar silica filler must be considered to enhance the predictive value of the model.

#### Distribution selectivity

The constant  $\alpha$  and the solubility parameter for the membrane stationary phase,  $\delta_s$ , from Equation 3.16 were calculated simultaneously. Rearrangement of Equation 3.16 yields the following relation:

$$[RT/v_i][ln(K_i) + 1] = 2 \cdot [\delta_s - \alpha] \cdot \delta_i + [\alpha^2 - \delta_s^2]$$
(3.37)

The plot of  $[RT/v_i][ln(K_i) + 1]$  vs.  $\delta_i$  in Figure 3.3 yields a straight line with a slope of  $2 \cdot [\delta_s - \alpha] = 21.8$  and y-intercept of  $[\alpha^2 - \delta_s^2] = -223$ .



#### Key:

X = gases
dark circles = alkanes
circles = aromatics
dark diamonds = chloromethanes
diamonds = chloroethenes
triangles = bromomethanes
dark squares = alcohols.

Figure 3.3. Correlation between distribution ratio and solubility parameter for substances in a silicone elastomer membrane at 25 °C.

By simultaneous solution of these equations, experimental values are obtained for  $\alpha = 4.8 \, (J/cm^3)^{1/2}$  and  $\delta_s = 15.7 \, (J/cm^3)^{1/2}$ . The solubility parameter reported in the literature for poly(dimethylsiloxane) is  $14.9 \, (J/cm^3)^{1/2}$  (29). The value for the filled silicone membrane is expected to be higher due to the polar nature of the silica filler, whose estimated solubility parameter is 32.2  $(J/cm^3)^{1/2}$  (30). The solubility parameter for a mixture is estimated from the contributions of the individual components according to Equation 3.9 (8). When the solubility parameter values and the volume fractions ( $\Phi_p = 0.75$ ,  $\Phi_f = 0.25$ ) for the polymer and filler are substituted into Equation 3.9, the calculated solubility parameter for the stationary phase is  $19.2 \, (J/cm^3)^{1/2}$ . The discrepancy between this calculated value and the experimental value of 15.7 (J/cm<sup>3</sup>)<sup>1/2</sup> suggests that the filled membrane does not exhibit the mass transport properties that would be expected for a homogeneous mixture of the individual phases. In addition, the filler is impermeable so that sorption occurs only in the volume associated with the polymer/filler interfacial layer. Since the volume of this interfacial layer is difficult to define, the experimentally determined value for  $\delta_{\text{S}}$  will be used in the present model.

The experimental values for the distribution ratios and the theoretical values calculated from Equation 3.16 are given in Table 3.3. The distribution selectivities,  $K_i/K_j$ , with respect to methane and to methanol were determined experimentally and were calculated using the model described by Equation 3.17. These values are presented in Table 3.4.

Table 3.3. Experimental and theoretical distribution ratios for substances in a silicone elastomer membrane, at 25 °C.

	distribution ratio		
compound	exp.	theor.	
gases			
nitrogen	0.10	0.090	
oxygen	0.19	0.20	
argon	0.19	0.51	
carbon dioxide	1.9	0.99	
alkanes			
methane	0.60	0.68	
ethane	2.3	2.7	
propane	9.7	3.1	
butane	12	9.5	
pentane	120	23	
hexane	190	80	
heptane	530	200	
aromatic hydrocarbons			
benzene	210	310	
toluene	580	650	
ethylbenzene	1900	1600	
chloromethanes			
chloromethane	13	39	
dichloromethane	93	79	
chloroform	180	180	
carbon tetrachloride	320	200	
chloroethenes			
chloroethene	13	12	
1,1-dichloroethene	100	120	
trichloroethene	370	330	
tetrachloroethene	1400	880	
bromomethanes	1.0		
bromomethane	16	37	
dibromomethane	290	550	
bromoform	3900	2700	
alcohols	0=0	222	
methanol	950	390	
ethanol	2100	1200	
l-propanol	2100	4000	
1-butanol	2200	13000	

Table 3.4. Experimental and theoretical distribution selectivities for substances relative to methane and to methanol in a silicone elastomer membrane at 25 °C.

	distribution selectivity			
	relative to m	ethane	relative to m	ethanol
compound	exp.	theor.	exp.	theor.
gases			_	
nitrogen	0.17	0.13	1.1X10 <sup>-4</sup>	2.3X10 <sup>-4</sup>
oxygen	0.31	0.30	2.0X10 <sup>-4</sup>	5.2X10 <sup>-4</sup>
argon	0.31	0.75	2.0X10 <sup>-4</sup>	1.3X10 <sup>-3</sup>
carbon dioxide	3.2	1.5	2.0X10 <sup>-3</sup>	2.5X10 <sup>-3</sup>
alkanes				_
methane	1.0	1.0	6.3X10 <sup>-4</sup>	1.8X10 <sup>-3</sup>
ethane	3.8	4.0	2.4X10 <sup>-3</sup>	$7.0X10^{-3}$
propane	16	4.5	0.010	8.0X10 <sup>-3</sup>
butane	20	14	0.013	0.025
pentane	190	34	0.12	0.059
hexane	320	120	0.20	0.21
heptane	880	290	0.56	0.51
aromatic hydrocarbon	S			
benzene	350	450	0.22	0.79
toluene	950	950	0.60	1.7
ethylbenzene	3100	2400	2.0	4.2
chloromethanes				
chloromethane	21	57	0.014	0.099
dichloromethane	150	120	0.10	0.20
chloroform	310	270	0.19	0.47
carbon tetrachloride	530	290	0.33	0.50
chloroethenes				
chloroethene	22	17	0.014	0.030
1,1-dichloroethene	170	180	0.11	0.31
trichloroethene	610	480	0.38	0.83
tetrachloroethene	2400	1300	1.5	2.3
bromomethanes				
bromomethane	26	54	0.017	0.095
dibromomethane	480	800	0.30	1.4
bromoform	6500	3900	4.1	6.9
alcohols				
methanol	1600	570	1.0	1.0
ethanol	3500	1800	2.2	3.1
l-propanol	3500	5900	2.2	10
1-butanol	3600	20000	2.3	34

The correlation between the experimental and theoretical values appears quite reasonable for most of the substances. Whereas the distribution ratios vary over a range greater than four orders of magnitude, the difference between the experimental and theoretical values is typically within a factor of two or three. With few exceptions, the selectivity data show similarly good correlations. The most significant discrepancy is seen for 1-butanol, where the theoretical distribution selectivity is a factor of six greater than the experimental value. The experimental selectivities for the alcohols are quite similar, as are the solubility parameters (Table 3.1). Conversely, the theoretical selectivities for the alcohols more closely follow the molar volume than they do the solubility parameter. The theoretical selectivities are consistent with the experimental selectivities for the other classes of substances studied. These data suggest that the -OH group dominates the sorption process for the alcohols.

### Diffusion selectivity

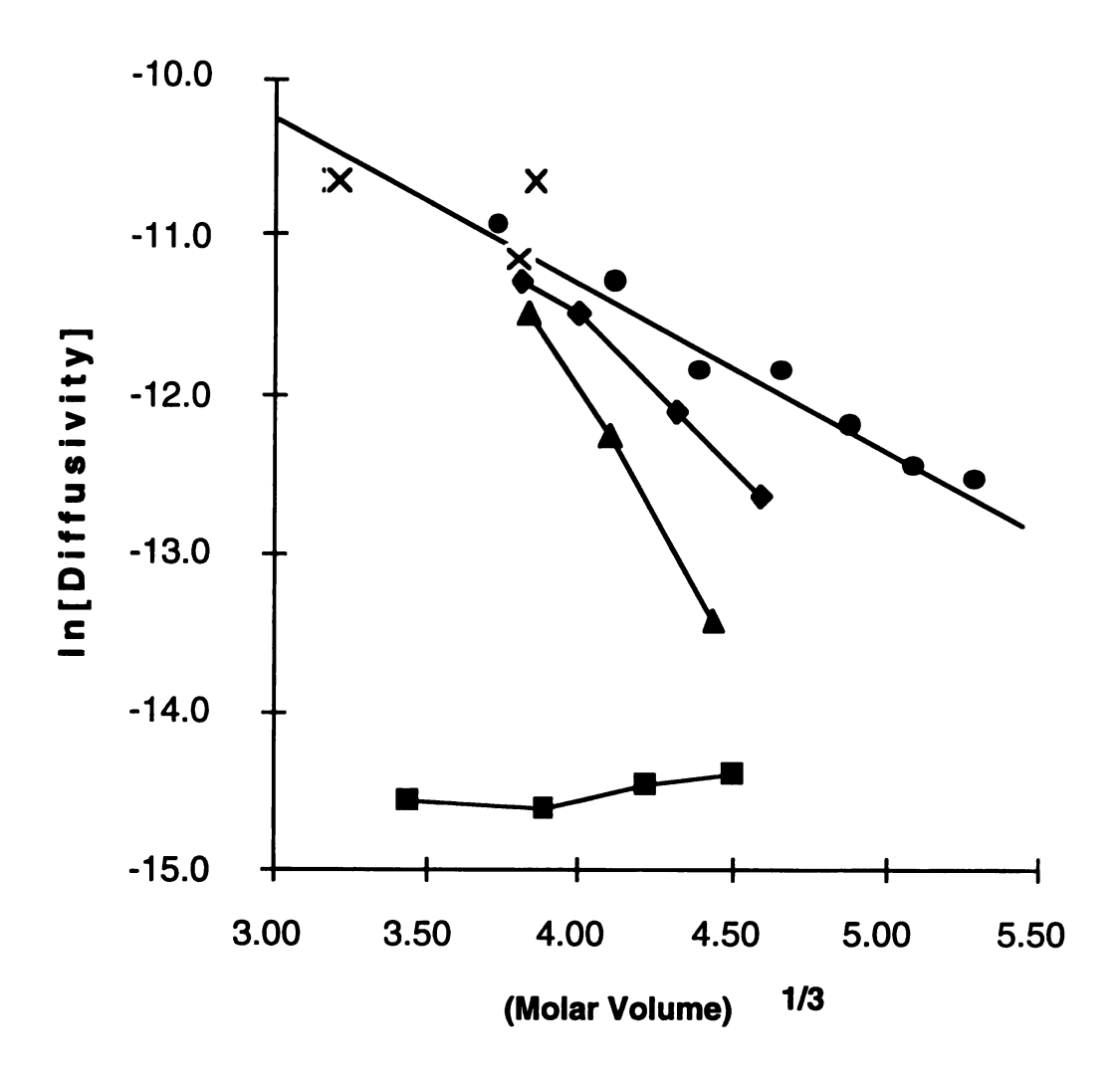
If no adsorption on the filler occurs, the diffusivity of a molecule in a given membrane is dependent upon the size of the molecule and is independent of chemical properties (Equation 3.20). With correction for tortuosity (Equation 3.25), a plot of  $\ln[(1 + \Phi_f/2) \cdot (D_{i,s})]$  vs.  $v_i^{1/3}$  is shown in Figure 3.4 for substances in the filled membrane. Although all substances within a given class exhibit a linear relationship, a single line is not observed for all classes as predicted theoretically.

The presence of two distinct phases in the membrane, a non-polar polymer phase and a polar silica phase, results in a marked decrease in diffusive flow for the substances with greater hydrogen-bonding character. As the functional groups exhibit greater hydrogen bonding (i.e. -OH > -Br > -Cl > -CH<sub>3</sub>), the behavior deviates further from a simple correlation with molar volume. These deviations are predicted by Equation 3.27. In the most extreme case, the diffusivities of the alcohols show no correlation with molar volume, which suggests that only the partial molar volume of the -OH group is involved in retention on the silica filler. For clarity, the aromatic hydrocarbons and chloroethenes are not shown in this plot. The diffusivity behavior of the aromatic hydrocarbons closely follows that of the alkanes and the chloroethenes exhibit transport properties very similar to the chloromethanes.

If the alkanes are assumed to diffuse through the membrane without retention by the silica ( $k'_i = 0$ ), then the slope of the regression line in Figure 3.4 gives the value for the polymer-dependent term,  $\vartheta$ , in Equation 3.27, while the pre-exponential term,  $D_{o,p}$ , is found from the intercept (not shown). This plot suggests that diffusion in the polymer is described by:

$$D_{i,p} = 8.25X10^{-4} \exp[-1.06 \cdot v_i^{1/3}]$$
 (3.38)

In the diffusion-retention (D-k) model of Equation 3.27 for diffusivity in the filled elastomer, both the physical and chemical properties of the system are considered. To predict diffusivities in



## Key:

X = gases dark circles = alkanes dark diamonds = chloromethanes triangles = bromomethanes dark squares = alcohols.

Figure 3.4. Correlation between diffusivity, corrected for tortuosity, and the molar volume for substances in a silicone elastomer membrane at 25 °C.

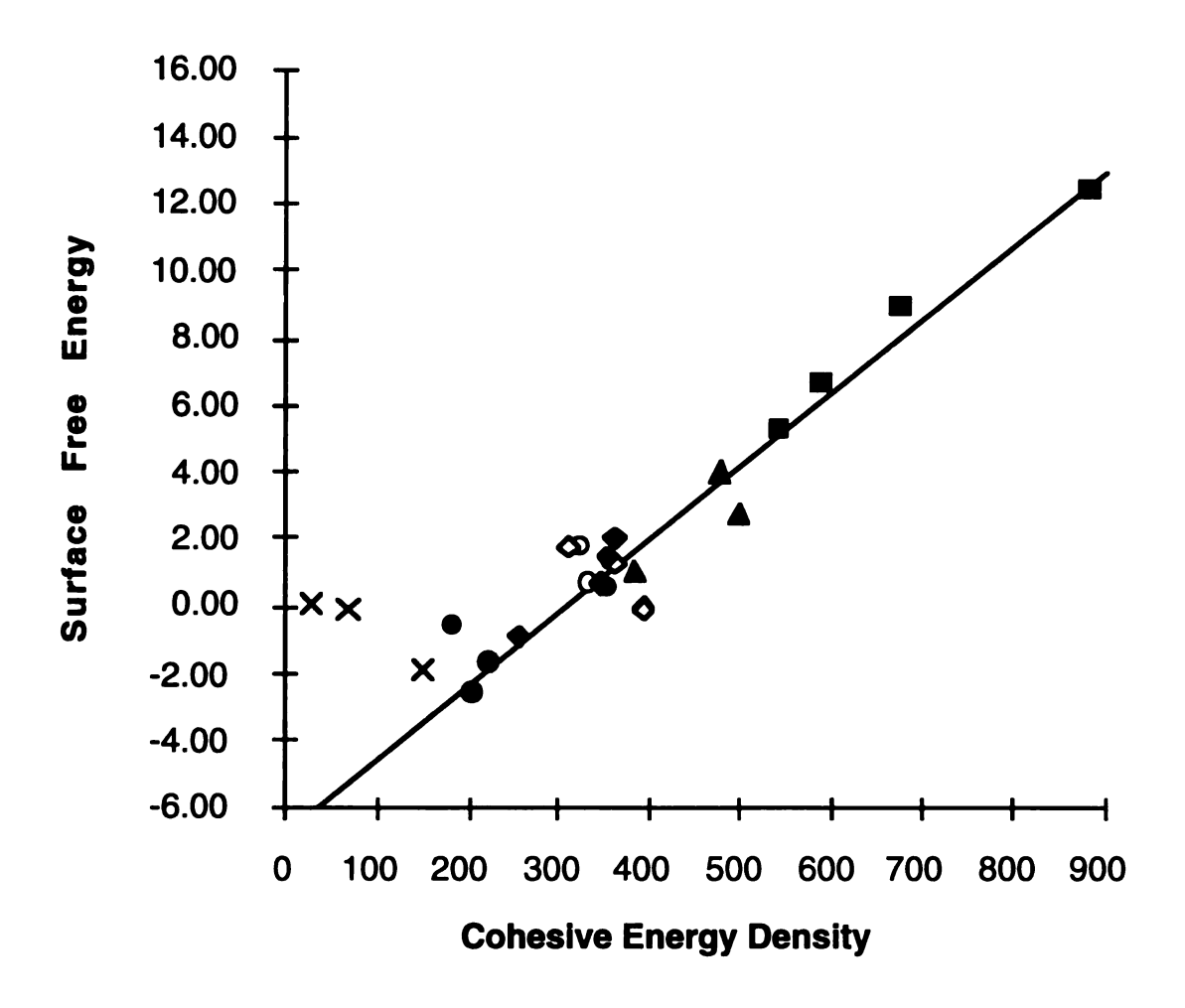
the filled elastomer, it is necessary to estimate  $k_i$  by means of either Equation 3.34 or 3.35. In the model described by Equation 3.34, the proportionality constants A and B were determined from a plot of the surface free energy,  $[RT/(N^{1/3} \bullet v_i^{2/3})] \bullet [ln(k_i) - ln(V_f/V_p)]$  vs. the cohesive energy density,  $\delta_i^2$ , where the actual filler to polymer volume ratio,  $V_f/V_p = 0.33$ , was used. From this plot, shown in Figure 3.5, it was determined that A = 1.84 and B = -569 when the Avogadro's number term,  $N^{1/3}$ , is incorporated into these parameters. The solution for the molar adsorption coefficient now becomes

$$\ln(\mathbf{k}'_{i}) = -1.10 + [v_{i}^{2/3}/(RT)] \cdot [1.84 \cdot \delta_{i}^{2} - 569]$$
(3.39)

The model described by Equation 3.35 requires knowledge of the partial molar volumes of the surface-active functional groups,  $v_i$ . These partial molar volumes have been defined by Fedors (31) and are given in Table 3.5.

Table 3.5. Partial molar volumes,  $v_i$ , for surface-active functional groups from Reference 31.

functional group	<u>molar volume, cm<sup>3</sup>/mole</u>
Cl	24.0
Cl(disubstituted)	26.0
Cl(trisubstituted)	27.3
Br	30.0
Br(disubstituted)	31.0
Br(trisubstituted)	32.4
ОН	10.0



# Key:

X = gases
dark circles = alkanes
circles = aromatics
dark diamonds = chloromethanes
diamonds = chloroethenes
triangles = bromomethanes
dark squares = alcohols.

Figure 3.5. Correlation between surface free energy,  $[RT/(N^{1/3} \circ \vee_i^{2/3})] \circ [ln(k'_i) - ln(V_f/V_p)]$ , and cohesive energy density,  $\delta_i^2$ , for substances in a silicone elastomer membrane, at 25 °C. The line is fitted to the halogenated compound and alcohol data only.

Partial molar volumes were not used for the gases, alkanes, and aromatic compounds, since no significant orientation effects are predicted for these substances. For these substances, it was assumed that  $\nu'_1 = \nu_i$ . As noted previously, a value for the active volume ratio,  $V'_f/V_p$ , was not known. By comparing the experimental values for  $\ln(k'_i)$  and the theoretical values for  $\ln(K'_i)$  for the series of alcohols, the active volume ratio was estimated. Values for  $\ln(k'_i)$  were determined from Equation 3.24 using experimental diffusivities and Equation 3.36 where

$$\ln(\mathbf{k'_i}) = \ln[\{(8.25\times10^{-4}/D_{i,s}) \cdot \exp(-1.06 \cdot v^{1/3})\} - 1]$$
 (3.40)

Theoretical values for ln(K'<sub>i</sub>) were determined from Equation 3.35 where

$$\begin{split} \ln(\mathbf{k'}_i) &- \ln(V'_f/V_p) = \ln(K'_i) = [v_i/(RT)] \bullet [\delta_i - 14.9]^2 \\ &- [v'_i/(RT)] \bullet [\delta_i - 32.2]^2 \end{split} \tag{3.41}$$

These results are summarized in Table 3.6.

Table 3.6. Data for determining the active volume ratio,  $V_f/V_p$ , in a silicone elastomer membrane at 25 °C.

	ln(k' <sub>i</sub> )	ln(K' <sub>i</sub> )	$ln(V_f/V_p) =$
compound	Eqn. 3.39	<u>Eqn. 3.41</u>	$ln(k'_i/K'_i)$
methanol	3.92	3.57	0.35
ethanol	3.49	2.75	0.74
1-propanol	2.94	2.43	0.51
1-butanol	2.56	2.29	0.27

The mean value for the active volume ratio is 1.6, which is approximately five times greater than the total volume ratio,  $V_f/V_p = 0.33$ . This result is consistent with the expectation that the active filler surface area or interfacial volume is expected to be greater than the actual volume of the filler.

For the silica-filled elastomer, the solution to the D-k model using the surface areas of sorbed substances is given by

$$D_{i,s} = 8.25X10^{-4} \cdot \exp[-1.06 \cdot v_i^{1/3}]/[1 + 0.33 \cdot \exp\{[v_i^{2/3}/(RT)] \cdot [1.84 \cdot \delta_i^2 - 569]\}$$
(3.42)

The solution using the partial molar volumes of the surface-active functional groups is given by

$$\begin{split} D_{i,s} &= 8.25 \times 10^{-4} \cdot \exp[-1.06 \cdot v_i^{1/3}] / [1 \\ &+ 1.6 \cdot \exp\{[v_i/(RT)] \cdot [\delta_i - 14.9]^2 \\ &- [v_i'/(RT)] \cdot [\delta_i - 32.2]^2\}] \end{split} \tag{3.43}$$

Both of these solutions were applied to the substances studied. The results are given in Table 3.7 along with experimental diffusivities and theoretical values calculated from Equation 3.38 for non-retained transport. The D-k models (Equation 3.42 and Equation 3.43) generally exhibit a better correlation with the experimental values than does the non-retained transport model. Both D-k models successfully predict little retention on the filler by the alkanes but widely varying degrees of retention for the other organic compounds.

Table 3.7. Experimental and theoretical diffusivities for substances in a silicone elastomer membrane at 25  $^{\circ}$ C.

	diffusivity, $X10^{-6}$ cm <sup>2</sup> /s			
		theor.		
		Eqn. 3.38	Eqn. 3.42	Eqn. 3.43
<u>compound</u>	exp.	No Retention	D-k Model	D-k Model
gases				
nitrogen	21	<b>2</b> 8	27	28
oxygen	21	<b>2</b> 8	26	27
argon	21	14	13	14
carbon dioxide	13	15	14	15
alkanes				
methane	16	16	15	16
ethane	11	10	9.8	10
propane	6.4	7.8	7.5	7.8
butane	6.3	5.9	5.6	5.9
pentane	4.5	4.7	4.4	4.7
hexane	3.5	3.8	3.5	3.8
heptane	3.2	3.1	2.9	3.1
aromatic hydrocarbon	18			
benzene	4.9	7.2	4.4	7.2
toluene	3.5	5.4	3.6	5.4
ethylbenzene	1.7	4.2	2.9	4.2
chloromethanes				
chloromethane	11	15	8.0	9.0
dichloromethane	7.9	12	6.3	7.5
chloroform	4.9	8.5	5.0	6.0
carbon tetrachloride	2.9	6.3	4.7	5.3
chloroethenes				
chloroethene	9.1	11	9.3	9.6
1,1-dichloroethene	5.8	8.8	5.6	6.4
trichloroethene	3.7	7.1	4.3	5.0
tetrachloroethene	2.4	5.9	3.3	3.9
bromomethanes				
bromomethane	9.1	14	8.1	10
dibromomethane	4.2	11	2.4	3.4
bromoform	1.3	7.5	1.6	2.4
alcohols				
methanol	0.42	22	0.41	0.37
ethanol	0.40	13	0.64	0.52
1-propanol	0.47	9.4	0.64	0.49
1-butanol	0.50	7.0	0.57	0.42

Table 3.8. Experimental and theoretical (D-k model, Equation 3.42) diffusivity selectivities for substances relative to methane and to methanol in a silicone elastomer membrane at 25 °C.

	diffusion selectivity			
	relative to me	ethane	relative to me	ethanol
<u>compound</u>	<u>exp.</u>	theor.	exp.	theor.
gases				
nitrogen	1.3	1.8	50	66
oxygen	1.3	1.8	50	63
argon	1.3	0.90	50	<b>32</b>
carbon dioxide	0.81	0.92	31	33
alkanes				
methane	1.0	1.0	38	36
ethane	0.69	0.65	26	23
propane	0.40	0.50	15	18
butane	0.39	0.38	15	13
pentane	0.28	0.30	11	11
hexane	0.22	0.24	8.4	8.5
heptane	0.20	0.19	7.6	6.9
aromatic hydrocarbons	<b>3</b>			
benzene	0.31	0.24	12	8.6
toluene	0.22	0.22	8.4	7.7
ethylbenzene	0.11	0.18	4.1	6.5
chloromethanes				
chloromethane	0.69	0.38	26	13
dichloromethane	0.49	0.30	19	11
chloroform	0.31	0.26	12	9.5
carbon tetrachloride	0.18	0.29	6.9	10
chloroethenes				
chloroethene	0.57	0.58	22	21
1,1-dichloroethene	0.36	0.31	14	11
trichloroethene	0.23	0.24	8.8	8.4
tetrachloroethene	0.15	0.18	5.7	6.6
bromomethanes				
bromomethane	0.57	0.39	22	14
dibromomethane	0.26	0.10	10	3.6
bromoform	0.081	0.071	3.1	2.5
alcohols				
methanol	0.026	0.028	1.0	1.0
ethanol	0.025	0.032	0.95	1.1
1-propanol	0.029	0.030	1.1	1.1
1-butanol	0.031	0.027	1.2	0.97

The solution to the D-k model given in Equation 3.42 was used to determine the diffusion selectivities (Equation 3.36) relative to methane and to methanol. The experimental and D-k model diffusion selectivities are given in Table 3.8. The results from the D-k model show reasonable correlation to experimental selectivities relative to a non-retained reference (methane) as well as a highly retained reference (methanol).

### Enrichment

The correlations between the experimentally determined enrichment factors,  $\mathcal{E}_{i/j}$ , and the product of the theoretical diffusion and distribution selectivities,  $(D_i/D_j) \cdot (K_i/K_j)$ , are given relative to methane and relative to methanol in Table 3.9. The theoretical distribution selectivities were determined based on Equation 3.17 and the diffusion selectivities were based on the D-k model given by the combination of Equations 3.36 and 3.42. With the notable exceptions of 1-propanol and 1-butanol, reasonable correlation is observed between the experimental and theoretical enrichment factors.

For most of the substances studied, the deviation between the experimental and theoretical values for the distribution selectivities are opposite in direction from the diffusion selectivities.

Consequently, these errors compensate for one another, such that the enrichment factors are accurately predicted. For some substances, however, these deviations are in the same direction so that poorer correlation between the experimental and theoretical enrichment factors is observed.

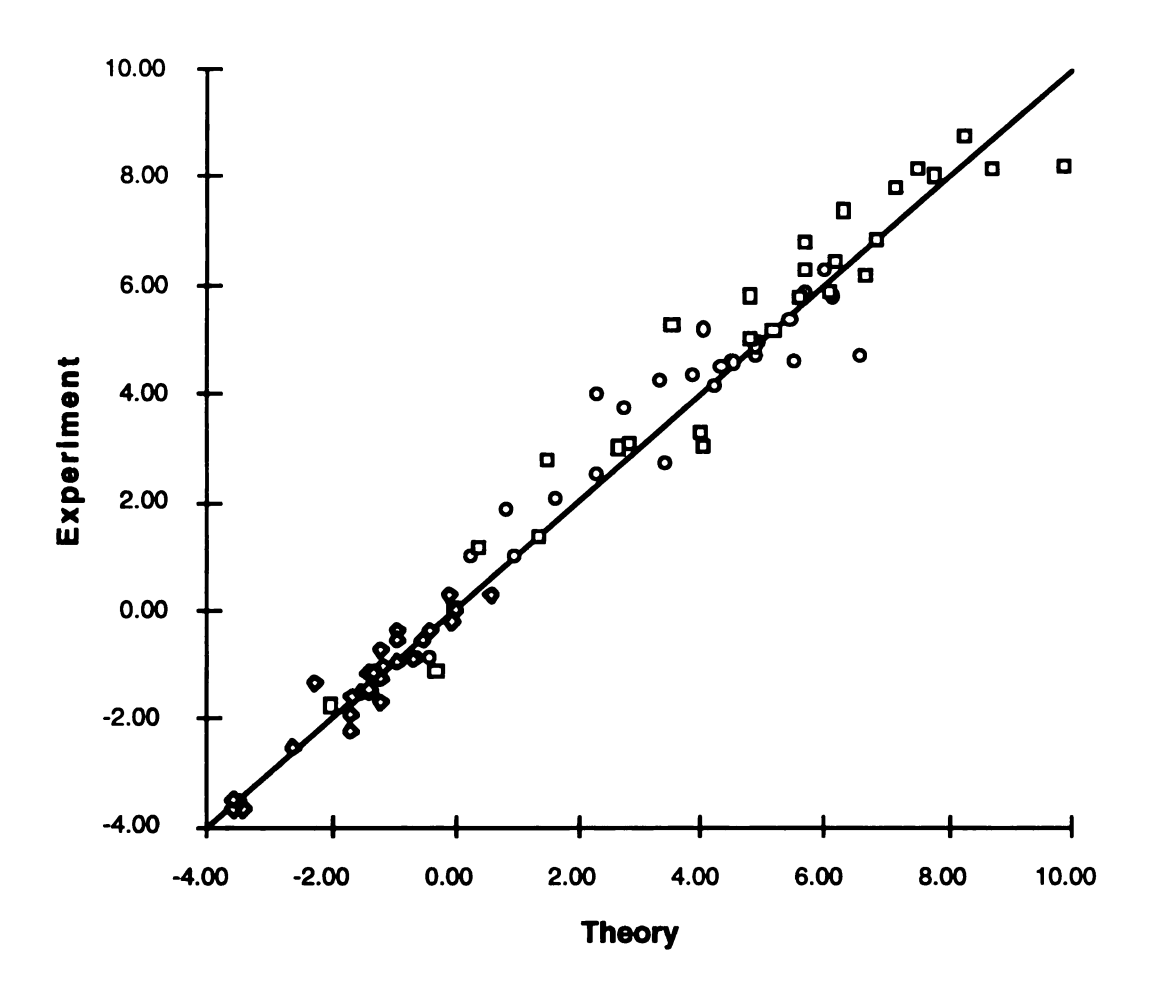
Table 3.9. Enrichment factors for compounds relative to methane and to methanol in a silicone elastomer membrane at 25 °C. Theoretical values were obtained from the product of distribution (Equation 3.16) and diffusion selectivities (D-k model, Equations 3.36 and 3.42).

	enrichment factors			
	relative to methane		relative to me	ethanol
<u>compound</u>	exp.	theor.	<u>exp.</u>	theor.
gases	_		_	
nitrogen	0.22	0.24	5.2X10 <sup>-3</sup>	0.015
oxygen	0.41	0.52	0.010	0.033
argon	0.41	0.67	0.010	0.042
carbon dioxide	2.6	1.3	0.063	0.085
alkanes				
methane	1.0	1.0	0.024	0.063
ethane	2.6	2.6	0.063	0.17
propane	6.4	2.3	0.15	0.14
butane	7.9	5.2	0.19	0.33
pentane	<b>54</b>	10	1.3	0.64
hexane	70	28	1.7	1.8
heptane	180	56	4.2	3.5
aromatic hydrocarbons	}			
benzene	110	130	2.6	8.4
toluene	210	230	5.0	15
ethylbenzene	330	470	7.9	30
chloromethanes				
chloromethane	15	30	0.35	1.9
dichloromethane	76	49	1.8	3.1
chloroform	94	90	2.3	5.7
carbon tetrachloride	95	91	2.3	5.8
chloroethenes				
chloroethene	12	10	0.30	0.66
1,1-dichloroethene	63	67	1.5	4.3
trichloroethene	140	140	3.4	8.7
tetrachloroethene	360	<b>2</b> 90	8.6	18
bromomethanes				
bromomethane	15	30	0.36	1.9
dibromomethane	130	130	3.0	8.1
bromoform	530	410	13	26
alcohols				
methanol	41	16	1.0	1.0
ethanol	87	<b>76</b>	2.1	4.8
1-propanol	100	<b>250</b>	2.5	16
1-butanol	110	740	2.7	47

Error analysis (see Appendix) indicates that the estimated relative standard deviations for the diffusivity and distribution selectivity measurements are 60 % and the relative standard deviation for the enrichment factor measurements are 14 %. In addition, experimental error may result from absorption of a substance into the walls of the sampling bag used to prepare the mobile phase gas mixtures.

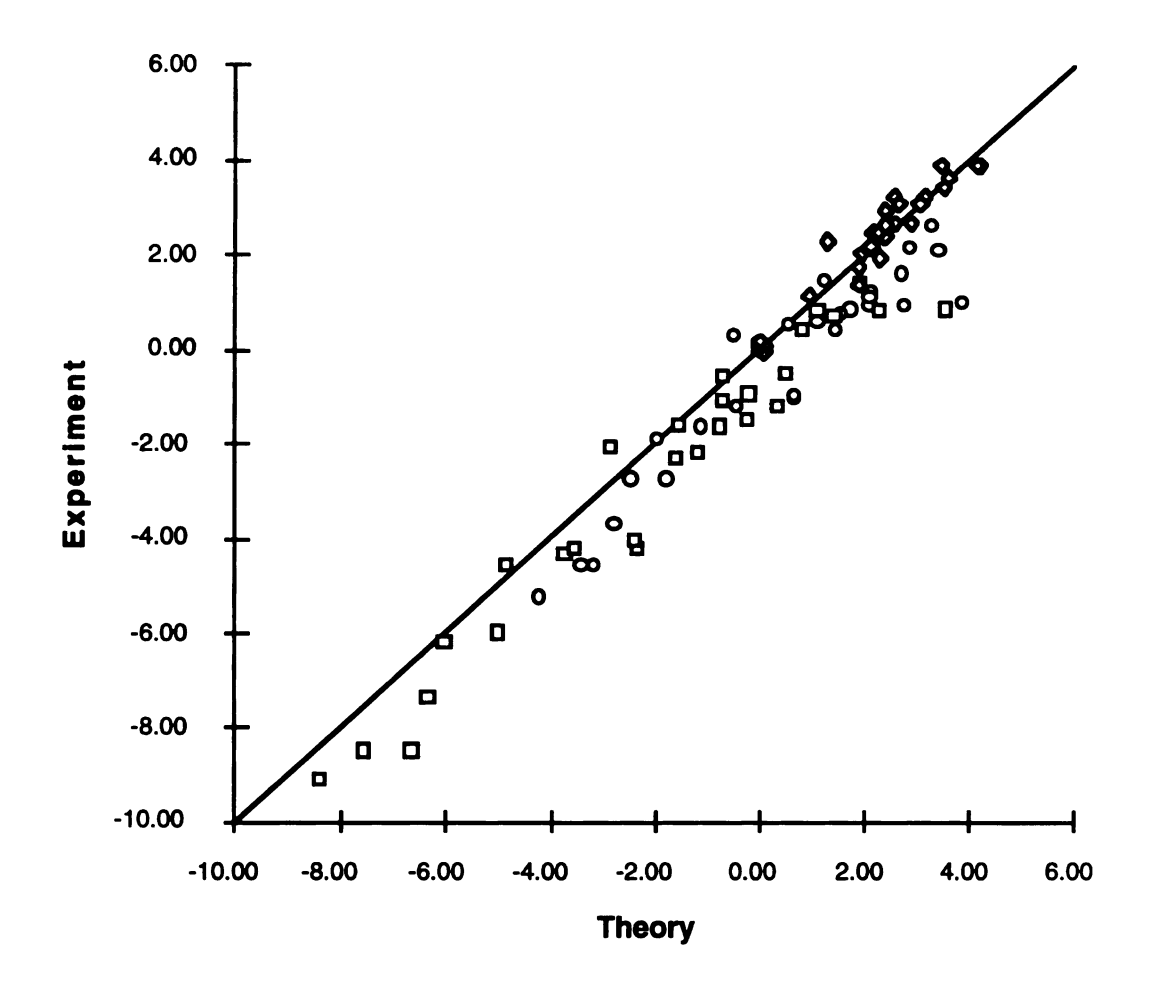
Graphically, the correlation for experimental and theoretical values for the distribution, diffusion, and permeation selectivities relative to methane are shown in Figure 3.6. The same correlation for selectivities relative to methanol are shown in Figure 3.7. These plots demonstrate the predictive capabilities of the model.

Although the predictive ability of the model was quite good, it could be improved by an expanded solubility parameter treatment that takes into account specific chemical interactions between the sorbed substances, the polymer, and the filler. The consistency of the model possibly suffers from the use of molar volumes and solubility parameters that were not all generated by a single researcher. However, the reasonable application of a predictive permeation model using readily available parameters has been demonstrated for a wide variety of substances.



# **Key:** circles = permeation diamonds = distribution ratio squares = diffusivity.

Figure 3.6. Correlation between experimental and theoretical selectivities for substances relative to methane in a silicone elastomer at 25 °C.



# **Key:** circles = permeation diamonds = distribution ratio squares = diffusivity.

Figure 3.7. Correlation between experimental and theoretical selectivities for substances relative to methanol in a silicone elastomer at 25 °C.

### REFERENCES

- (1) C. Hansen and A. Beerbower, Solubility parameters, in: A. Standen (Ed.), <u>Kirk-Othmer Encyclopedia of Chemical Technology</u>, Suppl. Vol. 2nd. Ed.: 1971.
- (2) A. F. M. Barton, Solubility parameters, Chem. Rev. 1975, 75, 731.
- (3) H. Burrell, Solution Properties: Solubility Parameter Values, in: J. Brandrup and E. H. Immergut (Eds.), <u>Polymer Handbook</u>, 2nd ed.; Wiley-Interscience: New York, NY; 1975.
- (4) B. Schneier, J. Appl. Polym. Sci. 1972, 16, 2343.
- (5) A. F. M. Barton, <u>Handbook of Polymer-Liquid Interaction</u> <u>Parameters</u>; CRC Press: Boca Raton, FL; 1990.
- (6) H. W. Starkweather, Jr., Macromolecules 1977, 10, 1161.
- (7) J. H. Hildebrand and R. L. Scott, <u>The Solubility of Nonelectrolytes</u>, 3rd ed.; Reinhold: New York, NY; 1950.
- (8) J. H. Hildebrand, J. M. Prausnitz, and R. L. Scott, <u>Regular and Related Solutions</u>; Van Nostrand-Reinhold: Princeton, NJ; 1970.
- (9) B. L. Karger, L. R. Snyder, and C. Eon, *Anal. Chem.* **1978**, 50, 2126.
- (10) V. Stannett, Simple gases, in: J. Crank and G. S. Park (Eds.), Diffusion in Polymers; Academic Press: New York, NY; 1968.
- (11) H. F. Mark, N. M. Bikales, C. G. Overberger, G. Menges, and J. I. Kroschwitz (Eds.), <u>Encyclopedia of Polymer Science and Engineering</u>, Vol. 3; Wiley-Interscience: New York, NY; 1985.
- (12) J. M. Prausnitz and F. H. Shair, A.I.Ch.E. J. 1961, 7, 682.

- (13) J. C. Giddings, M. N. Myers, L. McLaren, and R. A. Keller, *Science* **1968**, 162, 67.
- (14) W. W. Brandt, J. Phys. Chem., Wash. 1959, 63, 1080.
- (15) K. D. Ziegel, H. K. Frensdorff, and D. E. Blair, *J. Polym. Sci.* **1969**, A-2, 809.
- (16) R. M. Barrer, J. A. Barrie, and N. K. Raman, *Polymer* **1962**, 3, 605.
- (17) R. M. Barrer, J. A. Barrie, and M. G. Rogers, *J. Polym. Sci.* **1963**, A-1, 2565.
- (18) A. S. Michaels and H. J. Bixler, J. Polym. Sci. 1961, 50, 413.
- (19) G. J. van Amerongen, Rubber Chemistry and Technology 1964, 37, 1065.
- (20) S. Wu, J. Phys. Chem. 1968, 72, 3332.
- (21) A. Beerbower, Surface free energy: A new relationship to bulk energies, J. Colloid Interface Sci. 1971, 35, 126.
- (22) L. B. Westover, J. C. Tou, and J. H. Mark, Anal. Chem. 1974, 46, 568.
- (23) Standard test method for C1 through C5 hydrocarbons in the atmosphere by gas chromatography, in: 1990 Annual Book of ASTM Standards: Volume 11.03, ASTM, 1916 Race Street, Philadelphia, PA, 19103-1187.
- (24) J. C. Fjeldsted, presented at the Instrument Society of America International Conference and Exhibition, New Orleans, LA, 1990.

- (25) Analytical Sciences Mass Spectral Data Base, The Dow Chemical Co., Midland, MI, internal communication, based on method by V. Caldecourt, *Anal. Chem.* **1955**, 27, 1670.
- (26) M. A. LaPack, J. C. Tou, and C. G. Enke, *Anal. Chem.* **1990**, 62, 1265.
- (27) M. E. Hodgson, Filtr. and Separ. 1973, July, 418.
- (28) A. F. M. Barton, <u>Handbook of Solubility Parameters and Other Cohesion Parameters</u>; CRC Press: Boca Raton, FL; 1983.
- (29) G. L. Lee, S. A. Stern, J. E. Mark, and E. Hoffman, <u>Investigation of Structure-Sermeability Selationships of Silicone Solymer Sembranes</u>: Final Report October 1982 September 1986, Gas Research Institute, Chicago, IL.
- (30) P. J. Shoenmakers, H. A. H. Billiet, and L. de Galan, *Chromatographia* **1982**, 15, 205.
- (31) R. F. Fedors, Polym. Eng. Sci. 1974, 14, 147.

# **CHAPTER 4**

# A Model for Characterizing and Predicting Membrane Extractions based on Chromatographic Retention

As demonstrated in Chapter 3, the capacity to separate components in a mixture can be predicted utilizing fundamental separation principles. Chromatography is governed by these same fundamental principles and can therefore be a useful tool for characterizing the sorption and transport properties of polymeric materials (1, 2). A membrane extraction model based upon chromatographic principles is developed in this chapter. The effect of chemical properties and experimental conditions on permeability parameters are discussed in the context of this model. Finally, the model provides a quantitatively useful rule of thumb with simple correlations between membrane extraction efficiencies and such readily available data as boiling points and solubility parameters.

### **EXPERIMENTAL METHODS**

# Gas chromatography

The chromatography column was a 15 meter-long, 250 µm-i.d., 1 µm-film thickness DB-1 (poly(dimethylsiloxane) bonded phase) capillary from J&W Scientific, Folsom, CA. The helium or nitrogen

mobile phase linear velocity was 50 cm/s. The column temperature was 25 °C isothermal. Mass analysis of the chromatographic effluent was performed with the first quadrupole of a Finnigan TSQ-70 GC/MS. The scan rate was 0.2 seconds/scan for a 10-300 dalton range. The secondary electron multiplier voltage was -1000 V. The dynode voltage was -2000 V.

### Membrane extraction

A flow-through silicone hollow fiber membrane separator with mass spectrometric detection was used for the measurement of the permeation data. The membrane was a 2.5 cm length of Dow Corning Silastic<sup>™</sup> Medical Grade Tubing (0.0635 cm o.d., 0.0305-cm i.d., 69 % poly(dimethylsiloxane), 31 % silica by weight) mounted in a stainless steel tee (3). The nitrogen mobile phase flow through the hollow fiber membrane was 100 cm³/minute. The membrane temperature was 25 °C isothermal. The permeation measurements were made with the ME device interfaced directly with a Hewlett-Packard 5971-A MSD quadrupole mass spectrometer modified for process analysis applications (4). The scan rate was 0.3 s/scan for a 10-180 dalton range. The electron multiplier voltage was -1500 V.

Reviewing the solution-diffusion model (5), permeation through a membrane may be described by three processes: 1) selective partitioning of a substance between the membrane stationary phase and the mobile phase, 2) selective diffusion of the substance through the membrane phase, and 3) desorption of the substance from the

membrane phase into a sweep fluid or vacuum. The permeation rate,  $F_i$ , for a component, i, is described by Fick's first law:

$$F_i = A \cdot D_{i,s} \cdot K_i \cdot c_{i,m} / d$$
(4.1)

where A is the membrane surface area,  $D_{si}$  is the diffusivity of component i in the stationary (membrane) phase,  $K_i$  is the distribution ratio for component i in equilibrium between the membrane stationary phase and the mobile phase,  $c_{i,m}$  is the concentration of component i in the mobile phase, and d is the membrane thickness. The product  $D_{i,s}K_i$  is the permeability constant,  $P_i$ , for component i in the membrane. Just as with chromatography, the ability of a membrane phase to separate two components from a mobile phase is dependent upon both thermodynamic (distribution ratio) and kinetic (diffusivity) parameters. The analytical power of membranes lies in their ability to provide an enriched analyte stream to the analyzer. The permeation enrichment factor,  $\mathbf{E}_{i/j}$ , for component i over component j is given by the relative permeation rates of the two components normalized with respect to their concentrations in the sample

$$\mathcal{E}_{i/j} = [F_i/F_j]/[c_{i,m}/c_{j,m}] = [D_{i,s}/D_{j,s}] \cdot [K_i/K_j] = P_i/P_j \tag{4.2}$$

The method for determining membrane permeation parameters such as distribution ratios and diffusivities is described in detail in the Appendix of this work. In this chapter, the two selective processes (distribution and diffusion) are discussed separately and then their implications to the extraction process are presented.

## **RETENTION AND DISTRIBUTION**

The difference in the ability of two different phases to solvate a substance is a major driving force for many membrane and chromatographic separation processes. These solvation processes have been shown to exhibit a fundamental relationship that may be described by regular solution theory, as modified by Flory-Huggins (6-8). Hildebrand et. al. (9) have proposed that the solubility of a gas in a liquid solvent can be described as a two-step process involving first the compression of the gas into some hypothetical liquid state followed by sorption of this hypothetical liquid into the solvent. The extension of this model to gases dissolving in a polymer, with Flory-Huggins correction, has been given in Chapter 3 as follows:

$$\ln[K_i] = [v_i/RT] \cdot [(\delta_i - \alpha)^2 - (\delta_i - \delta_s)^2] - 1$$
 (4.3)

Where  $K_i$  is the concentration distribution ratio  $(c_{i,s}/c_{i,m})$ ,  $v_i$  is the molar volume of the partitioning substance i, R is the ideal gas constant, T is the absolute temperature,  $\delta_i$  and  $\delta_s$  are the solubility parameters for the partitioning compound i and the stationary phase, respectively, and  $\alpha$  is an experimentally determined constant that corrects for non-ideal behavior and approximates the solubility parameter of the hypothetical compressed mobile phase. Values for molar volumes, solubility parameters (7, 8, 10), and boiling point temperatures (11) used in these studies are presented in Table 4.1.

Table 4.1. Molar volumes, Hildebrand solubility parameters (7, 8, 10), and boiling points (11) for the compounds used in this study.

compound	<u>v<sub>i</sub>, cm<sup>3</sup>/mole</u>	$\delta_i$ , (MPa) <sup>1/2</sup>	<u>T<sub>b</sub>, K</u>
nitrogen	32.4	5.3	77.4
oxygen	33.0	8.2	90.2
argon	57.1	10.9	87.5
carbon dioxide	55.0	12.3	194.7
methane	<b>52.0</b>	11.6	109.2
ethene	65.0	13.5	169.5
ethane	70.0	13.5	184.6
propane	89.4	13.4	231.1
butane	101.4	13.9	272.7
pentane	116.2	14.3	309.3
hexane	131.6	14.9	342.2
heptane	147.4	15.1	371.6
benzene	89.4	18.8	353.3
toluene	106.8	18.2	383.8
ethylbenzene	123.1	18.0	409.4
chlorobenzene	102.1	19.4	405.2
chloromethane	55.4	19.8	249.0
dichloromethane	63.9	19.8	313.3
chloroform	80.7	19.0	334.9
carbon tetrachloride	97.1	17.6	349.7
chloroethene	68.1	16.0	<b>259.8</b>
1,1-dichloroethene	79.0	18.6	310.2
trichloroethene	90.2	18.8	360.2
tetrachloroethene	101.1	19.0	394.2
bromomethane	56.1	19.6	276.8
dibromomethane	68.9	22.3	370.2
bromoform	87.5	21.8	422.7
water	18.0	47.9	373.2
methanol	40.7	29.7	338.1
ethanol	58.5	26.0	351.7
1-propanol	75.2	24.3	370.6
2-propanol	76.8	23.3	355.6
1-butanol	91.5	23.3	390.4
acetone	74.0	20.3	329.4
2-butanone	90.1	19.0	352.8

For identical mobile and stationary phases, the chromatographically determined distribution ratio for an analyte will be the same as that determined from permeation measurements. The equilibrium distribution of a substance between the stationary and mobile phases may be determined from chromatographic retention times and the phase ratio using the following relation:

$$K_i = k_i \cdot \beta = [(t_{ri} - t_o)/t_o] \cdot [V_m/V_s]$$

$$(4.4)$$

where  $k_i$  is the molar partition coefficient,  $t_{ri}$  is the elution time for a retained component i, to is the elution time for a non-retained component, and  $\beta$  is the volumetric phase ratio.

The distribution ratios for several substances obtained from GC and ME measurements are given in Table 4.2. The distribution ratio for the permanent gases is so low that their retention in the chromatographic stationary phase is essentially zero. The time observed for the elution of the air peak (N<sub>2</sub>, O<sub>2</sub>, Ar, and CO<sub>2</sub> are not separated) is taken to be to. In practice, nitrogen carrier gas is more representative of the air sample matrix that is reported in most ME applications, while helium is a more common carrier gas since its lower density allows for higher linear velocities (12). As demonstrated in Table 4.2, no significant differences are observed in the GC retention time data when the two different carrier gases are used.

The ME data described below were obtained with nitrogen carrier gas while the GC data were obtained with helium carrier gas.

Table 4.2. Experimental distribution ratios,  $K_i$ , determined by ME and GC at 25  $^{\circ}$ C.

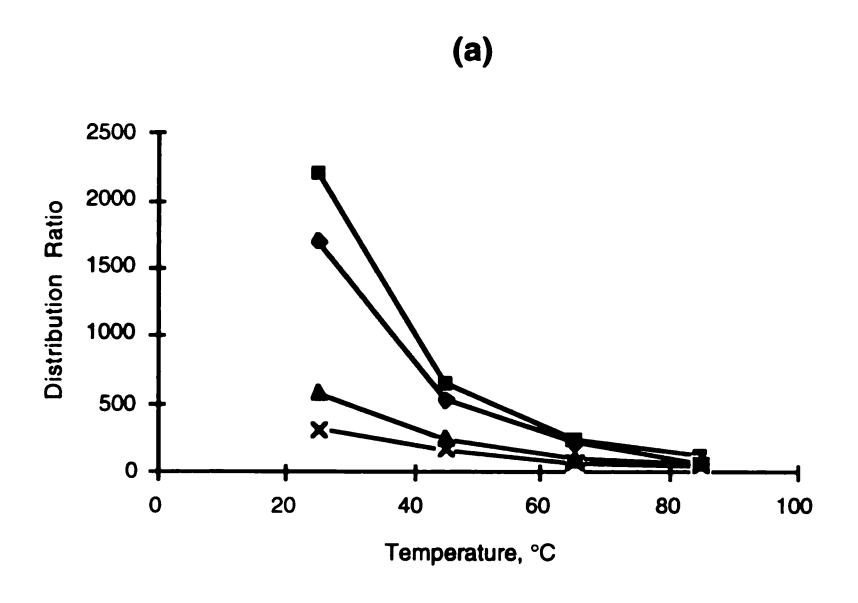
	ME with N <sub>2</sub>	GC with He	GC with N <sub>2</sub>
<u>compound</u>	mobile phase	mobile phase	mobile phase
nitrogen	0.10	0.0	0.0
oxygen	0.19	0.0	0.0
argon	0.19	0.0	0.0
carbon dioxide	1.9	0.0	0.0
methane	0.60	0.0	-
ethene	2.2	3.1	-
ethane	2.3	3.1	-
propane	9.7	6.2	-
butane	12	21	-
pentane	120	67	64
hexane	190	190	180
heptane	530	530	490
benzene	210	310	290
toluene	580	870	820
ethylbenzene	1900	2200	2000
chlorobenzene	1600	1800	1700
chloromethane	13	12	-
dichloromethane	93	81	77
chloroform	180	190	180
carbon tetrachloride	320	330	300
chloroethene	13	19	-
1,1-dichloroethene	100	76	73
trichloroethene	370	450	420
tetrachloroethene	1400	1300	1200
bromomethane	16	28	-
dibromomethane	290	410	380
bromoform	3900	2200	2100
water	340	9.3	-
methanol	950	15	23
ethanol	2100	37	41
1-propanol	2100	110	120
2-propanol	834	56	59
1-butanol	2200	310	330
acetone	1000	49	50
2-butanone	1500	140	150

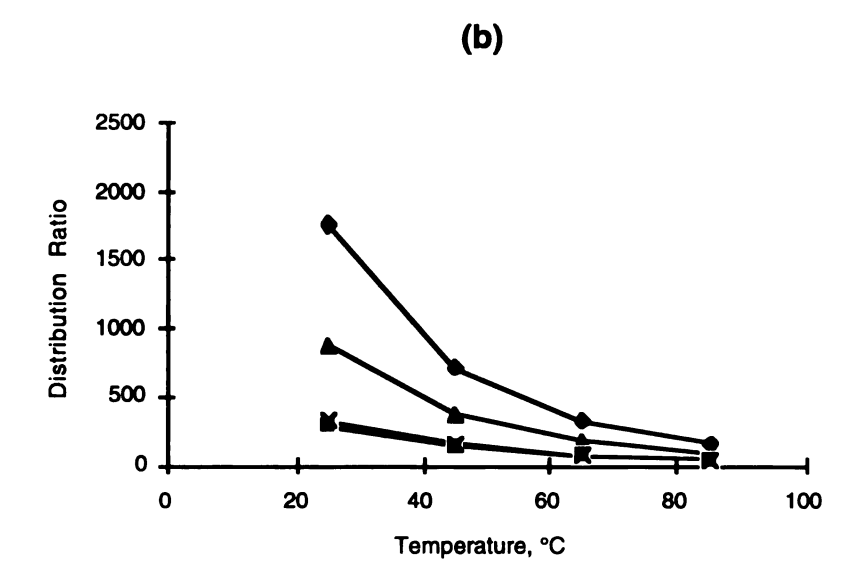
Within experimental error, most of the compounds that exhibit weak or no hydrogen bonding show good agreement for the two techniques. The effect of the silica particles dispersed in the membrane is apparent when comparing the distribution ratios obtained by the two techniques for the strong hydrogen bonding substances. The silica provides a hydrogen-bonding component to the membrane, resulting in a much higher affinity for compounds that exhibit hydrogen bonding than does the otherwise non polar silicone phase.

Just as with chromatographic systems, the capacity of the membrane to perform thermodynamic separations decreases as the temperature of the system increases. This effect is shown in Figure 4.1 in the plot of  $K_i$  vs. T for various components. Due to the presence of the silica in the membrane, a dramatic difference in the position of the curves for 1-butanol is seen when comparing the ME data (Figure 4.1a) with the GC data (Figure 4.1b). Since they exhibit little affinity for the silica, the non polar compounds in these plots demonstrate nearly identical behavior between the two systems. The temperature dependence of the distribution ratio illustrated in these plots is given by the following relation:

$$\partial(\ln[K_i])/\partial(1/T) = -\Delta H_{Si}/R \tag{4.5}$$

where  $\Delta H_{Si}$  is the difference in enthalpy of solution for the substance in the stationary phase and the mobile phase ( $\Delta H_{Si} = H_{Si}$ (stationary phase) -  $H_{Si}$ (mobile phase)). Values for  $\Delta H_{Si}$  were obtained from the slope of a plot of  $\ln[K_i]$  vs. 1/T for selected compounds and are





# Key:

X = carbon tetrachloride square = 1-butanol diamond = chlorobenzene triangle = toluene.

Figure 4.1. The effect of temperature on the stationary phase/mobile phase distribution ratio,  $K_i$ , obtained by ME (a) and by GC (b).

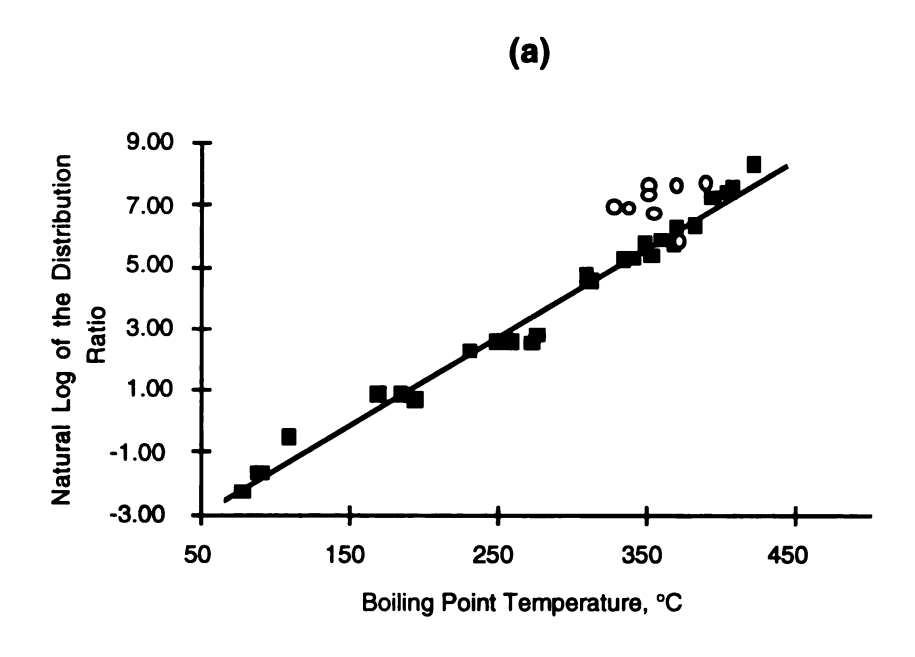
presented in Table 4.3. Generally,  $\Delta H_{si}$  values for gas-phase organic compounds are negative, and the magnitude of  $\Delta H_{si}$  indicates the ability of the silicone stationary phase to extract the compound from the mobile phase. Deviations in these  $\Delta H_{si}$  determinations may result from interactions between the compounds and the silica filler as well as imprecision in chromatographic elution time and permeation measurements.

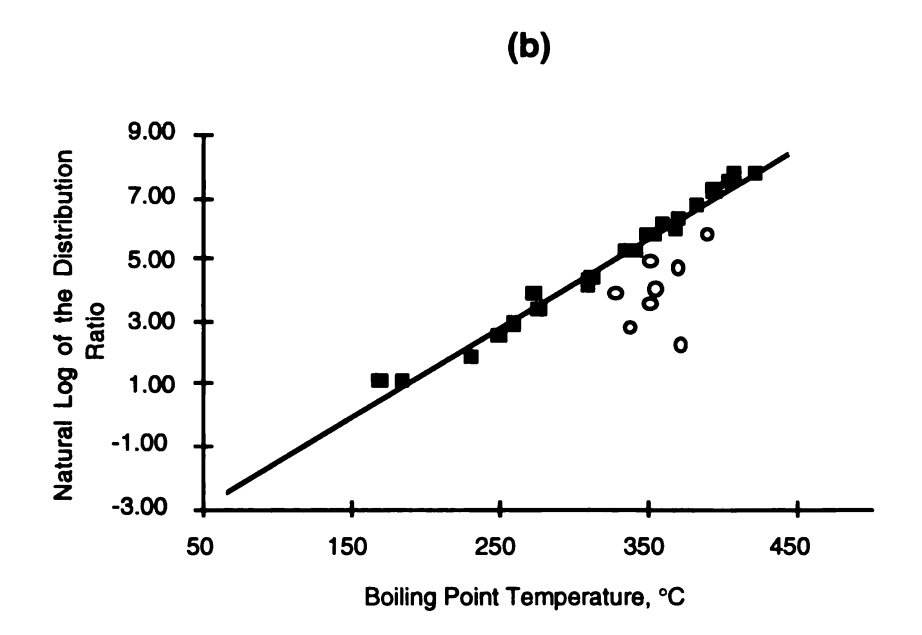
Table 4.3. Values for the heats of solution for selected compounds in the membrane and chromatographic stationary phases.

	H <sub>Si</sub> (kJ/mole)			
compound	<u>ME</u>	<u>GC</u>		
nitrogen	-8			
heptane	-27	-33		
toluene	-34	-34		
chlorobenzene	-48	-36		
carbon tetrachloride	-31	-29		
1-butanol	-46	-31		

By the Hildebrand rule (6), a strong correlation exists between the solubility parameter and the boiling point,  $T_{bi}$ , for a substance. Thus, a correlation also exists between  $ln[K_i]$  and  $T_{bi}$  where, for a homologous series of compounds, the correlation may be given by (13)

$$ln[K_i] = m \cdot T_{bi} + b \tag{4.6}$$





**Key:** square = weak or non-hydrogen bonding compound circle = strong hydrogen bonding compound.

Figure 4.2. The correlation of the distribution ratio,  $K_i$ , with boiling point,  $T_{\rm bi}$ , at 25 °C, obtained by ME (a) and by GC (b).

where M is the slope and B is the y-axis intercept for the plot of  $ln[K_i]$ vs. T<sub>bi</sub>. A plot of ln[K<sub>i</sub>] vs. T<sub>bi</sub> is given for the ME and GC data in Figure 4.2. The compounds that exhibit strong hydrogen bonding are seen to deviate significantly from the straight line plot resulting from linear regression of data for the compounds that exhibit weak or no hydrogen bonding. For the silicone membrane at 25 °C, this linear regression yields values for the slope, where  $m = 2.85 \times 10^{-2}$ , and for the y-intercept, where b = -4.38. For the lowest boiling point compounds, distribution ratios could not be determined by gas chromatography because no retention was observed. However, even with fewer data points, the chromatographic experiments yielded a nearly identical line with a slope  $m = 2.87X10^{-2}$  and the intercept b =-4.37. Most of the strong hydrogen bonding compounds exhibit ln[K<sub>i</sub>] values that are higher than predicted by the straight line plot for the ME experiments (Figure 4.2a). This result is consistent with the affinity of these compounds for the silica in the membrane. In the case of the GC data, a plot of ln[K<sub>i</sub>] vs. T<sub>bi</sub> yields a negative deviation from a straight line plot for the hydrogen bonding compounds (Figure 4.2b) because hydrogen bonding interactions result in boiling point temperatures that are higher than predicted from dispersion interactions alone (14).

The selectivity of the membrane to perform a given thermodynamic separation on the basis of known boiling points can be predicted from with a general form of Equation 4.6.

$$K_i/K_i = \exp\{2.85X10^{-2} \cdot (T_{bi} - T_{bi})\}$$
 (4.7)

Table 4.4. Distribution selectivities for compounds over nitrogen and heptane at 25 °C.  $T_b$  = predicted from boiling points (Equation 4.7); SP = predicted from solubility parameter theory (Equation 4.3); ME = experimental from ME data; GC = experimental from GC data.

	relative to nitrogen		relative to heptane				
<u>compound</u>	$\overline{\mathrm{T_{b}}}$	SP	ME	$\underline{\mathrm{T}}_{\mathrm{b}}$	SP	ME	CC
nitrogen	1.0	1.0	1.0	2.2X10-4	4.5X10 <sup>-4</sup>	1.9X10 <sup>-4</sup>	0
oxygen	1.4	2.3	1.9	3.3X10 <sup>-4</sup>	1.0X10 <sup>-3</sup>	3.6X10 <sup>-4</sup>	0
argon	1.3	5.7	1.9	3.0X10 <sup>-4</sup>	2.6X10 <sup>-3</sup>	3.6X10 <sup>-4</sup>	0
carbon dioxide	<b>2</b> 8	11	19	6.5X10 <sup>-3</sup>	5.0X10 <sup>-3</sup>	3.6X10 <sup>-3</sup>	0
methane	2.5	7.6	6.0	5.7X10 <sup>-4</sup>	3.4X10 <sup>-3</sup>	1.1X10 <sup>-3</sup>	0
ethene	14	26	22	3.2X10 <sup>-3</sup>	1.2X10 <sup>-2</sup>	4.1X10 <sup>-3</sup>	5.8X10 <sup>-3</sup>
ethane	21	30	23	4.8X10 <sup>-3</sup>	1.4X10 <sup>-2</sup>	4.3X10 <sup>-3</sup>	5.8X10 <sup>-3</sup>
propane	80	49	97	1.8X10 <sup>-2</sup>	2.2X10 <sup>-2</sup>	1.8X10 <sup>-2</sup>	1.2X10 <sup>-2</sup>
butane	260	106	120	6.0X10 <sup>-2</sup>	4.8X10 <sup>-2</sup>	2.2X10 <sup>-2</sup>	3.9X10 <sup>-2</sup>
pentane	740	260	1200	0.17	0.12	0.22	0.12
hexane	1900	890	1900	0.43	0.40	0.36	0.36
heptane	4400	2200	5300	1.0	1.0	1.0	1.0
benzene	2600	3400	2100	0.59	1.5	0.40	0.58
toluene	6200	<b>7200</b>	5800	1.4	3.3	1.1	1.6
ethylbenzene	13000	18000	19000	2.9	8.2	3.5	4.1
chlorobenzene	11000	15000	16000	2.6	6.9	3.1	3.3
chloromethane	130	430	130	3.0X10 <sup>-2</sup>	0.20	2.4X10 <sup>-2</sup>	2.3X10 <sup>-2</sup>
dichloromethane	830	880	930	0.19	0.40	0.17	0.15
chloroform	1500	2000	1800	0.35	0.93	0.35	0.36
carbon							
tetrachloride	2300	2200	3200	0.54	0.99	0.60	0.61
chloroethene	180	130	130	4.1X10 <sup>-2</sup>	5.8X10 <sup>-2</sup>	2.4X10 <sup>-2</sup>	3.5X10 <sup>-2</sup>
1,1-dichloroethene	760	1300	1000	0.17	0.62	0.20	0.14
trichloroethene	3200	3600	3700	0.72	1.6	0.69	0.84
tetrachloroethene	8300	9800	14000	1.9	4.5	2.7	2.5
bromomethane	160	400	150	6.7X10 <sup>-2</sup>	0.19	3.0X10 <sup>-2</sup>	5.2X10 <sup>-2</sup>
dibromomethane	4200	6100	2900	0.96	2.8	0.55	0.76
bromoform	19000	30000	39000	4.3	13	7.4	4.2
water	4600	1600	3400	1.0	0.72	0.64	1. <b>7</b> X10 <sup>-2</sup>
methanol	1700	4300	9500	0.39	2.0	1.8	2.9X10 <sup>-2</sup>
ethanol	2500	14000	21000	0.57	6.2	3.9	6.9X10 <sup>-2</sup>
1-propanol	4300	44000	21000	0.97	20	4.0	0.20
2-propanol	2800	28000	8300	0.63	13	1.6	0.10
1-butanol	7500	150000	22000	1.7	68	4.1	0.58
acetone	1300	2800	10000	0.30	1.3	2.0	9.2X10 <sup>-2</sup>
2-butanone	2600	4200	15000	0.59	1.9	2.8	0.27

Examples of distribution selectivities are given in Table 4.4 along with those predicted by modified regular solution theory (Equation 4.3) and by boiling point correlations (Equation 4.7). Since nitrogen is assumed to be non retained by the GC stationary phase, the selectivities compared with nitrogen cannot be presented for the chromatographic data. Instead, distribution selectivities with respect to heptane are presented for both ME and GC as well as the selectivities predicted from Equation 4.7. Although the hydrogen bonding substances deviate from the values predicted by Equation 4.7, significant selectivities for these compounds (i) with respect to nitrogen (j) are still predicted for the membrane.

The predictive models and the data demonstrate that the distribution ratio selectivities increase as the molar volume (or molecular weight) of the compounds increase within a series. For a selectivity model, a factor of two or three difference between the predicted values and the experimental values may be considered quite good considering that one of the most widely used ME applications of separating organic analytes from air is a process that favors the analytes by one to four orders of magnitude. With a few exceptions, most of the selectivity data relative to nitrogen meet this criterion. As expected, the predictions based upon the boiling points show the greatest deviation from the experimental data for the compounds that exhibit strong hydrogen bonding. Using the solubility parameter model, the predicted selectivity for 1-butanol is a factor of seven higher than observed by the ME method. An expanded model (7, 15) that contains specific solubility parameters for dipole interactions and

hydrogen bonding may provide better correlations. However, even the simple models in the present work provide a reasonably quantitative approximation.

Except for the strong hydrogen bonding compounds, the selectivity values relative to heptane obtained by ME are in excellent agreement with the values obtained by GC. The values predicted by the solubility parameter model show less agreement for the most part because heptane exhibits a factor of more than two higher distribution ratio than is predicted by the model, as discussed in Chapter 3. In any case, the thermodynamic relationship between the ME and the GC processes is evident and the rules that guide the use of one technique readily apply to the other.

### **BAND SPREADING AND DIFFUSION**

The band widths of chromatographic peaks are highly diffusion-dependent as described by the Van Deemter equation (16) for packed columns and the Golay equation (17) for open tubes. The Golay equation states that for open tubular columns, effective theoretical plate height, h<sub>i</sub>, for a component is the sum of plate height contributions from the stationary phase, h<sub>i,s</sub>, and from the mobile phase, h<sub>i,m</sub>, where

$$h_i = h_{i,s} + h_{i,m}$$
 (4.8)

The plate height contributions in both phases are due to transport in both the radial, r, and longitudinal, l, directions in the column, where

$$h_{i.s} = h_{i.sr} + h_{i.sl}$$
 (4.9)

and

$$h_{i,m} = h_{i,mr} + h_{i,ml}$$
 (4.10)

Therefore, band spreading is due to longitudinal diffusion and radial diffusion in both phases. Bandspreading in the stationary phase is dependent upon the diffusivity,  $D_{i,s}$  of component i, in the stationary phase of thickness d, the partition coefficient,  $k_i$ , and the linear velocity of the mobile phase, u, where

$$h_{i,sr} = [2/3] \cdot [k_i/(1+k_i)^2] [d^2/D_{i,s}] u$$
(4.11)

and

$$\mathbf{h_{i,sl}} = 2 \cdot \mathbf{D_{i,s}} \cdot \mathbf{k_i} / \mathbf{u} \tag{4.12}$$

Bandspreading in the mobile phase is dependent upon the inner radius, r, of the open tubular column, the partition coefficient, the linear velocity of the mobile phase, and the diffusivity,  $D_{i,m}$ , of component i in the mobile phase gas, where

$$h_{i,mr} = [(1+6 \cdot k_i + 11 \cdot k_i^2)/(24 \cdot (1+k_i)^2)][r^2/D_{i,m}]u$$
 (4.13)

and

$$h_{i,ml} = 2 \cdot D_{i,m} / u$$
 (4.14)

Values for  $D_{i,m}$  are readily estimated from the method developed by Fuller, Shettler, and Giddings (18) where, in a helium mobile phase,

$$D_{i,m} = 1.75X10^{-3} \cdot T \cdot [(M_i + M_{He})/(M_i \cdot M_{He})]^{1/2}$$

$$/\{p \cdot [(\Sigma v)_i^{1/3} + V_{He}^{1/3}]^2\}$$
(4.15)

where T is the absolute temperature,  $M_i$  and  $M_{He}$  are the molecular weights for the component i and helium, respectively, and p is the gas pressure. In the present model, the empirical molecular diffusion volume for substance i,  $(\Sigma v)_i$ , given by the sum of the empirical diffusion volumes for the atoms comprising substance i and the atomic diffusion volume of helium,  $V_{He}$ , are replaced by molar volume terms,  $v_i$ , given in Table 4.1, factored by Avogadro's number,  $N_A$ , where

$$(\Sigma v)_i = v_i / N_A \tag{4.16}$$

By combining and rearranging Equations 4.8, 9, 11, and 12, the following quadratic equation is obtained for determining diffusivities in the stationary phase:

$$0 = [2 \cdot k_i / u] \cdot D_{i,s}^2 - [h_i - h_{i,m}] \cdot D_{i,s} + [2/3] \cdot [k_i / (1 + k_i)^2] \cdot d^2 \cdot u$$
 (4.17)

The solution for D<sub>i,s</sub> is given by

$$D_{i,s} = [h_i - h_{i,m}] \cdot u / [4 \cdot k_i]$$

$$- \{ ([h_i - h_{i,m}] \cdot u / [4 \cdot k_i])^2 - [1/3] \cdot [d \cdot u / (1 + k_i)]^2 \}^{1/2}$$
(4.18)

Experimentally, the plate height,  $h_i$ , is determined from the column length, L, the experimental retention time,  $t_{ri}$ , and the band width at half maximum,  $W_i$ , (19) where

$$h_i = L \cdot W_i^2 / (5.54 \cdot t_{ri}^2)$$
 (4.19)

Calculated gas-phase diffusivities, longitudinal and radial components of band spreading, and experimental plate heights are summarized in Table 4.5 for the components of interest. The measurements of Wi are made with much less certainty for poorly retained compounds. In fact, Wi was impossible to determine for some of these compounds under the present experimental conditions, because only two or three data points could be obtained for an eluting band, which was an insufficient number to obtain a measurable peak profile. This common problem is difficult to resolve with a scanning instrument (20). A thicker chromatographic stationary phase might help alleviate this problem, but would result in extremely long retention times and broad bands for the compounds with higher boiling points. Recording the analog signal from, for example, a flame ionization detector might provide more accurate profiles. However, band overlap at higher temperatures would pose an even more serious problem. The mass spectrometer provides an additional degree of separation in such cases.

Table 4.5. Mobile phase diffusivities,  $D_{i,m}$ , and chromatographic band spreading components used to calculate diffusivities in the stationary phase at 25 °C.

	$D_{i,m}$	$h_{i,mr}$	$h_{i,ml}$	$\mathbf{h_{i}}$
<u>compound</u>	(Eqn. 4.15)	(Eqn. 4.13)	<u>(Eqn. 4.14)</u>	(Eqn. 4.19)
nitrogen	0.32	1.2X10 <sup>-3</sup>	1.1X10 <sup>-2</sup>	-
oxygen	0.31	1.2X10 <sup>-3</sup>	1.1X10 <sup>-2</sup>	-
argon	0.25	1.5X10 <sup>-3</sup>	8.8X10 <sup>-3</sup>	-
carbon dioxide	0.26	1.4X10 <sup>-3</sup>	8.8X10 <sup>-3</sup>	-
methane	0.28	1.3X10 <sup>-3</sup>	9.7X10 <sup>-3</sup>	-
ethene	0.24	2.4X10 <sup>-3</sup>	6.5X10 <sup>-3</sup>	-
ethane	0.24	2.4X10 <sup>-3</sup>	6.3X10 <sup>-3</sup>	-
propane	0.21	3.2X10 <sup>-3</sup>	5.6X10 <sup>-3</sup>	-
butane	0.20	7.4X10 <sup>-3</sup>	6.9X10 <sup>-3</sup>	-
pentane	0.19	9.3X10 <sup>-3</sup>	6.4X10 <sup>-3</sup>	5.1X10 <sup>-2</sup>
hexane	0.18	1.6X10 <sup>-2</sup>	6.1X10 <sup>-3</sup>	4.6X10 <sup>-2</sup>
heptane	0.17	2.1X10 <sup>-2</sup>	5.8X10 <sup>-3</sup>	3.8X10 <sup>-2</sup>
benzene	0.21	1.5X10 <sup>-2</sup>	7.2X10 <sup>-3</sup>	4.0X10 <sup>-2</sup>
toluene	0.19	1.9X10 <sup>-2</sup>	6.6X10 <sup>-3</sup>	3.3X10 <sup>-2</sup>
ethylbenzene	0.18	2.2X10 <sup>-2</sup>	6.2X10 <sup>-3</sup>	4.3X10 <sup>-2</sup>
chlorobenzene	0.19	2.0X10 <sup>-2</sup>	6.7X10 <sup>-3</sup>	3.4X10 <sup>-2</sup>
chloromethane	0.25	3.5X10 <sup>-3</sup>	6.8X10 <sup>-3</sup>	4.2X10 <sup>-2</sup>
dichloromethane	0.24	8.1X10 <sup>-3</sup>	8.2X10 <sup>-3</sup>	$3.6X10^{-2}$
chloroform	0.21	1.3X10 <sup>-2</sup>	7.4X10 <sup>-3</sup>	4.0X10 <sup>-2</sup>
carbon tetrachloride	0.20	1.6X10 <sup>-2</sup>	6.8X10 <sup>-3</sup>	4.6X10 <sup>-2</sup>
chloroethene	0.23	4.6X10 <sup>-3</sup>	6.2X10 <sup>-3</sup>	8.8X10 <sup>-2</sup>
1,1-dichloroethene	0.22	8.6X10 <sup>-3</sup>	7.5X10 <sup>-3</sup>	4.3X10 <sup>-2</sup>
trichloroethene	0.20	1.7X10 <sup>-2</sup>	7.1X10 <sup>-3</sup>	$3.6X10^{-2}$
tetrachloroethene	0.19	$2.0X10^{-2}$	6.7X10 <sup>-3</sup>	$3.6X10^{-2}$
bromomethane	0.25	5.5X10 <sup>-3</sup>	6.6X10 <sup>-3</sup>	7.4X10 <sup>-2</sup>
dibromomethane	0.23	1.5X10 <sup>-2</sup>	7.8X10 <sup>-3</sup>	3.1X10 <sup>-2</sup>
bromoform	0.20	1.9X10 <sup>-2</sup>	7.1X10 <sup>-3</sup>	3.4X10 <sup>-2</sup>
water	0.40	1.9X10 <sup>-3</sup>	1.1X10 <sup>-2</sup>	3.7X10 <sup>-2</sup>
methanol	0.29	3.4X10 <sup>-3</sup>	7.7X10 <sup>-3</sup>	3.9X10 <sup>-2</sup>
ethanol	0.25	6.5X10 <sup>-3</sup>	6.6X10 <sup>-3</sup>	5.1X10 <sup>-2</sup>
1-propanol	0.22	1.3X10 <sup>-2</sup>	6.0X10 <sup>-3</sup>	0.11
2-propanol	0.22	9.2X10 <sup>-3</sup>	5.9X10 <sup>-3</sup>	4.0X10 <sup>-2</sup>
l-butanol	0.20	2.0X10 <sup>-2</sup>	5.5X10 <sup>-3</sup>	9.4X10 <sup>-2</sup>
acetone	0.22	8.5X10 <sup>-3</sup>	6.0X10 <sup>-3</sup>	3.9X10 <sup>-2</sup>
2-butanone	0.21	1.6X10 <sup>-2</sup>	5.5X10 <sup>-3</sup>	4.7X10 <sup>-2</sup>

For organic substances in poly(dimethylsiloxane), diffusivities are typically less than  $1X10^{-5}$  cm<sup>2</sup>/s and molar partition coefficients,  $k_i$ , are typically less than 100. Consequently, longitudinal bandbroadening in the stationary phase (Equation 4.12) may be neglected to yield the following solution for  $D_{i,s}$ :

$$D_{i,s} = [2/3] \cdot [k_i/(1+k_i)^2] \cdot [d^2 \cdot u]/[h_i - h_{i,m}]$$
(4.20)

In some applications where very narrow bore columns and high linear velocity mobile phases are used, the mobile phase components of band spreading,  $h_{i,m}$ , may also be neglected (2). Under these conditions, the diffusivity of a substance in the stationary phase can be estimated entirely from experimental data combining Equations 4.19 and 20, after substituting  $u = L/t_0$  and  $k_i = (t_{ri}-t_0)/t_0$ , to yield the following simple relation:

$$D_{i.s} = 3.69 \cdot d^{2} \cdot (t_{ri} - t_{o}) / W_{i}^{2}$$
(4.21)

From Table 4.5, it is apparent that for the experimental conditions in the present study, band spreading in the mobile phase is not negligible. Therefore, Equations 4.18 or 4.20 are applicable to the current work. Within three significant figures, identical results are obtained for calculations using Equations 4.18 and 4.20, indicating that  $h_{i,sl}$  is negligible. Values for  $D_{i,s}$  determined for the membrane and the chromatographic phase, using Equation 4.20, are provided in Table 4.6. The diffusivities in the membrane for compounds that exhibit hydrogen bonding are lower when compared with the data for

Table 4.6. Diffusivities at 25 °C in the stationary phase for compounds of interest determined by membrane extraction experiments (ME), and gas chromatographic experiments (GC).

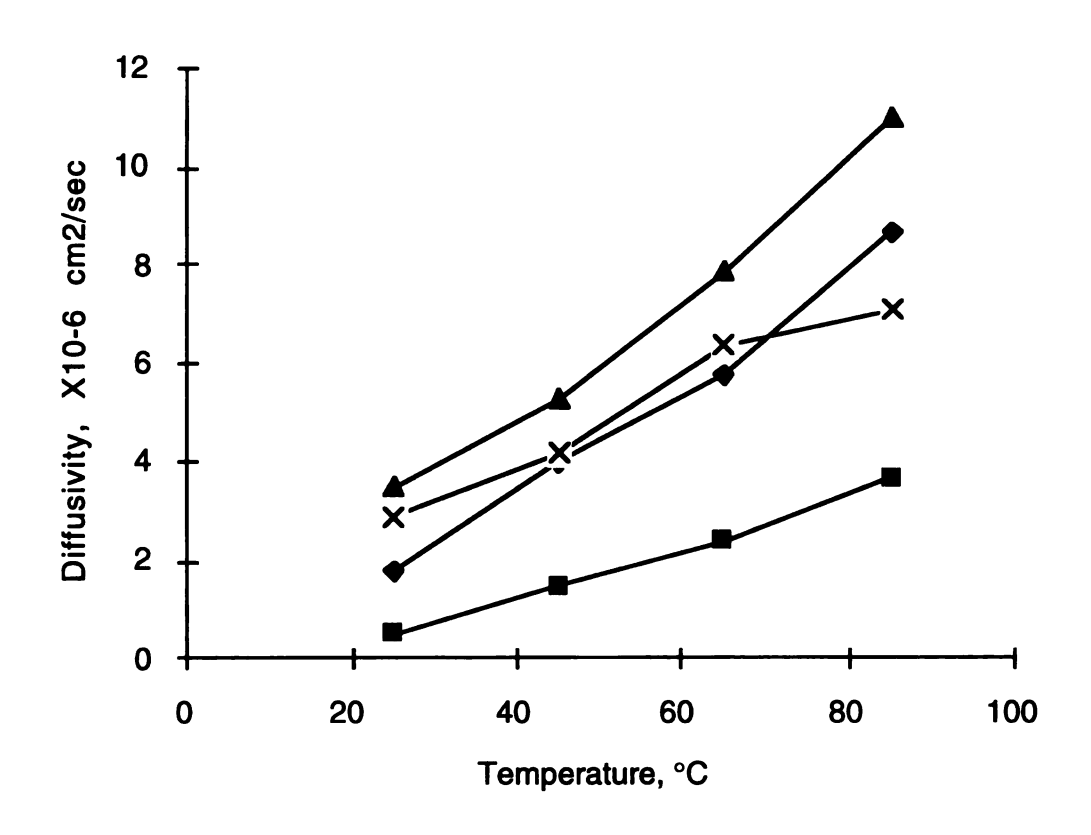
compound	ME	GC (Eqn. 4.20)
pentane	4.4X10 <sup>-6</sup>	2.7X10 <sup>-6</sup>
hexane	3.6X10 <sup>-6</sup>	2.9X10 <sup>-6</sup>
heptane	3.2X10 <sup>-6</sup>	3.1X10 <sup>-6</sup>
benzene	4.8X10 <sup>-6</sup>	2.9X10 <sup>-6</sup>
toluene	3.6X10 <sup>-6</sup>	3.6X10 <sup>-6</sup>
ethylbenzene	1.7X10 <sup>-6</sup>	6.9X10 <sup>-7</sup>
chlorobenzene	1.8X10 <sup>-6</sup>	1.7X10 <sup>-6</sup>
chloromethane	1.1X10 <sup>-5</sup>	2.2X10 <sup>-6</sup>
dichloromethane	8.0X10 <sup>-6</sup>	4.8X10 <sup>-6</sup>
chloroform	4.8X10 <sup>-6</sup>	3.6X10 <sup>-6</sup>
carbon tetrachloride	2.9X10 <sup>-6</sup>	2.3X10 <sup>-6</sup>
chloroethene	9.0X10 <sup>-6</sup>	1.1X10 <sup>-6</sup>
1,1-dichloroethene	5.9X10 <sup>-6</sup>	3.6X10 <sup>-6</sup>
trichloroethene	3.8X10 <sup>-6</sup>	3.3X10 <sup>-6</sup>
tetrachloroethene	2.3X10 <sup>-6</sup>	1.7X10 <sup>-6</sup>
bromomethane	9.0X10 <sup>-6</sup>	1.7X10 <sup>-6</sup>
dibromomethane	4.2X10 <sup>-6</sup>	5.3X10 <sup>-6</sup>
bromoform	1.3X10 <sup>-6</sup>	1.3X10 <sup>-6</sup>
water	2.5X10 <sup>-6</sup>	2.3X10 <sup>-6</sup>
methanol	4.2X10 <sup>-7</sup>	2.9X10 <sup>-6</sup>
ethanol	4.0X10 <sup>-7</sup>	3.1X10 <sup>-6</sup>
l-propanol	4.6X10 <sup>-7</sup>	1.2X10 <sup>-6</sup>
2-propanol	3.2X10 <sup>-7</sup>	5.1X10 <sup>-6</sup>
1-butanol	4.8X10 <sup>-7</sup>	1.0X10 <sup>-6</sup>
acetone	5.0X10 <sup>-7</sup>	5.1X10 <sup>-6</sup>
2-butanone	8.6X10 <sup>-7</sup>	4.1X10 <sup>-6</sup>

the GC stationary phase. This effect is due to adsorption of these compounds on the silica in the membrane. This adsorption results in decreased diffusive transport, as described below. While the treatment resulting in Equation 4.21 will be discussed again, calculations from the more rigorous Equation 4.20 will be used in the correlations with membrane extraction data.

Diffusivities increase with increasing temperatures, as illustrated in Figure 4.3 for diffusivities for selected compounds in the membrane vs. temperature. This effect results in narrower chromatographic bands for GC analyses and faster response to steady state in membrane extraction analyses. The effect of temperature on diffusivity is described by the Arrhenius relation

$$\partial(\ln[D_{i,s}])/\partial(1/T) = -E_{Di}/R \tag{4.22}$$

where  $E_{Di}$  is the energy of activation for diffusion. The activation energies for diffusion for selected compounds were obtained and are presented in Table 4.7. The activation energies for diffusion are always positive so that diffusion increases with increasing temperature. As stated above, because the diffusivities increase with increasing temperatures, the measurements of  $t_{ri}$  and  $W_i$  by GC were made with less reliability at temperatures higher than 25 °C. The diffusivity in the membrane for 1-butanol and other strong hydrogen-bonding substances are decreased relative to the other compounds when compared with the data for the GC stationary phase (Table 4.7). This



### Key:

X = carbon tetrachloride square = 1-butanol diamond = chlorobenzene triangle = toluene

Figure 4.3. The effect of temperature on diffusivity,  $D_{i,s}$ , in the ME stationary phase.

is a result of the adsorption of the hydrogen-bonding substances on the silica in the membrane.

Table 4.7. Values for the activation energies for diffusion for selected compounds in the membrane stationary phase.

	E <sub>Di</sub> (kJ/mole)
compound	<u>ME</u>
nitrogen	16
heptane	15
toluene	17
chlorobenzene	23
carbon tetrachloride	14
1-butanol	30

In the free-volume theory of diffusion (21), diffusive transport of a substance in an unfilled, rubbery polymer is related to the molar volume of the substance as described in Chapter 3. This relationship can be expressed as follows:

$$D_{i,p} = D_{o,p} \cdot \exp\{[-\Theta/(RT)] \cdot v_i^{1/3}\}$$
 (4.23)

where  $D_{i,p}$  is the diffusivity of component i in the polymeric membrane, the pre-exponential term,  $D_{o,p}$ , is the diffusivity of some hypothetical substance with zero molar volume, and  $\Theta$  is a constant that is related to the free-volume and the cohesive energy density of the polymer. In addition, the boiling points of a homologous series of weak or non hydrogen bonding compounds display a direct

relationship with molecular diameter and, therefore, with  $v_i^{1/3}$ . Consequently, a useful correlation may be obtained from a plot of  $\ln(1/D_{i,s})$  vs.  $T_{bi}$ , as shown in Figure 4.4. The solution to the curve in Figure 4.4a for the compounds that exhibit weak or non hydrogen bonding shows a slope of  $6.96 \times 10^{-3}$  and an intercept of 10.1. Because of the inability to determine the diffusivities of the compounds with low boiling points (i.e., the poorly retained compounds) by the chromatographic method, the line plotted in Figure 4.4b was obtained from the ME data. The diffusion selectivity with the silicone membrane may be estimated from

$$D_{i,s}/D_{j,s} = \exp\{6.96X10^{-3} \cdot (T_{bj}-T_{bi})\}$$
 (4.24)

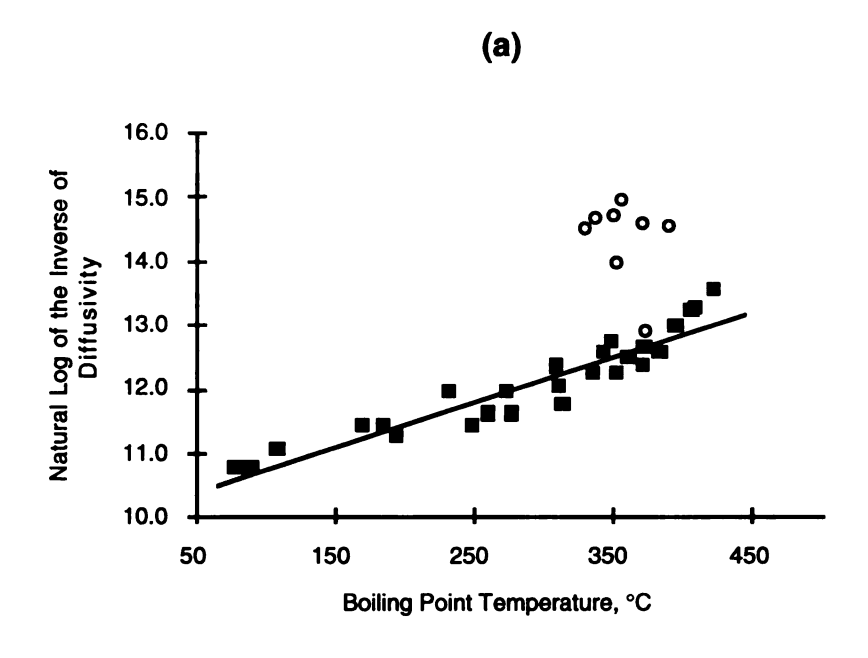
Again, the effect of silica on the transport of the strong hydrogen bonding substances is observed in the ME measurements. The silica inhibits the diffusive transport of these substances in a process akin to frontal or integral chromatography (22). This retention process is described in Chapter 3 by the following relation:

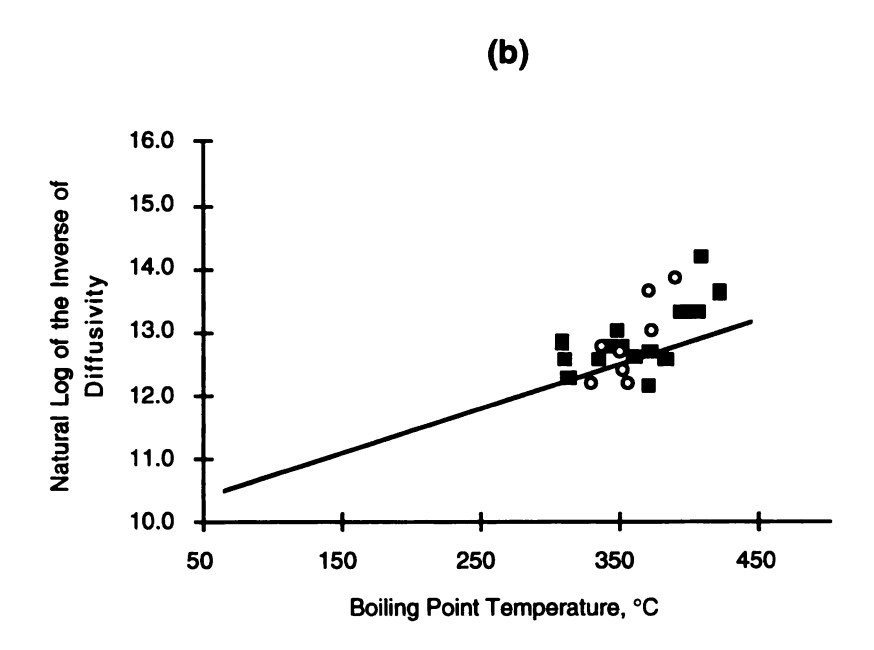
$$D_{i,p}/D_{i,s} = 1+k'_i$$
 (4.25)

which is derived from the definition of chromatographic retention (23),

$$t_r/t_o = 1+k'_i$$
 (4.26)

and the solution for determining diffusion in a membrane (24),





Key:
square = weak or non-hydrogen bonding compound
circle = strong hydrogen bonding compound

Figure 4.4. The correlation of diffusivity,  $D_{i,s}$ , with boiling point,  $T_{bi}$ , at 25 °C, obtained by ME (a) and by GC (b).

$$D_{i.s} = 0.14 \cdot d^2 / t_{50} \tag{4.27}$$

where  $D_{i,s}$  is the diffusive transport that is observed with retention by the silica phase,  $D_{i,p}$  is the diffusivity through the polymer phase in the absence of a retentive phase,  $k'_i$  is the molar partition coefficient for compound i at equilibrium between the silica and polymer phases, and  $t_{50}$  is the time required to achieve 50 % steady state permeation following a step change in concentration in the mobile phase. The diffusivity of substance in polymers containing fillers have also been shown to be effected by the tortuous path the substances must travel (25) so that the relation describing the effect of a filler on diffusive transport is given by

$$D_{i,s} = D_{i,p}/[1+k'_i] \cdot [1+(\Phi_f/2)]$$
 (4.28)

where  $\Phi_f$  is the volume fraction of the filler in the stationary phase. In the case of the silicone elastomer,  $\Phi_f = 0.25$ . It is easily seen that for the chromatographic stationary phase (or for an unfilled membrane), the values for  $k'_i$  and  $\Phi_f$  are zero so that  $D_{i,s} = D_{i,p}$ . By combining Equations 4.23 and 4.28, the following general solution to the retention-modified diffusion process is obtained:

$$D_{i,s} = D_{o,p} \cdot \exp\{[-\Theta/(RT)] \cdot v_i^{1/3} / \{[1 + k'_i] \cdot [1 + (\Phi_f/2)]\}$$
 (4.29)

The constant values  $D_{o,p}$ ,  $\Theta$ , and  $\Phi_f$  have been determined experimentally (Chapter 3) to yield the following solution for diffusivities in the silicone elastomer at 25 °C:

$$D_{i,s} = 8.25X10^{-4} \exp\{-1.06 \cdot v_i^{1/3}\}/[1 + k_i']$$
 (4.30)

It is believed that the forces that govern separations by liquid-solid chromatography (26, 27) also govern this retention and would therefore depend upon the nature of both the polymer phase and the filler phase. For describing the process of a substance partitioning between a permeable mobile phase and an impermeable stationary phase, i.e., adsorption, the molar area, rather than the molar volume of the partitioning substance is typically used (6-9, 15). In liquid-solid chromatography, the thermodynamic description has been presented as a linear relationship between energy of adsorption and the square of the solubility parameter (15). Similarly, the following relationship has been shown in Chapter 3 to describe the process of adsorption of a substance onto a silica filler from a poly(dimethylsiloxane) phase:

$$\ln(k'_{i}) = \ln(V_{f}/V_{p}) + [v_{i}^{2/3}/(RT)][A \cdot \delta_{i}^{2} + B]$$
(4.31)

where the filler/polymer volume phase ratio,  $V_f/V_p$ , is known to be 0.33, and the constants A and B have been experimentally determined in Chapter 3. With these values, and combining Equations 4.29 and 4.30, the following solution to the diffusion-partition process is given:

$$D_{i,s} = 8.25X10^{-4} \cdot \exp\{-1.06 \cdot v_i^{1/3}\}$$

$$/[1 + 0.33 \cdot \exp\{[v_i^{2/3}/(RT)] \cdot [1.84 \cdot \delta_i^2 - 569]\}]$$
(4.32)

Presented in Table 4.8 are the diffusion selectivity,  $D_{i,s}/D_{j/s}$ , values predicted from this equation and from the boiling point model

Table 4.8. Diffusion selectivities for compounds over nitrogen and over heptane at 25 °C.  $T_b$  = predicted from boiling point model (Equation 4.24); SP = predicted from solubility parameter theory (Equation 4.31); ME = experimental from ME data; GC = experimental from GC data.

relative to nitrogen relative to heptane	relative to heptane			
compound Tb SP ME Tb SP ME G	<u> </u>			
nitrogen 1.0 1.0 1.0 6.7 9.1 6.6				
oxygen 0.91 1.0 1.0 6.2 8.8 6.6	-			
argon 0.93 0.50 1.0 6.3 4.5 6.6	-			
carbon dioxide 0.44 0.51 0.62 3.1 4.7 4.1	-			
methane 0.80 0.55 0.76 5.4 5.0 5.0	-			
ethene 0.52 0.40 0.52 3.7 3.7 3.4	-			
ethane 0.47 0.36 0.52 3.3 3.3 3.4	-			
propane 0.34 0.25 0.30 2.5 2.3 2.0	-			
butane 0.26 0.21 0.30 1.9 1.9 2.0	-			
	.88			
	.93			
	.0			
	.0			
	.1			
• • • • • • • • • • • • • • • • • • • •	.22			
	.56			
	.70			
	.6			
chloroform 0.17 0.19 0.23 1.1 1.7 1.5 1.	.2			
carbon				
	.73			
	.37			
	.2			
trichloroethene 0.14 0.16 0.18 1.1 1.5 1.2 1.				
	54			
	.56			
	.7			
	40			
water $0.13$ $2.3 \times 10^{-4}$ $0.12$ $0.99$ $2.1 \times 10^{-3}$ $0.78$ $0.99$	74			
methanol $0.16$ $1.5X10^{-2}$ $2.0X10^{-2}$ $1.2$ $0.14$ $0.13$ $0.14$	93			
	99			
	39			
2-propanol 0.14 3.9X10 <sup>-2</sup> 1.5X10 <sup>-2</sup> 1.1 0.36 0.10 1.				
	32			
acetone 0.17 0.16 2.4X10 <sup>-2</sup> 1.3 1.4 0.16 1.				
2-butanone 0.15 0.15 4.1X10 <sup>-2</sup> 1.1 1.4 0.27 1.				

(Equation 4.24) for selective diffusion over nitrogen and heptane for the compounds studied. Again, the boiling point model exhibits the poorest correlation with the ME data for the strong hydrogen bonding compounds. The boiling point model typically predicts relative diffusivities that are five to ten times higher than observed by ME for these compounds. On the other hand, this model yields good correlation with the GC data. The solubility parameter model for the membrane considers the effect of the silica on the diffusive transport and yields a very good correlation for most of the compounds. The compounds that yield low distribution ratios for the GC stationary phase yield the poorest correlation between the GC and ME data because of the inability to accurately measure the widths of these GC bands as discussed above.

Just as with the distribution ratio selectivities, the diffusion selectivities may be modeled by the chromatographic process. For the best correlation, both the GC and the ME phases should be identical, since the presence of polymer additives and fillers may significantly affect the thermodynamic and kinetic transport properties. As demonstrated, the presence of such additives and fillers may be taken into account using known chromatographic principles.

#### **EFFICIENCY AND ENRICHMENT**

Since the permeation enrichment factor,  $\mathcal{E}_{i/j} = (D_{i,s}/D_{j,s})(K_i/K_j)$ , is comprised of parameters that have been characterized by solubility parameter theory, then the enrichment factor may be modeled by

combining Equation 4.3 for the distribution ratio with Equation 4.32 for the diffusivity.

From chromatography, the distribution selectivity may be written as

$$K_i/K_i = k_i/k_i = (t_{ri}-t_o)/(t_{ri}-t_o)$$
 (4.33)

and from Equation 4.20, after substituting  $u = L/t_0$  and  $k_i = (t_{ri}-t_0)/t_0$ , the diffusion selectivity may be written as

$$D_{i,s}/D_{j,s} = [(t_{ri}-t_o)/(t_{rj}-t_o)] \cdot [t_{rj}/t_{ri}]^2 \cdot [(h_j-h_{j,m})/(h_i-h_{i,m})]$$
(4.34)

Therefore, the relationship between the permeation enrichment factor,  $\mathcal{E}_{i/j} = (D_{i,s}/D_{j,s})(K_i/K_j)$ , and chromatographic measurements may be written as follows:

$$\mathcal{E}_{i/i} = [(t_{ri} - t_o) / (t_{ri} - t_o)]^2 \cdot [(t_{ri} / t_{ri})]^2 \cdot [(h_i - h_{i,m}) / (h_i - h_{i,m})]$$
(4.35)

If ideal conditions prevail, where the band spreading in the mobile phase is negligible, then Equation 4.21 is used to determine diffusivities so that the relationship between the permeation enrichment factor and chromatographic measurements is given by:

$$\mathcal{E}_{i/i} = [W_i/W_i]^2 \cdot [(t_{ri} - t_o)/(t_{ri} - t_o)]^2 \tag{4.36}$$

Since the chromatographic effective theoretical plate number for component i is defined as (19)

$$N_{i} = 5.54 \cdot [(t_{ri} - t_{o})/W_{i}]^{2}$$
(4.37)

The resulting relationship between E and N can be expressed as

$$\mathcal{E}_{i/j} = (N_i/N_j) \tag{4.38}$$

The effect of temperature on the enrichment factor is given by

$$\partial(\ln \mathcal{E}_{i/j})/\partial(1/T) = -\Delta E_P/R \tag{4.39}$$

where  $\Delta E_P$  is the difference in activation energy for permeation between compounds i and j, given by  $\Delta E_P = E_{Pi} - E_{Pj}$ . Values of  $E_{Pi}$  for selected compounds in the silicone elastomer are given in Table 4.9.

Table 4.9. Values for the activation energies for permeation for selected compounds in the membrane stationary phase.

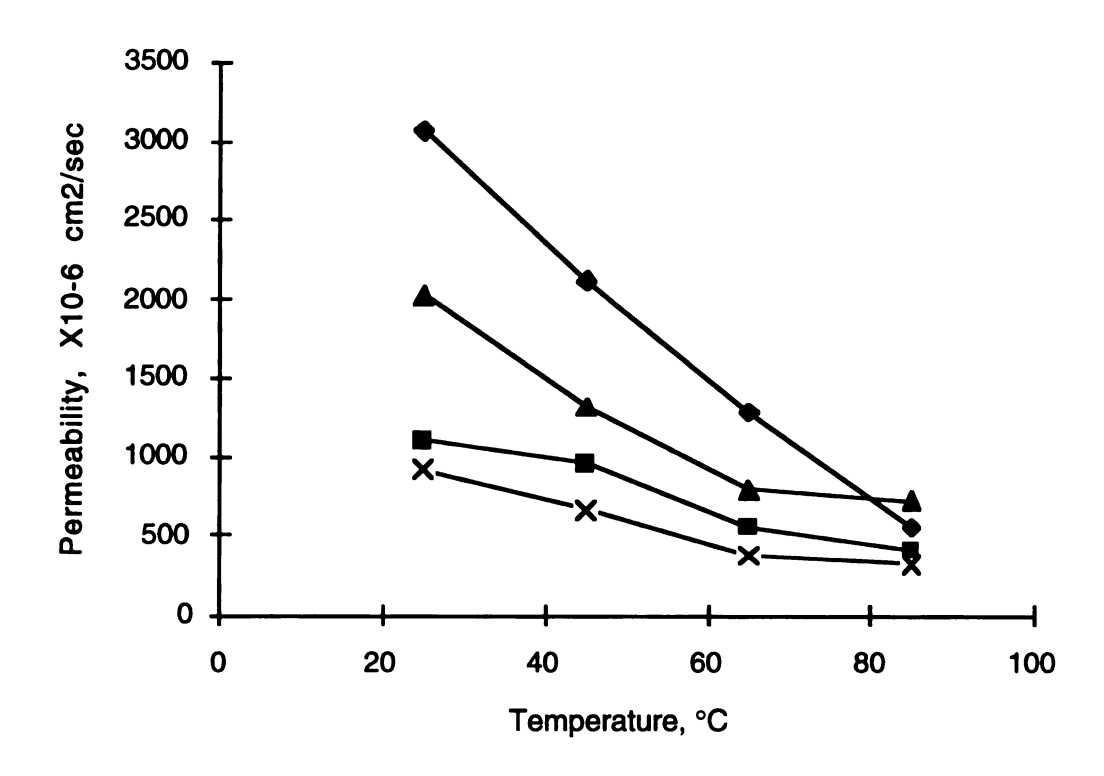
	E <sub>Pi</sub> (kJ/mole)
compound	<u>ME</u>
nitrogen	8
heptane	-12
toluene	-17
chlorobenzene	-25
carbon tetrachloride	-17
1-butanol	-16

The activation energy for permeation is in fact the sum of the heat of solution and the activation energy for diffusion. In the case of the silicone stationary phases, the heats of solution for most organic compounds are greater in magnitude than their activation energies for diffusion, therefore an increase in temperature results in a reduced permeability. The plots of  $\ln(P_{ij})$  vs. temperature in Figure 4.5 demonstrate the dominance of the distribution ratio in the effect that temperature has on the permeation of organic compounds in the silicone materials. For gases such as nitrogen and oxygen, the activation energies for diffusion dominate so that their permeabilities increase with increasing temperature. The result is that as the temperature increases, the enrichment factor for the organic compounds over nitrogen (and air) decreases. Since measurements of the chromatographic band widths at temperatures above 25 °C were not reliable, these data are not shown.

The plot of  $\ln[\mathcal{E}_{(i/N2)}]$  vs.  $T_{bi}$  shown in Figure 4.6 illustrates the dominance that the distribution ratio exhibits for the permeation process. The correlation between enrichment factor and boiling point for the non- and weakly hydrogen bonding compounds is given by

$$\mathbf{\varepsilon}_{i/j} = \exp\{2.15X10^{-2} \cdot (T_{bi} - T_{bj})\}\$$
 (4.40)

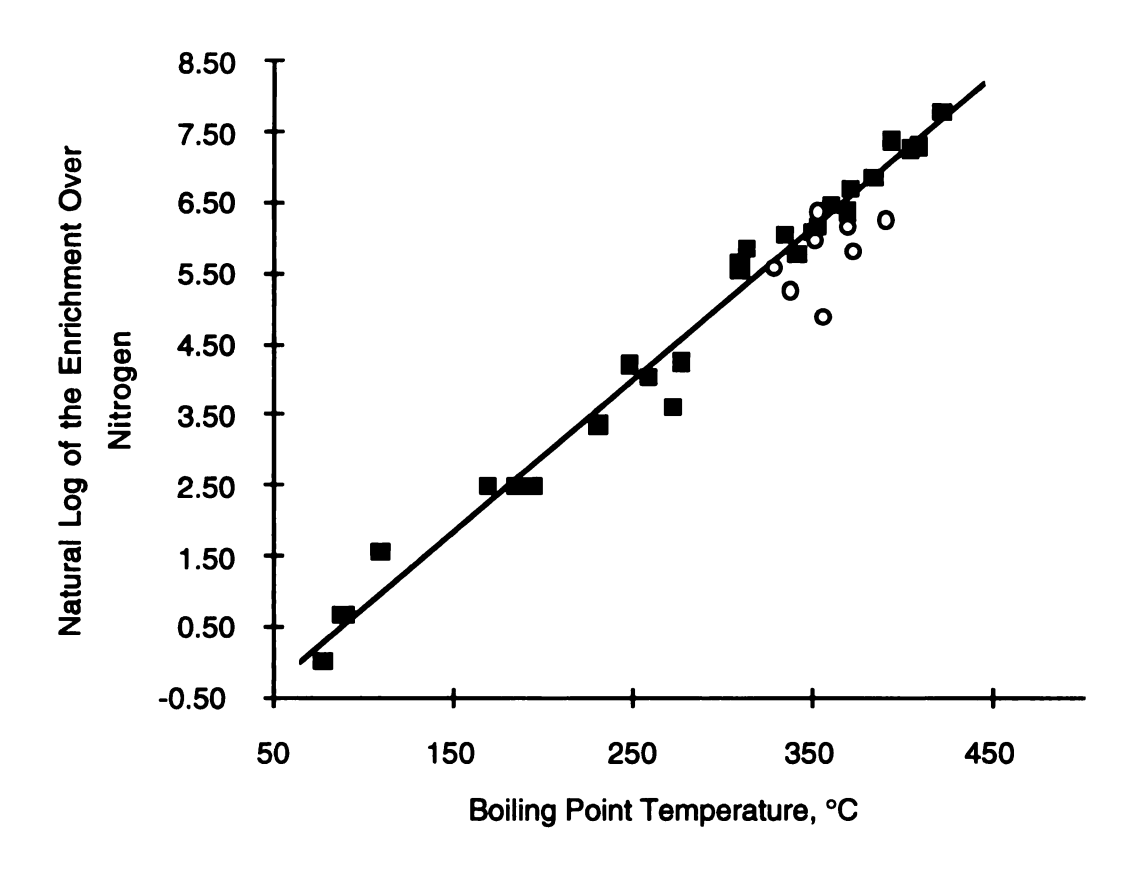
which is the product of Equations 4.7 and 4.24. The hydrogen bonding compounds show a reasonable correlation with the line plotted for the compounds that exhibit weak or no hydrogen bonding.



## Key:

X = carbon tetrachloride square = 1-butanol diamond = chlorobenzene triangle = toluene.

Figure 4.5. The effect of temperature on permeability,  $P_i$ , in the ME stationary phase.



**Key:** square = weak or non-hydrogen bonding compound circle = strong hydrogen bonding compound

Figure 4.6. The correlation of enrichment factor (over nitrogen),  $\mathcal{E}_{1/N2}$ , with boiling point,  $T_{bi}$ , for data obtained by ME at 25 °C.

This improved correlation may be due to the inhibited diffusion from the silica being offset by enhanced partitioning.

The enrichment factors over nitrogen and over heptane are presented in Table 4.10 for the boiling point and solubility parameter models as well as the ME and  $N_i/N_j$  data. The solubility parameter model showed good correlation with the ME data for the enrichment of the compounds over nitrogen. Only for pentane, hexane, heptane, 2-propanol, and 1-butanol do the values predicted from this model deviate significantly from the experimental data. Many of the values for the selectivity over heptane again showed deviation from the experimental values using this solubility parameter model. In general, the correlation between the ME and GC enrichment factors was quite good.

#### **FURTHER CONSIDERATIONS**

The results described in this chapter suggest that chromatographic data may be the basis for a simple and practical method for selecting a membrane for a specific separation application. In general, if two components are readily separated by chromatography, then they will be readily separated by a membrane composed of the chromatographic stationary phase. The distribution ratios for compounds between the stationary and mobile phases will be linear with the chromatographic retention times, while the diffusivities will roughly be inversely proportional to the retention times. The implication of this "rule-of-thumb" to an analysis is that the

Table 4.10. Enrichment factors for compounds over nitrogen and heptane at 25 °C.  $T_b$  = predicted from the boiling point model (Equation 4.40); SP = predicted from solubility parameter theory (Equations 4.3 and 4.32); ME = experimental from ME data ( $P_i/P_j$ ); GC = experimental from GC data (Equation 4.35).

	relati	ve to ni	itrogen	1		o heptane	
compound	Tb	SP	ME	Tb	SP	ME	GC
nitrogen	1.0	1.0	1.0	1.8X10-3	4.1X10 <sup>-3</sup>	1.2X10-3	-
oxygen	1.3	2.2	1.9	2.4X10-3	9.0X10 <sup>-3</sup>	2.3X10-3	-
argon	1.2	2.8	1.9	2.2X10-3	1.2X10 <sup>-2</sup>	2.3X10-3	-
carbon dioxide	12	5.6	12	2.2X10-2	2.3X10 <sup>-2</sup>	1.5X10 <sup>-2</sup>	-
methane	2.0	4.2	4.6	3.5X10 <sup>-2</sup>	1.7X10 <sup>-2</sup>	5.6X10 <sup>-3</sup>	-
ethene	7.2	11	12	1.3X10 <sup>-2</sup>	4.4X10 <sup>-2</sup>	1.4X10 <sup>-2</sup>	-
ethane	10	11	12	1.8X10 <sup>-2</sup>	4.5X10 <sup>-2</sup>	1.5X10 <sup>-2</sup>	-
propane	27	12	29	4.9X10 <sup>-2</sup>	5.1X10 <sup>-2</sup>	3.6X10 <sup>-2</sup>	-
butane	67	22	36	0.12	9.1X10 <sup>-2</sup>	4.4X10 <sup>-2</sup>	-
pentane	150	42	250	0.26	0.17	0.31	0.11
hexane	300	120	320	0.53	0.48	0.39	0.34
heptane	560	240	810	1.0	1.0	1.0	1.0
benzene	380	560	490	0.67	2.3	0.61	0.55
toluene	730	970	960	1.3	4.0	1.2	1.9
ethylbenzene	1300	1974	1500	2.3	8.2	1.9	0.91
chlorobenzene	1200	1600	1400	2.1	6.8	1.7	1.8
chloromethane	40	130	67	7.2X10 <sup>-2</sup>	0.53	8.4X10 <sup>-2</sup>	1.6X10 <sup>-2</sup>
dichloromethane	160	210	350	0.29	0.85	0.43	0.24
chloroform carbon	250	380	430	0.45	1.6	0.53	0.42
tetrachloride	350	380	440	2.0	1.6	0.54	0.44
chloroethene	50	44	57	9.0X10 <sup>-2</sup>	0.18	6.9X10 <sup>-2</sup>	1.3X10 <sup>-2</sup>
1.1-dichloroethene	150	280	290	0.27	1.2	0.35	0.16
trichloroethene	440	580	650	0.78	2.4	0.80	0.90
tetrachloroethene	910	1200	1600	1.6	5.0	2.0	1.4
bromomethane	73	120	69	0.13	0.52	8.6X10 <sup>-2</sup>	2.9X10-2
dibromomethane	540	540	580	0.97	2.2	0.72	1.3
bromoform	1700	1700	2400	3.0	7.1	3.0	1.7
water	580	0.37	390	1.0	1.5X10-3	0.48	1.3X10-2
methanol	270	67	190	0.49	0.28	0.24	2.7X10 <sup>-2</sup>
ethanol	360	320	400	0.65	1.3	0.49	6.9X10 <sup>-2</sup>
1-propanol	550	1100	490	0.98	4.4	0.59	7.9X10 <sup>-2</sup>
2-propanol	400	1100	130	0.71	4.5	0.16	0.17
1-butanol	840	3200	520	1.5	13	0.64	0.19
acetone	230	450	260	0.40	1.8	0.31	0.15
2-butanone	370	650	600	0.67	2.7	0.75	0.35

more permeable a compound is, the longer is its response time. These principles are illustrated in the gas chromatogram and the permeation parameters given in Figure 4.7.

In addition to gas analysis, analytical ME techniques are also commonly used for the analysis of aqueous samples. The same principles described above may be applied to these separations. In the case of compounds that exhibit weak or no hydrogen bonding, the compounds with the lower boiling points exhibit higher enrichment factors over water because of their low solubility in the water as shown in Chapter 2. The strong hydrogen bonding compounds partition poorly into the membrane from an aqueous matrix, which results in low permeabilities.

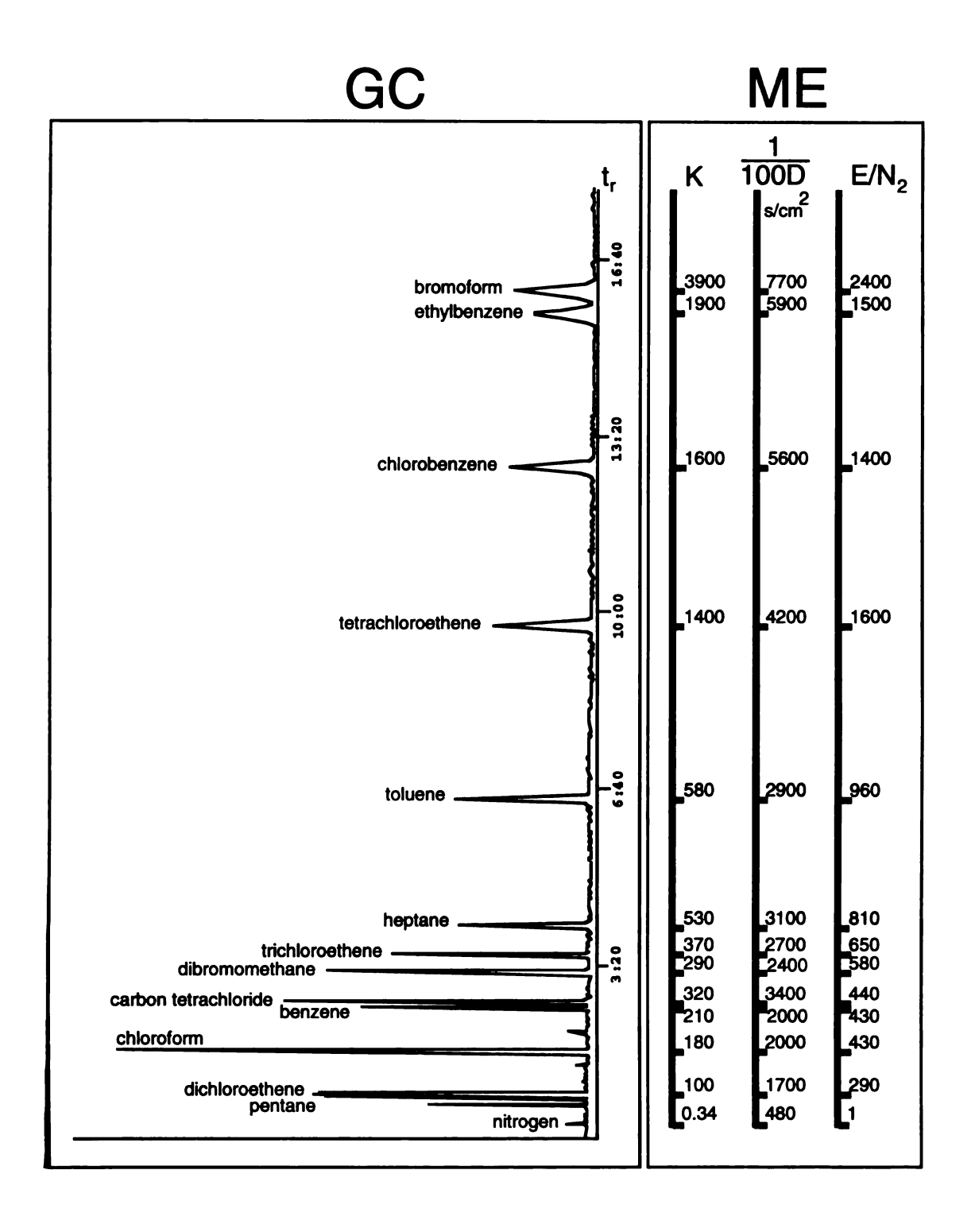


Figure 4.7. The correlation of GC retention times with ME permeation parameters at 25  $^{\circ}$ C.

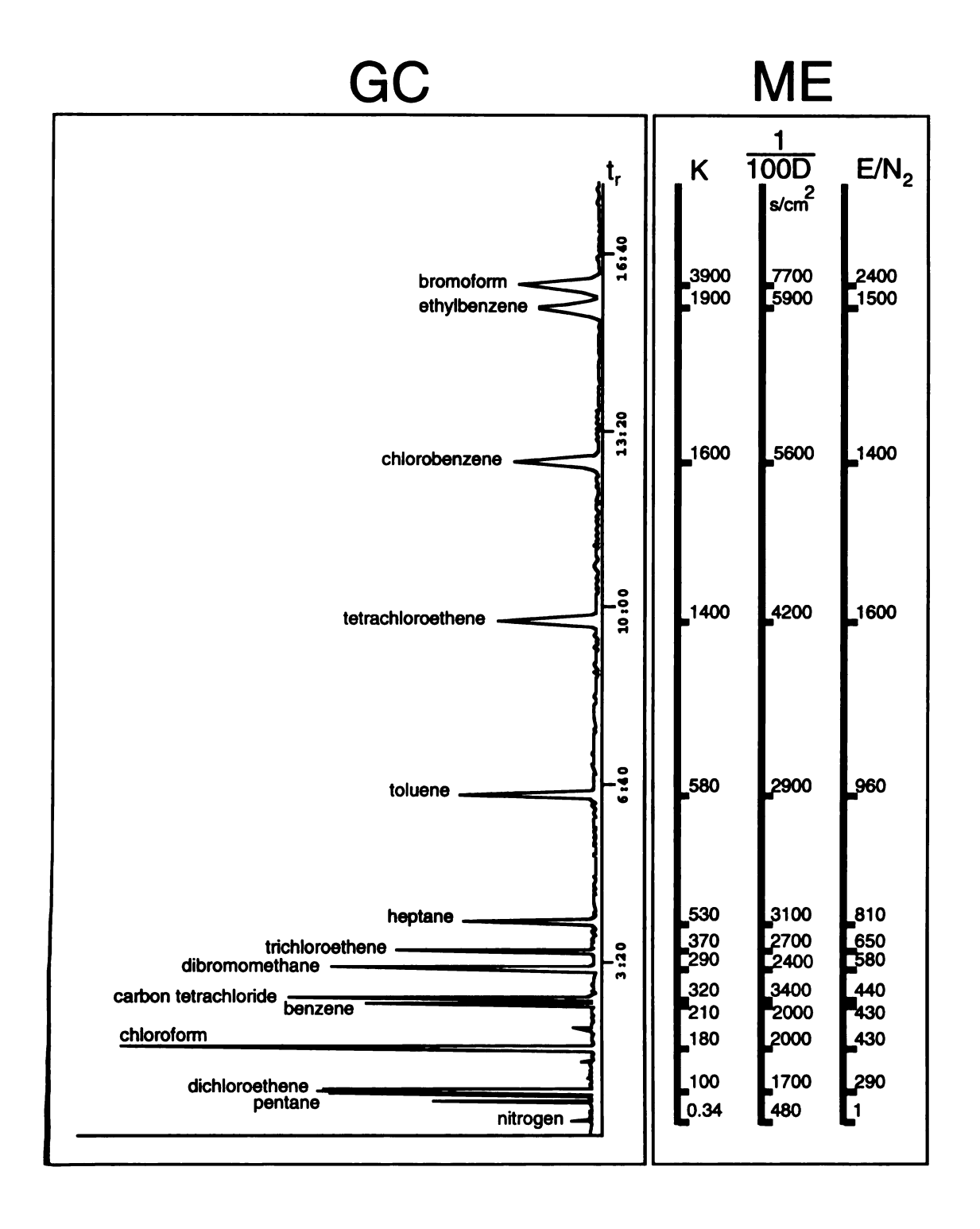


Figure 4.7. The correlation of GC retention times with ME permeation parameters at 25 °C.

#### REFERENCES

- (1) Braun, J.-M.; Guillet, J. E. Adv. Polym. Sci. 1976, 21, 107.
- (2) Lloyd, D. R.; Ward, T. C.; Schreiber, H. P., eds. <u>Inverse Gas Chromatography</u>, ACS Symposium Series; American Chemical Society: Washington D.C., 1989.
- (3) LaPack, M. A.; Tou, J. C.; Enke, C. G. Anal. Chem. 1990, 62, 1265.
- (4) Fjeldsted, J. C. Instrument Society of America International Conference and Exhibition, New Orleans, LA, 1990.
- (5) Mears, P. In: <u>Membrane Separation Processes</u>; Mears, P., Ed.; Elsevier: Amsterdam, Netherlands, 1976.
- (6) Hildebrand, J. H.; Scott, R. L. <u>The Solubility of Nonelectrolytes</u>, 3rd Ed.; Reinhold: New York, NY, 1950.
- (7) Hansen, C.; Beerbower, A. Solubility Parameters, In <u>Kirk-Othmer Encyclopedia of Chemical Technology</u>, Suppl. Vol., 2nd. Ed.; 1971.
- (8) Barton, A. F. M. <u>Handbook of Solubility Parameters and Other</u> Cohesion Parameters; CRC Press, Inc.: Baco Raton, FL, 1983
- (9) Hildebrand, J. H.; Prausnitz, J. M.; Scott, R. L. <u>Regular and Related Solutions</u>; VanNostrand-Rheinhold: Princeton, NJ, 1970.
- (10) Prausnitz, J. M.; Shair, F. H. A.I.Ch.E. J. 1961, 7, 682.
- (11) Weast, R. C., ed. <u>Handbook of Chemistry and Physics</u>,64th Ed.; CRC Press, Inc.: Baco Raton, 1983.
- (12) Jennings, W. <u>Gas Chromatography with Glass Capillary Columns</u>, 2nd Ed.; Academic Press: New York, NY, 1980.

- (13) Bermejo, J.; Guillen, M.D. Chromatographia 1983, 17, 664.
- (14) Karger, B. L.; Snyder, L. R.; Horvath, C. <u>An Introduction to Separation Science</u>; Wiley-Interscience: New York, NY, 1973.
- (15) Karger, B. L.; Snyder, L. R.; Eon, C. Anal. Chem. 1978, 50, 2126.
- (16) Van Deempter, J. J.; Zuiderweg, F. J.; Klikenberg, A. Chem. Eng. Sci. 1956, 5, 271.
- (17) Golay, M. J. E. In: <u>Gas Chromatography 1957</u>: East Lansing Symposium, Coates, V. J.; Noebels, H. J.; Fagerson, I. S., Eds.; Academic Press: New York, NY, 1958.
- (18) Fuller, E. N.; Schettler, P. D.; Giddings, J. C. *Ind. Eng. Chem.* **1966**, 58, 19.
- (19) Desty, D. H.; Goldup, A.; Swanton, W. T. In: <u>Gas Chromatography</u>, Brenner, N; Callen, J. E.; Weiss, M. D., Eds.; Academic Press: New York, NY, 1962.
- (20) Holland, J. F.; Enke, C. G.; Allison, J.; Stults, J. T.; Pinkston, J. D.; Newcome, B.; Watson, J. T. *Anal. Chem.* **1983**, 55, 997A.
- (21) Brandt, W. W. J. Phys. Chem., Wash., 1959, 63, 1080.
- (22) Grob, R. L. <u>Modern Practices of Gas Chromatography;</u> Wiley-Interscience: New York, NY; 1977.
- (23) Giddings, J. C. <u>Dynamics of Chromatography</u>, Vol. 1; Marcel Dekker: New York, NY; 1965.
- (24) Ziegel, K. D.; Frensdorff, H. K.; Blair, D. E. *J. Polym. Sci.* **1969**, 7, 809.
- (25) van Amerongen, G. J. Rubber Chem. Technol. 1964, 37, 1065.

- (26) Snyder, L. R. <u>Principles of Adsorption Chromatography;</u> Marcel Dekker: New York, NY; 1968.
- (27) Kirkland, J. J., (Ed.) Modern <u>Practice of Liquid</u> <u>Chromatography;</u> Wiley-Interscience: New York, NY; 1971.

## **CHAPTER 5**

# **Practical Aspects of Membrane Extractions**

In this chapter, practical aspects for optimizing experimental and instrumental parameters are discussed for membrane extraction mass spectrometry. Some experimental conditions that affect membrane extraction efficiencies include temperature and sample flow rate. The experimental conditions under which an analysis of a chemical process is performed are often dictated by the process itself. The instrumental parameters that may be more easily controlled include the membrane dimensions, the ME device configuration, and the distance between the membrane extractor and the analyzer. Another concern for the analyst is the potential for a thin-walled membranes to rupture, allowing the sample or process stream to vent the mass spectrometer. This is of particular concern in process applications where many process streams are complex and the membrane may degrade by physical, chemical, or thermal means.

A variety of devices for ME have been developed to separate compounds of interest from a sample matrix and introduce these compounds into a mass spectrometer. Hollow fiber or tube membranes have seen a great deal of use in ME-MS applications (1-7). Several groups have also devised systems for making sheet ME-MS interfaces (7-10). More recently, hollow fiber and sheet membrane

extractors have been incorporated directly into the vacuum chamber and even the ion source of the mass spectrometer with the goal of improving the sensitivities and response times (11-13).

Two hollow fiber membrane extractor configurations have been reported and contrasted. The flow-through device for ME is configured such that sample flows through the interior of the hollow fiber membrane while the analytes permeate radially to the outside, where they are analyzed. Conversely, the flow-over device for ME is configured such that the outside of the hollow fiber membrane is exposed to the sample while the inside is exposed to the MS vacuum. Basic designs for flow-over and the flow-through hollow fiber membrane extractors are illustrated in Figures 5.1 and 5.2.

The following points are important experimental considerations for on-line ME-MS techniques:

- 1) Experimental control is desired over parameters that affect permeability or that may damage the membrane, such as the membrane temperature and linear velocity of the sample.
- 2) The membrane should be protected from being torn due to pinching or abrasion.
- 3) In the event of a ruptured membrane, the analyzer should immediately be isolated from the ME device so that the mass spectrometer is not vented by the sample.
- 4) The surface area and void volume of the ME-MS interface should be minimized. Interface tubing, fittings, vacuum-protection valves,

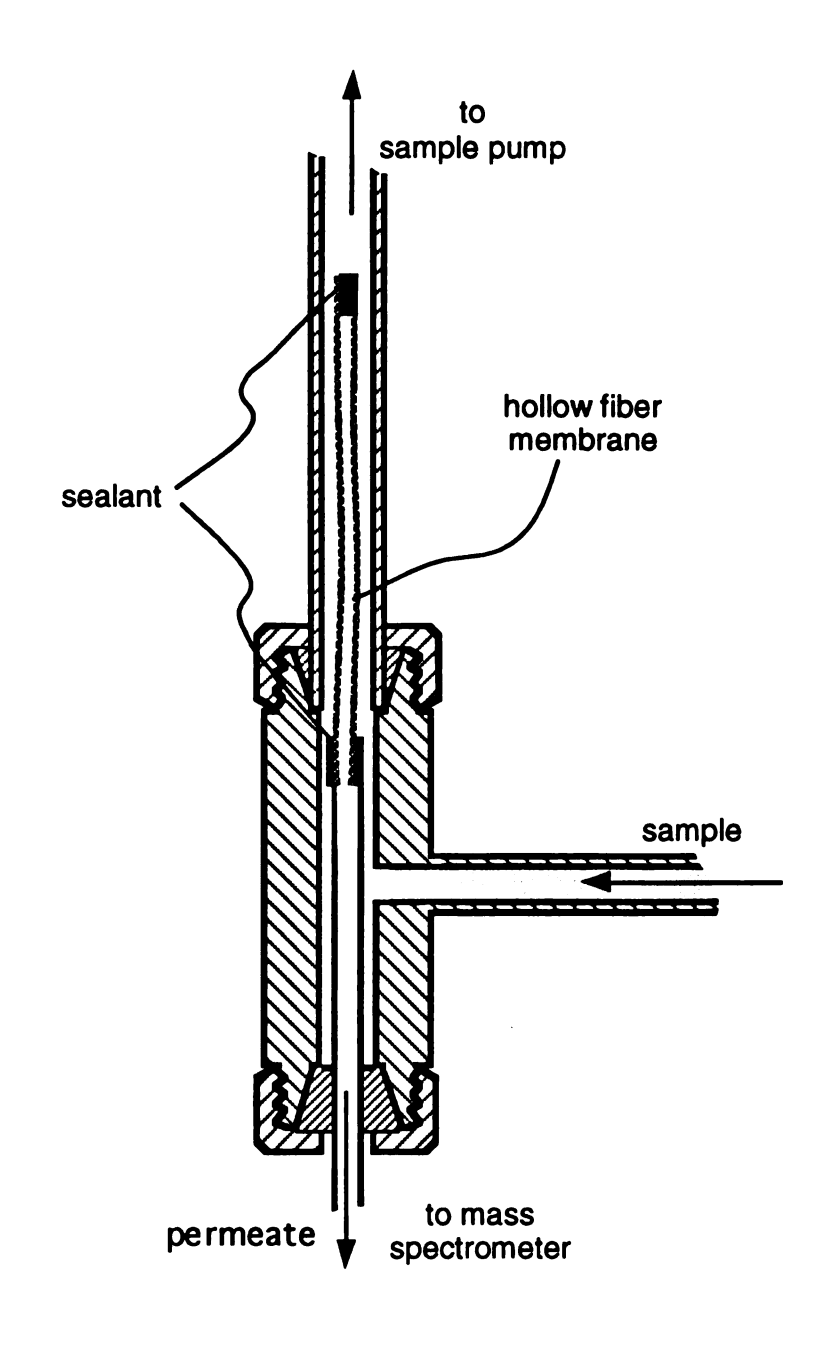


Figure 5.1. Flow-over hollow fiber membrane extractor.

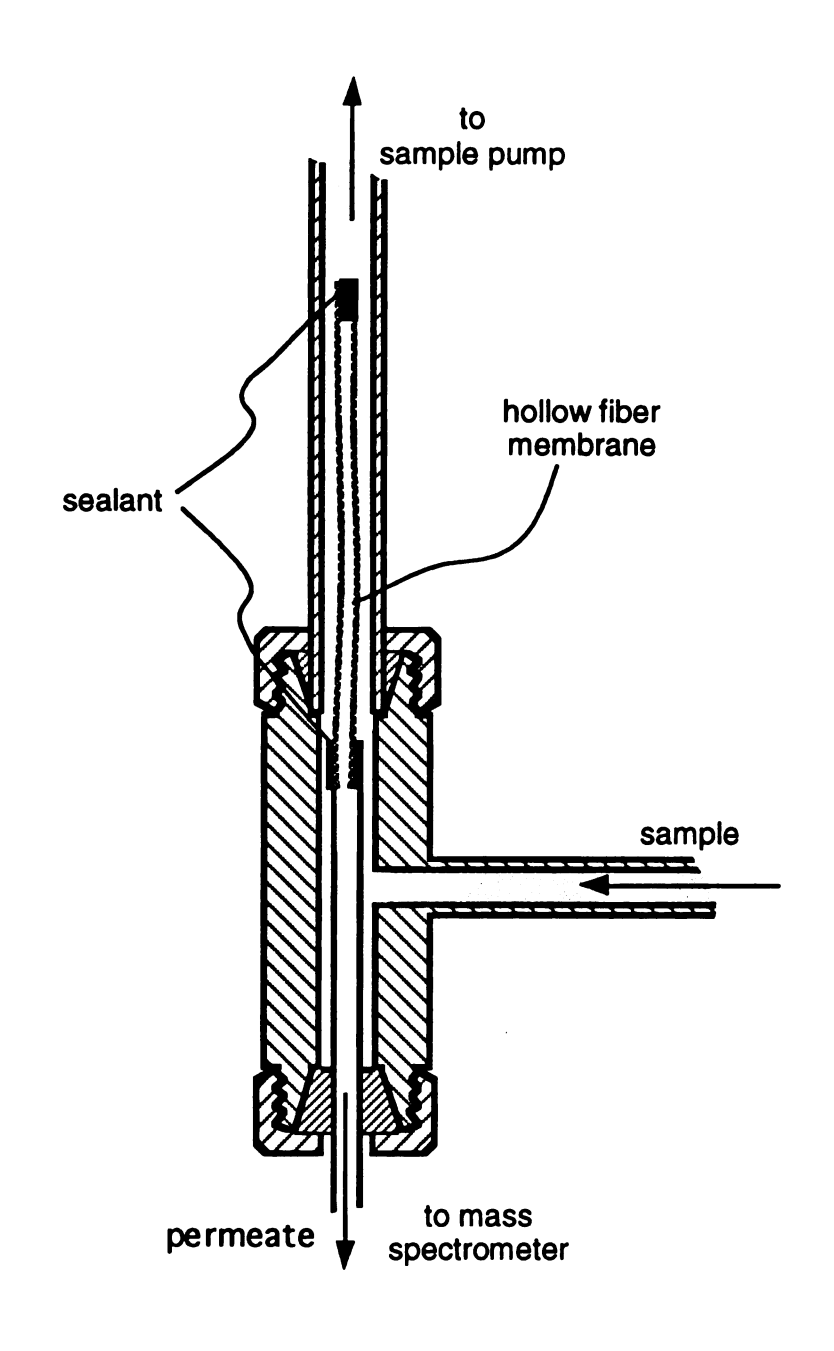


Figure 5.1. Flow-over hollow fiber membrane extractor.

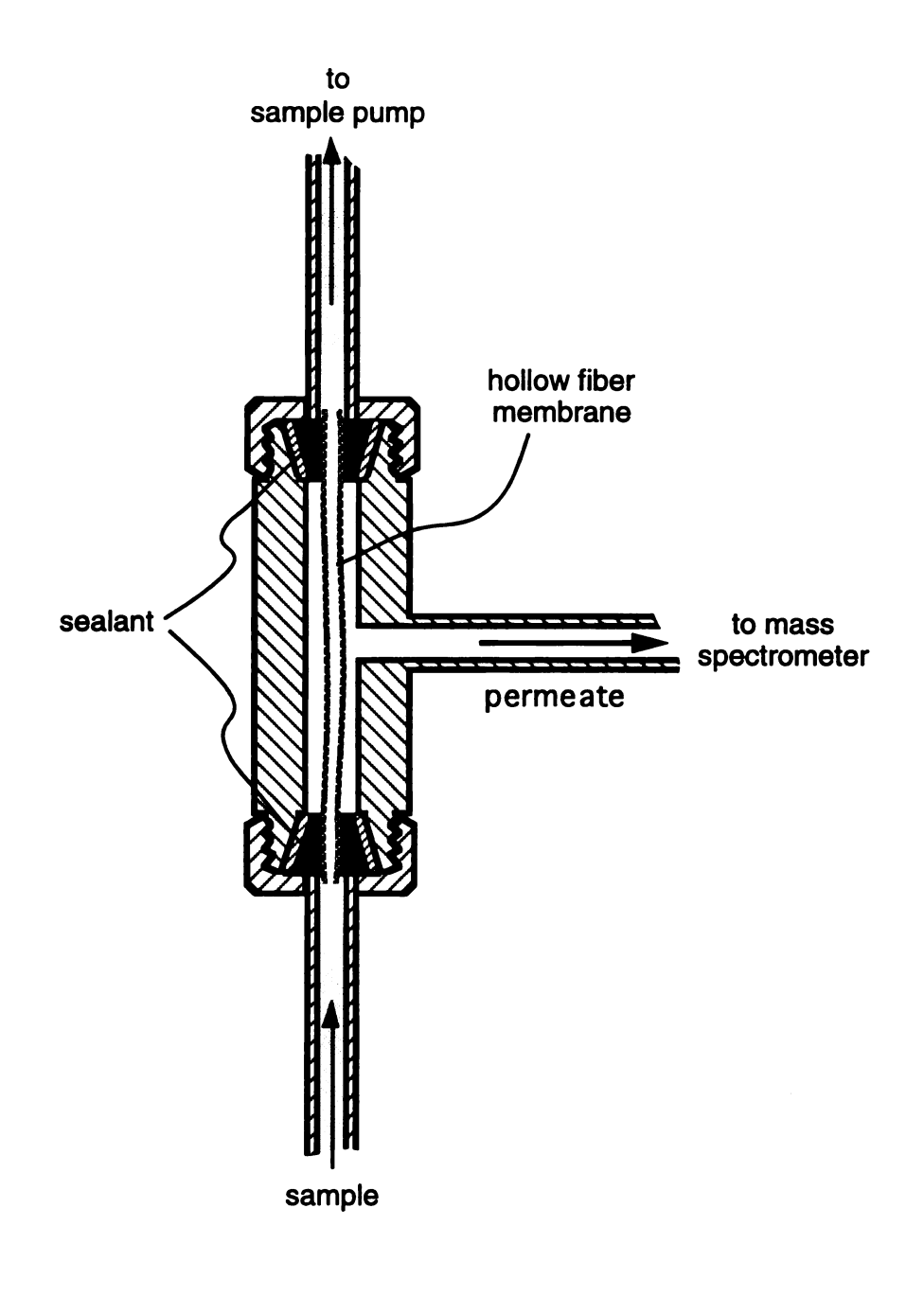


Figure 5.2. Flow-through hollow fiber membrane configuration.

and the ME device contribute to the surface area and void volume in the ME-MS interface.

- 5) In processes where highly reactive analytes or reaction kinetics are to be measured, the shortest distance possible between the sample and the membrane extractor is desired to minimize loss of the analyte or skewing of the reaction profile.
- 6) In some applications, it is desirable to monitor multiple streams of gas and liquid process streams, as discussed in Chapter 6, thus more than one ME device may be required.

Several experimental parameters are discussed below in the context of optimizing the analytical speed, sensitivity, and selectivity.

#### **MEMBRANE DIMENSION CONSIDERATIONS**

The permeation equations discussed in Chapter 2 show that the permeation rate increases, and therefore the detection limit decreases, as a function of sheet membrane area or hollow fiber membrane length. In the case of the hollow fiber membrane, the permeation rate for the analyte increases with increasing length only to the limit where the concentration of the analyte in the sample does not change along the hollow fiber due to efficient extraction into the membrane (14, 15). In such cases, it is preferred that the membrane extractor be constructed with several short hollow fiber membranes, rather than with a single long one to ensure uniform sample concentration along the membrane surface.

The amount of analyte removed by the permeation process per unit length of membrane is actually quite small as illustrated by the permeation rates per unit concentration through a silicone hollow fiber membrane given in Table 5.1 for several gas phase compounds. By pumping a water sample from a 48-cc volatile organic analysis (VOA) vial through the membrane and back into the vial, small samples have been analyzed without appreciable consumption of the sample and without formation of headspace in the vial. A water sample spiked with toluene and dichloromethane was pumped at various rates through three flow-through hollow fiber membrane extractors in series and their permeate streams were analyzed. No significant drop in permeation rate between the first and the third membrane in the series was observed.

The detection limit for an analyte is proportional to the thickness of a sheet membrane. In the case of hollow fiber membranes, the following treatment may be useful in understanding the permeation rate-hollow fiber wall thickness relationship. In Chapter 2, it was shown that the permeation rate through a hollow fiber membrane is given by

$$F_{i} = 2 \cdot \pi \cdot L \cdot P_{i} \cdot c_{mi} / \ln(o.d./i.d.)$$
(5.1)

Since o.d./i.d. = outer radius (o.r.)/inner radius (i.r.), and since d = o.r. - i.r., then Equation 5.1 can be written as

$$F_i = 2 \cdot \pi \cdot L \cdot P_i \cdot c_{mi} / \ln(1 + d/i.r.)$$
(5.2)

Table 5.1. Gas permeabilities and permeation rates/unit concentration (given per unit ppm by volume) through a 2.54-cm-long, 0.0305-cm-i.d., 0.0635-cm-o.d. silicone hollow fiber membrane.

	permeability	permeation rate
<u>compound</u>	$(10^{-6} \text{cm}^2/[\text{s} \cdot \text{c}_i])$	$(10^{-10} \text{cm}^3/[\text{s•ppm}])$
nitrogen	2.1	0.46
oxygen	4.0	0.87
argon	4.0	0.87
carbon dioxide	25	5.5
ethene	24	5.2
methane	9.7	2.1
ethane	25	5.5
propane	61	13
butane	76	16
pentane	530	110
hexane	670	150
heptane	1700	370
benzene	1000	220
toluene	2000	440
ethylbenzene	3200	690
chlorobenzene	3000	640
chloromethane	140	31
dichloromethane	740	160
chloroform	900	200
carbon tetrachloride	920	200
chloroethene	120	26
1,1-dichloroethene	600	130
trichloroethene	1400	290
tetrachloroethene	3500	750
bromomethane	140	31
dibromomethane	1200	260
bromoform	5100	1100
methanol	400	87
ethanol	840	180
1-propanol	1000	220
2-propanol	270	58
1-butanol	1100	240
acetone	540	120
2-butanone	1300	280
water	87	19

Therefore, a reduction of the thickness/inner radius ratio for a hollow fiber membrane results in an increase in permeation rates and thus an improvement in the detection limits.

In addition to improved detection limits, faster response times are achieved with thinner membranes. The membrane thickness-response time relationship given by Equation 2.13 shows the response time to be directly proportional to the square of the thickness for both the sheet and the hollow fiber membranes. As stated above, a concern for mass spectrometrists is the potential for the thin-walled membranes to rupture, allowing the sample or process stream to vent the mass spectrometer. In many cases, the polymer membrane is sufficiently strong that leaks are more likely to occur at the sealant used to attach the membrane to the ME device.

Because the enrichment factor is given by the ratio of the permeabilities for two components in a sample, it is not affected by the dimensions of the membrane. Therefore, utilizing membranes that have thinner walls or larger surface areas will improve the speed and sensitivity, but not the selectivity.

#### **TEMPERATURE CONSIDERATIONS**

As described in the previous chapters, the permeation rates for organic compounds from gas phase samples are dominated by the membrane/gas distribution ratio. Because their permeabilities decrease with increasing temperatures, their detection limits increase

(see Table 2.2). The effect of temperature on the permeabilities for organic compounds from water appears to be diffusion-dominated, therefore at higher temperatures, their detection limits improve. Higher temperatures result in increased diffusivities and therefore shorter response times. However, enrichment factors degrade at higher temperatures. In addition, for trace level organic samples, the analyzer pressure follows the permeabilities of the air or water matrix. Therefore, lower temperatures are desired for lower analyzer pressures and to minimize oxygen and water in the mass spectrometer.

For the most efficient membrane extractions, altering the membrane dimensions rather than increasing the temperature is generally better for obtaining improved detection limits and response times. But the choice of membrane thickness is limited to commercial availability or the capability to cast thin, supported membranes that will withstand the pressure differential imposed by the sample and mass spectrometer. With a given membrane, the desire for increased sensitivity and reduced response time must be balanced with the need for efficient separations. Higher temperatures may be warranted for kinetic studies requiring fast response. Processes have been studied at temperatures exceeding 100 °C (16) and performance evaluations have been carried out at temperatures greater than 200 °C (17). The membrane material is rated for a workable temperature range of -54 °C to 249 °C (18). However, the lifetime of the membrane is expected to be reduced at elevated temperatures. At room temperatures, the Silastic material has a

reported shelf-life (for medical uses) of 5 years. The operating lifetime will depend upon the conditions of the application.

#### **SAMPLE FLOW RATE CONSIDERATIONS**

Poor mixing at the sample/membrane interface can cause the formation of a layer of analyte depletion, resulting in low response. This phenomenon is commonly reported by the users of flat membranes (19, 20). The effect of the boundary layer is depicted in Figure 5.3 where the permeation rate is now given by

$$F_i = A \cdot P_i \cdot c_{mi} \cdot / d \tag{5.3}$$

The reduced concentration of analyte i,  $c_{mi}^{\phantom{mi}*}$ , at the interface of the boundary layer and the membrane now establishes the concentration gradient in the membrane. Turbulent flow is preferred, particularly for water samples where the rate of diffusion through the membrane may be greater than through water for many compounds. The transition from laminar flow to turbulent flow occurs at Reynolds number values of 2000-3000 (21),

$$N_{Re} = i.d. \bullet v \bullet \rho / \mu \tag{5.4}$$

where v is the sample linear velocity,  $\rho$  is the density of the fluid, and  $\mu$  is the fluid viscosity. To achieve these values however, volume flows of over 25 cm<sup>3</sup>/minute for water (25 °C) are required in a 0.0305-cm i.d. hollow fiber membrane.

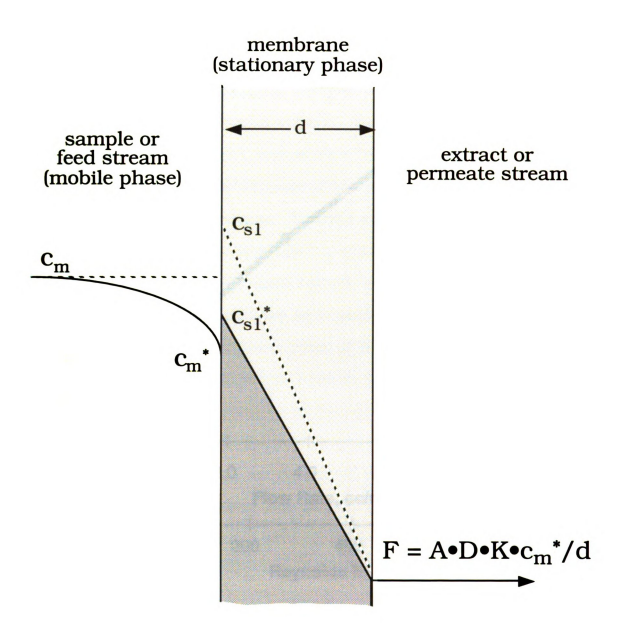


Figure 5.3. A cross-section view of the effect of boundary layers on the permeation process.

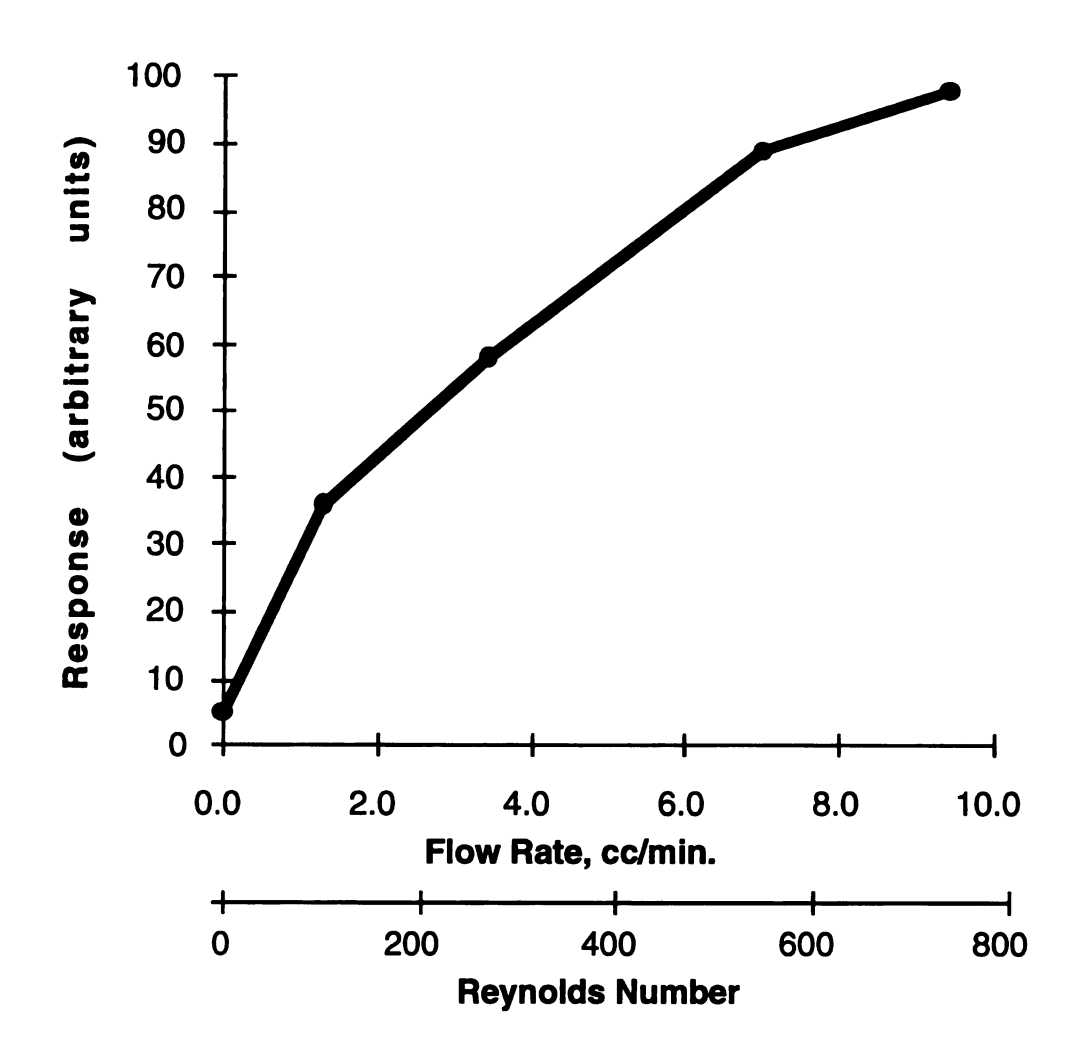


Figure 5.4. Response for toluene vs. sample flow rate through a 2.5-cm-long, 0.0305-cm i.d., 0.0635-cm o.d. hollow fiber.

The effect of linear velocity on response for toluene in water is shown in Figure 5.4. Flow rates approaching 10 cm<sup>3</sup>/minute appear to reduce the boundary layer to dimensions where the change in permeation rate with change in sample flow rate becomes small for most volatile organic analytes studied. When drawing the sample through the 0.0305-cm i.d. hollow fiber by pumping at the outlet, flow rates higher than 10 cm<sup>3</sup>/minute often result in the formation of bubbles in the sample stream. To avoid undue pressurization of the membrane, samples are generally not pushed through the membrane by the sample pump. Increased turbulence (and thus permeation rates) for a given flow rate have been achieved by segmenting the flow stream (22) and packing the interior of the hollow fiber membrane with inert beads (23). These techniques have not been employed in this work.

The observed increases in organic permeation rates from water with increasing temperature may in part be due to the fact that the Reynolds number increases with temperature according to the relation  $N_{Re} = d \cdot v \cdot (0.00538 \cdot T^2 + 2.38 \cdot T + 48.7)$  so that boundary layers are reduced at higher temperatures. This relation was determined from curve-fitting a plot of water density/viscosity ratios (24) vs. temperature.

In addition to reduced steady state response, poor mixing also results in longer response times due to the additional boundary layer through which the analyte must diffuse. Increasing the water flow rate through the hollow fiber from 1.3 cm<sup>3</sup>/minute to 3.5 cm<sup>3</sup>/minute

results in an approximately 50% decrease in  $t_{50}$  measurements for both toluene and dichloromethane. This effect on response time is dependent upon the diffusivity of the substance in the sample matrix and upon the thickness of the boundary layer. Elimination of this boundary layer reduces the response time to the limit imposed by the membrane. For toluene and dichloromethane, response time appear to become constant at flow rates greater than about 8 cm<sup>3</sup>/minute.

When an analyte-depleted boundary layer is established, the observed enrichment factor is reduced due to the depressed analyte/matrix ratio at the sample-membrane interface. A plot of the analyte/matrix response ratio vs. flow rate follows the same trend as that for the analyte response shown in Figure 5.4. The matrix is in such large excess that changes in its response are relatively small. When the permeation rates becomes independent of sample flow rate, so do the organic enrichments.

# THE EFFECTS OF DISTANCE BETWEEN THE MEMBRANE EXTRACTOR AND THE MASS SPECTROMETER

At least two phenomena associated with the ME-MS interface tube may result in extended response times and decreased sensitivities; poor conductance and adsorption. The membrane not only serves to separate the components of interest from the sample matrix, but because the flow rate through the membrane is so small, as shown in Table 5.1, the membrane also provides the necessary pressure drop from the ambient pressure sample to the high vacuum

in the mass spectrometer. For example, the permeabilities and flow rates through the membrane are given in Table 5.2 for nitrogen, dichloromethane, toluene, acetone, and 1-butanol. The nitrogen is the sample matrix and approaches 100% concentration. The organic compounds are 100 ppm by volume in the sample.

Table 5.2. Gas permeabilities and flow rates through a 2.5-cm-long, 0.0305-cm-i.d., 0.0635-cm-o.d. silicone hollow fiber membrane.

	concentration	permeability	flow rate
compound	% by volume	$\underline{\text{cm}}^2/(\underline{\text{s}}\underline{\text{c}}_i)$	$\underline{\text{cm}^3/\text{s}}$
nitrogen	100	2.1X10 <sup>-6</sup>	4.6X10 <sup>-5</sup>
dichloromethane	0.01	7.4X10 <sup>-4</sup>	1.6X10 <sup>-7</sup>
toluene	0.01	2.0X10 <sup>-3</sup>	4.4X10 <sup>-7</sup>
acetone	0.01	5.4X10 <sup>-4</sup>	1.2X10 <sup>-7</sup>
1-butanol	0.01	1.1X10 <sup>-3</sup>	2.4X10 <sup>-7</sup>

The permeate side of the membrane is under high vacuum, therefore molecular flow conditions prevail in the interface tube. In the two-step process of diffusion through an amorphous polymer followed by molecular flow through a tube, the diffusion step will be rate limiting. Since the analytical response for a component is dependent upon the conductance of the component into the ion source, then any effect that the interface tubing might have on conductance would be observed in both the response and the response time. The data in Table 5.3 for steady state response measurements for dichloromethane, toluene, acetone, and 1-propanol showed no significant change with the hollow fiber ME device at distances of 40

cm, 70 cm, and 100 cm from the ion source. In addition, no change in the analyzer pressure was observed for the different lengths of interface tubing.

Table 5.3. The effects of interface tube length on response.

		response factor (intensity/ppm)		
compound	m/z	<u>L=40 cm</u>	L=70 cm	L=100 cm
dichloromethane	84	1600	1600	1600
toluene	91	26000	24000	24000
acetone	58	550	550	550
1-butanol	56	5100	5000	5000

The effect of interface tube length on response times were examined by making step changes in the sample concentration and measuring the time required to reach steady state permeation. The effect of interface tube length on response time for toluene is illustrated in Figure 5.5. No significant changes in these response curves are observed. A plot of response time vs. interface tube length for dichloromethane, toluene, acetone, and 1-butanol are shown in Figure 5.6. Only 1-butanol showed a dependency on the tube length as shown in Figures 5.6 and 5.7. This pronounced dependency on the interface tube length or, more precisely, on the interface tube surface area for alcohols has also been reported by Lauritsen (13). In the present study, this adsorption phenomenon is shown to be minimized by simply heating the interface tube as demonstrated by the large square data point in Figure 5.6 and the plot designated **d** in Figure 5.7.

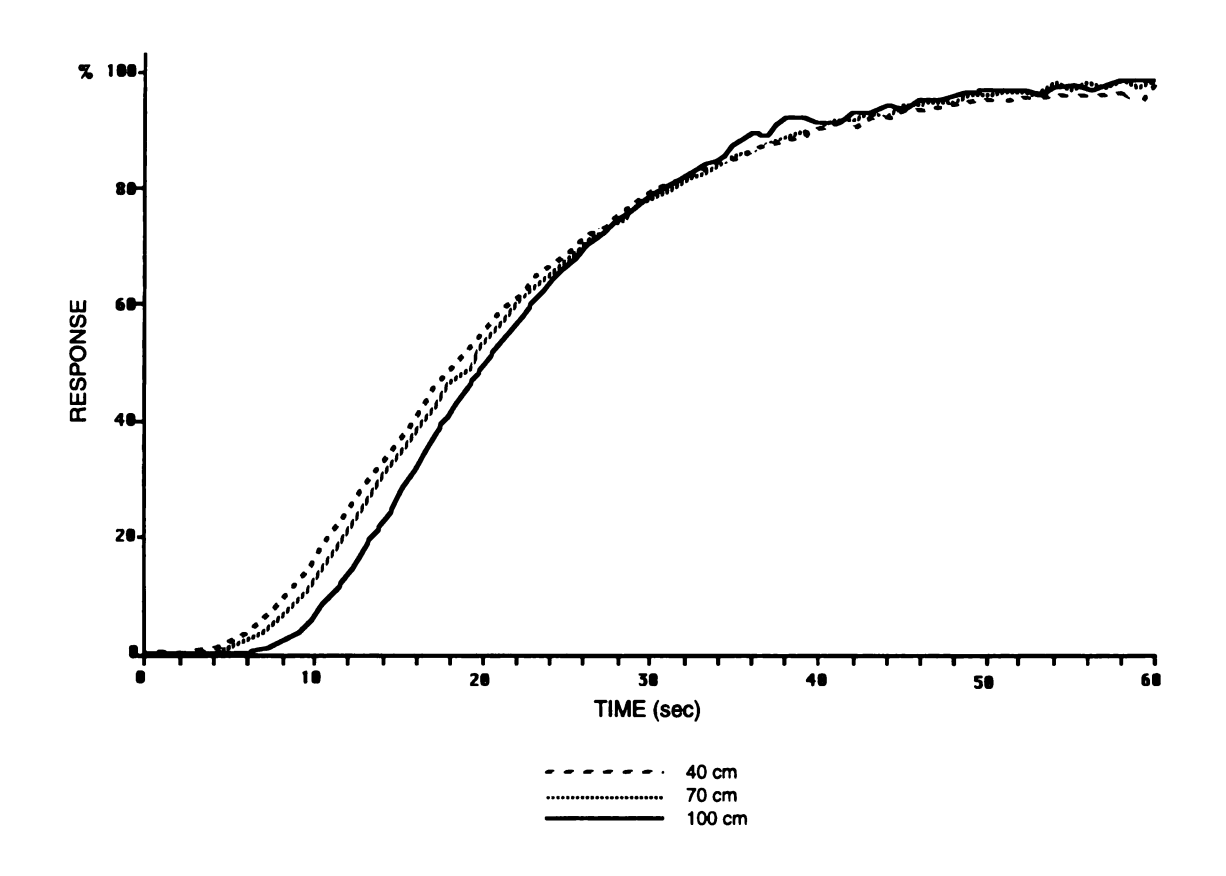
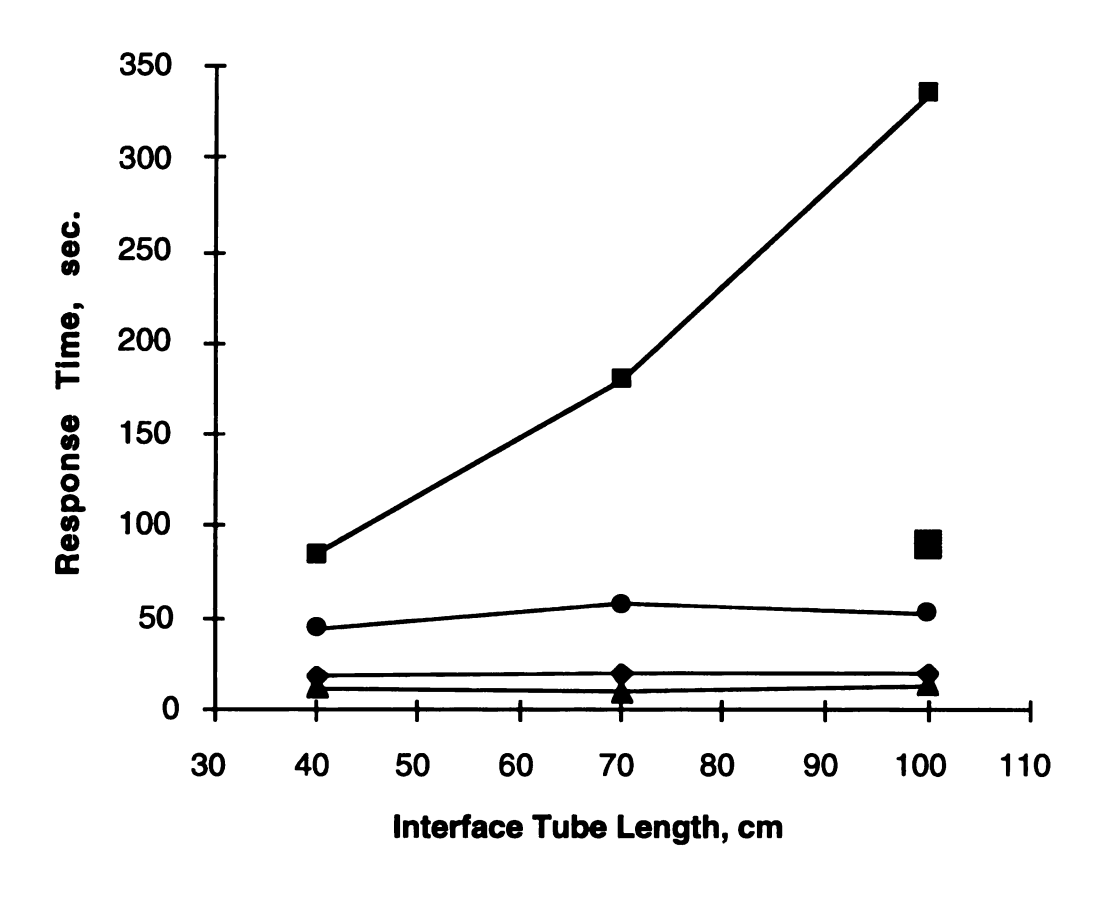


Figure 5.5. The response curves for m/z 92 following a step change in the concentration of toluene in a gas sample with different lengths of ME-MS interface tube lengths.



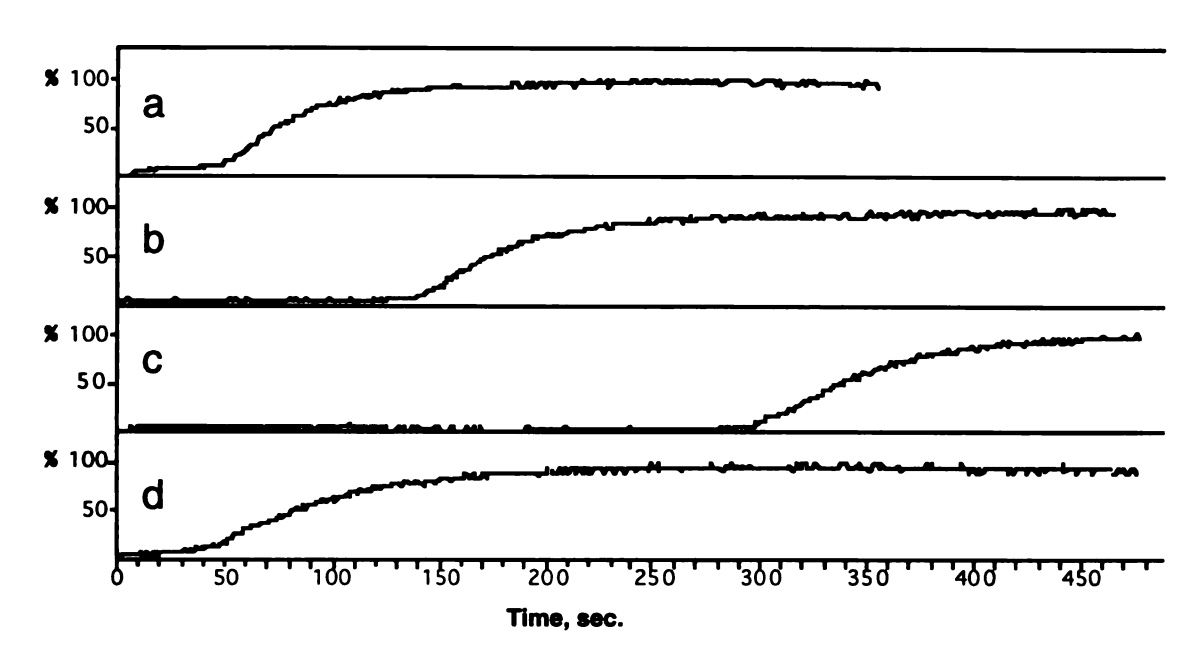
## Key:

square = 1-butanol circle = acetone diamond = toluene

triangle = dichloromethane

large square = 1-butanol with the interface tube heated to 150 °C

Figure 5.6. Response time vs. ME-MS interface tube length for various volatile compounds.



## Key:

- a) 1 = 40 cm, 23 °C
- b) 1 = 70 cm, 23 °C
- c) 1 = 100 cm, 23 °C
- d) 1 = 100 cm, 150 °C

Figure 5.7. The response curves for 1-butanol (m/z 56) with different lengths of ME-MS interface tube.

As discussed in Chapter 2, the response time for a component is defined as the time required to reach 50% of the steady state signal,  $t_{50}$ , following a step change in sample concentration at  $t_0$ . It may also be useful to use an experimental rise time from  $t_{10}$  to  $t_{90}$  to describe the response time of the membrane extraction technique. For Fickian behavior, the correlation of  $t_{50}$  to this rise time is approximated by

$$[t_{90}-t_{10}] = 0.6 \cdot [t_{50}-t_0] \tag{5.5}$$

If Fickian behavior is not observed (e.g., if adsorption/desorption of the analyte on the membrane or analyzer surfaces is the rate limiting step to attain steady state), then this rise time will yield a misleading system response time. The rise time measurement is determined only from the permeate response curve with no reference made to the sample. Values for the rise time and  $t_{50}$  are given in Table 5.4 for 1-butanol. These data illustrate that the rise time gives no indication of the system response time and therefore gives no indication when a change occurs in the sample or process.

Table 5.4. Comparisons between response time  $(t_{50}-t_0)$  and rise time  $(t_{90}-t_{10})$  for 1-butanol.

interface	t <sub>50</sub> -t <sub>0</sub>	$t_{90}$ - $t_{10}$
tube length	<u>seconds</u>	<u>seconds</u>
40 cm	<b>7</b> 5	95
70 cm	180	100
100 cm	340	100
100 cm, 150 °C	80	110

Other causes for non-Fickian behavior are common (25-27). Many rubbery membranes contain fillers such as silica or carbon black to provide mechanical strength (28). As described in Chapters 3 and 4, the silica has a dramatic effect on the response time for molecules that exhibit strong hydrogen bonding due to adsorption/desorption processes occurring within the membrane. If this adsorption/desorption process is reversible, as it appears to be for low molecular weight compounds, then Fickian behavior is observed. However, if a very strong interaction occurs between the filler and the permeating compound, non-Fickian transport would result, resembling the characteristics of adsorption/desorption at surfaces observed in this study.

When transport through the membrane is the rate-limiting step for the response time (i.e., the membrane is near the ion source or no interaction of the analyte with the interface surfaces is observed), then the rise time may yield erroneous values for the system response time. It would appear that the most useful characterization of response time should provide a reference to the sample, e.g.,  $t_{50}$ - $t_{0}$  or  $t_{90}$ - $t_{0}$  (if  $t_{90}$  can be accurately measured), in addition to the rise time (17).

Another major factor that may affect response time that has not been addressed in the previous discussion is the effect of the mass spectrometer. The geometry of the ion source and the vacuum chamber may have a significant effect upon the response time that is independent of the membrane extractor and interface tube. The response time for dichloromethane and toluene are given for three

different mass spectrometers in Table 5.5. Whereas the response time data collected with the MSD and the TSQ are comparable, the response times measured with the Balzers instrument are significantly longer. This phenomenon is presumably due to poor sample gas conductance through the 0.08-cm orifice in the Balzers gas-tight ion source to which the 1/8-inch ME-MS interface tube is connected.

Table 5.5. The effects of analyzer conductance on response time.

	response time (sec.)		
analyzer	dichloromethane	<u>toluene</u>	
Finnigan TSQ-70	11	14	
HP 5971-A MSD	10	11	
Balzers QMG-511	20	35	

#### **MEMBRANE EXTRACTOR CONFIGURATION CONSIDERATIONS**

In general, hollow fiber membranes provide greater extraction efficiencies than do sheet membranes because of the greater sample volume-to-membrane surface ratio and the higher sample linear velocities obtainable. In addition, a flow-over hollow fiber membrane probe can be inserted directly into samples, such as blood vessels in the *in vivo* analysis of blood gases (29), that are beyond the reach of sheet membranes. However, materials for sheet membranes are commercially available in a wider variety of materials and dimensions. In addition, without special equipment, custom-made membranes are more easily prepared in sheet form than hollow fibers. Although the

majority of ME-MS work reported in the literature utilizes poly(dimethylsiloxane) membranes, the development of practical sample-membrane interaction models such as described in Chapters 3 and 4 will undoubtedly result in the use of a variety of materials.

Evaluation of flow-over and flow-through membrane extractors

The comparisons of absolute signal from the analysis of a sample using a flow-over and a flow-through ME device shows a significant advantage for the flow-through configuration. Approximately 50-fold greater response was observed for the flow-through inlet as illustrated in Figure 5.8. Collapsing of the soft membrane in the flow-over configuration resulted in a significant reduction in effective membrane area. Conversely, the inverted pressure drop in the flow-through configuration takes maximum advantage of the membrane inner radius/thickness ratio. For identical volume flows, higher Reynolds numbers are more easily achieved with the flow-through configuration. However, there may be cases where the flow-over configuration is preferred, as it can be made into a probe convenient for on-line monitoring of hazardous or reactive chemicals (10, 16).

Neither the flow-through nor the flow-over inlet displays an advantage in response time when similar sample flow conditions are established. Under similar sample linear velocity conditions, the enrichment factor is also independent of the configuration. The plot in Figure 5.9 shows organic/water signal ratios for the flow-over inlet vs. that for the flow-through inlet with comparable feed linear flows.

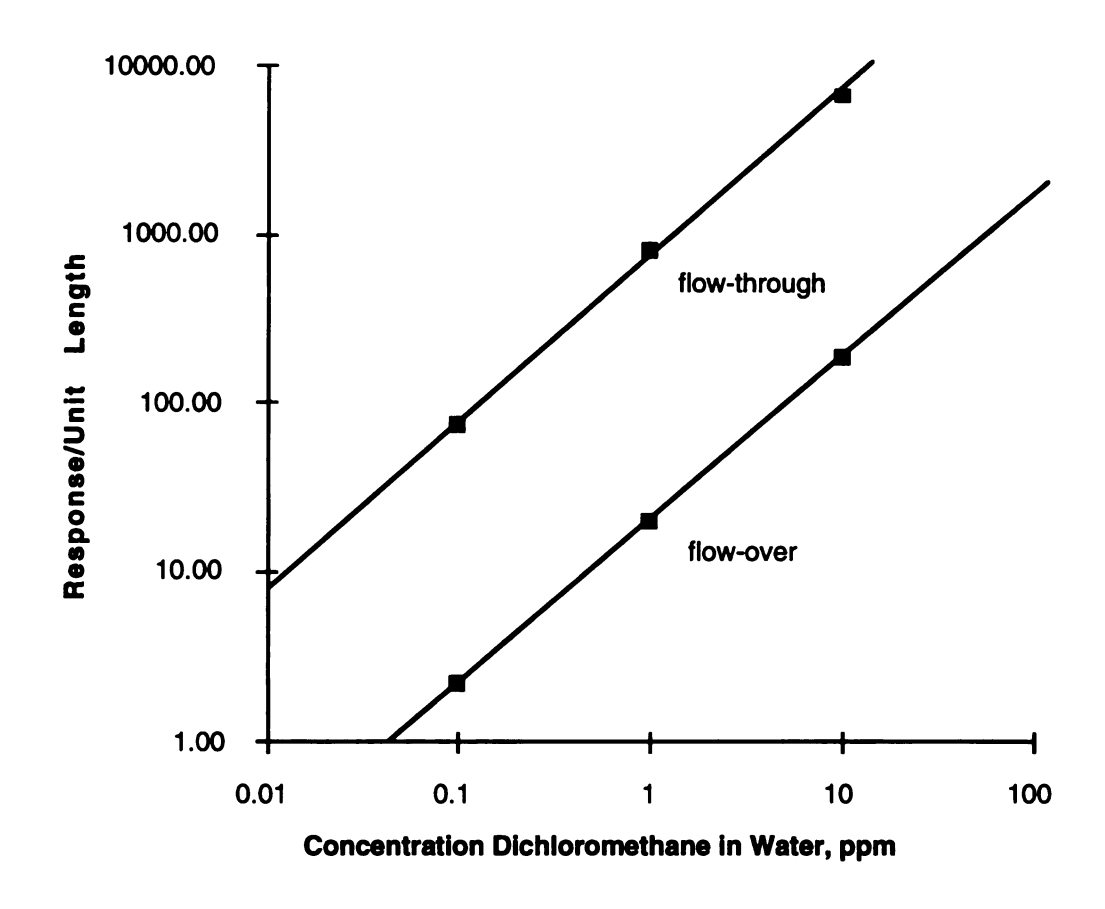
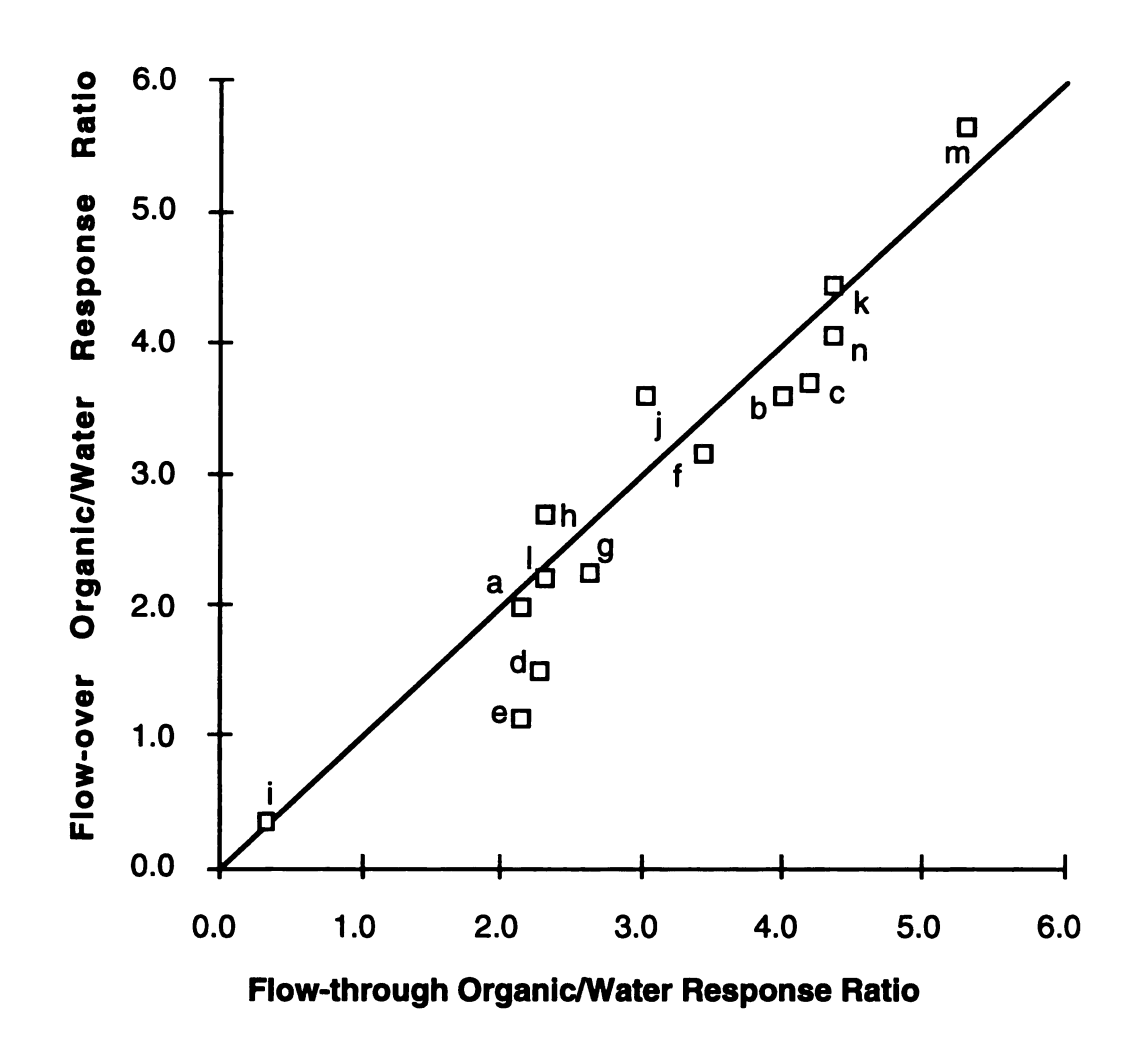


Figure 5.8. Comparison of response vs. concentration plots for the flow-over and the flow-through membrane extractor configurations.



## Key:

a = dichloromethane

c = bromodichloromethane

e = bromoform

g = trichloroethene i = 1,1-dichloroethane k = toluene

m = chlorobenzene

b = chloroform

d = dibromochloromethane f = 1,1-dichloroethene

h = tetrachloroethene

j = 1,1,1-trichloroethane l = ethylbenzene n = 1,2-dichlorobenzene.

Figure 5.9. Relative organic/water response ratios for flow-over vs. flow-through inlets obtained at comparable sample linear velocities.

As expected, no enrichment advantage is observed for either configuration since the permeation rate for water also is affected by the effective membrane area. Again, the flow-through configuration is generally preferred because of the capability to more easily achieve higher linear velocities at relatively low sample volume flows and the effective membrane surface area is maximized.

## Design of the ME Valve

An exploded view of the hollow fiber ME valve is shown in Figure 5.10. This ME device consists of two sections - upper and lower - of the valve body, a valve plunger, a hollow fiber membrane, and some sealant for attaching the membrane to the valve body. The lower section of the valve body was fabricated to fit the upper section and plunger from commercially available solenoid valves (1X259 24VDC normally-closed solenoid valve from Kip Incorporated). The lower section of the valve body is provided with two ports through which samples are pumped into the valve body, through the hollow fiber membrane, and out of the valve body. The membrane is a 2.5-cm length of 0.0305-cm-i.d., 0.0635-cm.-o.d. Silastic medical grade tubing from Dow Corning Corp. The hollow fiber membrane is sealed into the two sample port openings in the valve with Dow Corning RTV 734 Silastic sealant. The analytes selectively permeate through the membrane and into the valve cavity. The permeate stream flows into the mass spectrometer for analysis.

The sheet ME valve design in Figure 5.11 shows that the two sample ports are connected internally by a groove. The membrane

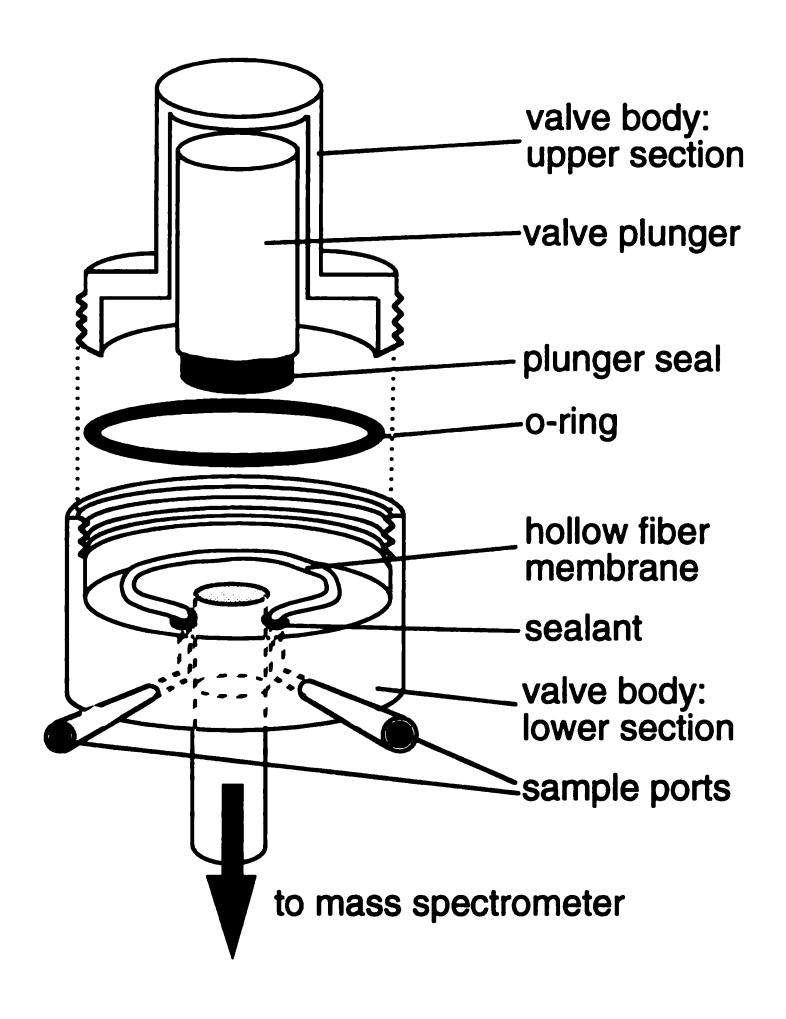


Figure 5.10. Exploded view of the hollow fiber membrane extractor valve.

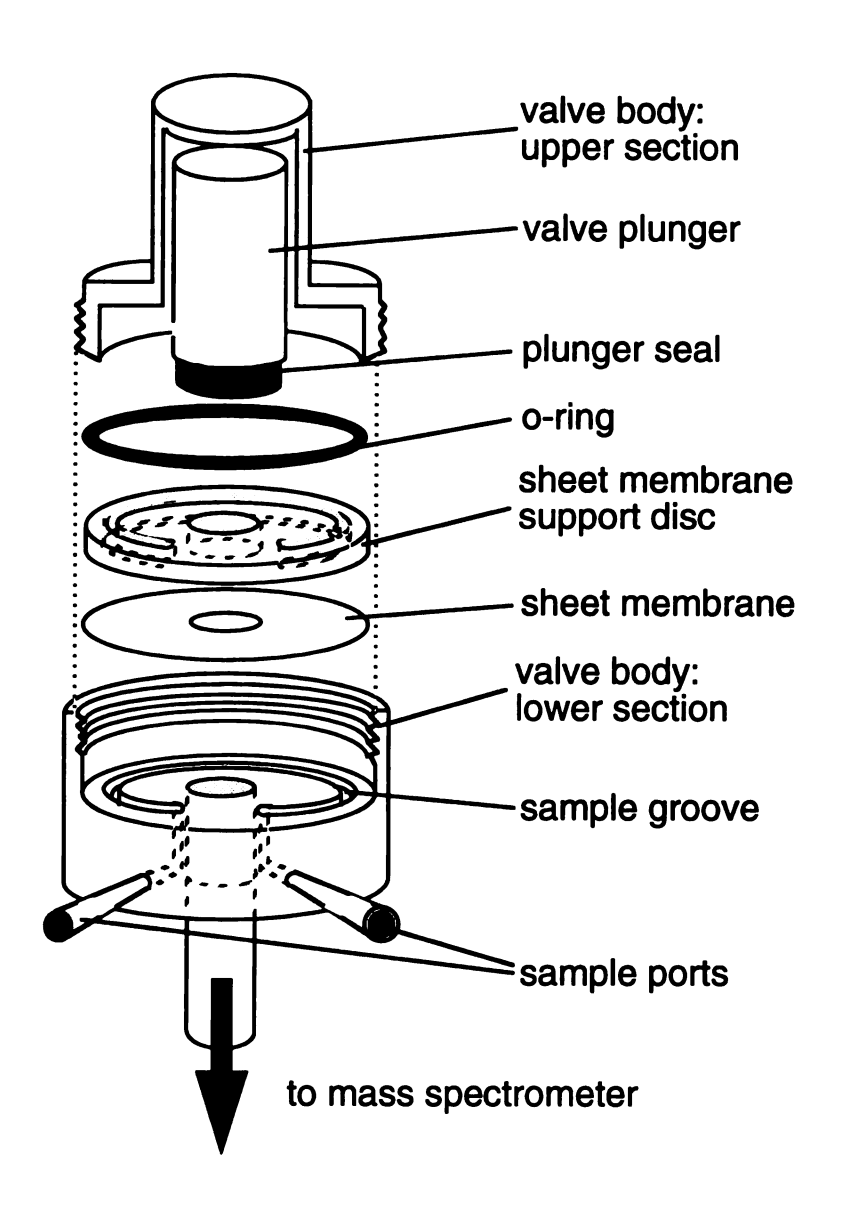


Figure 5.11. Exploded view of the sheet membrane extractor valve.

lays across this groove, separating the sample from the valve cavity. The preferred method for sealing the sheet membrane in the valve is to 'sandwich' the membrane between the valve body and a donut-like disc, as shown in Figure 5.11. A groove through the disc corresponds to the sample channel in the valve body and provides a passage for permeating materials to enter the valve cavity.

The ME valves were mounted to a probe and the ME-MS interface was made with a 1/8-inch (0.32-cm) o.d., 0.22-cm-i.d. stainless steel tube via the direct insertion probe inlet of the mass spectrometer, as shown in Figure 5.12. In addition to the direct insertion probe interface, the ME valve may be mounted directly to the mass spectrometer in a manner similar to solenoid valves commonly used for introducing calibration gases. The void volume in the ME valves (~1 cm<sup>3</sup>) does not cause an excessive pressure surge in the mass spectrometer when the valve was opened. Both the hollow fiber and the sheet ME valves have been successfully evaluated.

No known ME device fulfills all of the requirements stated at the beginning of this chapter for the ideal extraction/sampling device.

The advantages of the ME valve over some currently existing technology include a combination of the following attributes:

- 1) The temperature of the membrane and flow rate of the sample may be well controlled with the ME valve.
- 2) The valve body provides protection to the membrane from physical shock that may cause tearing or rupture.

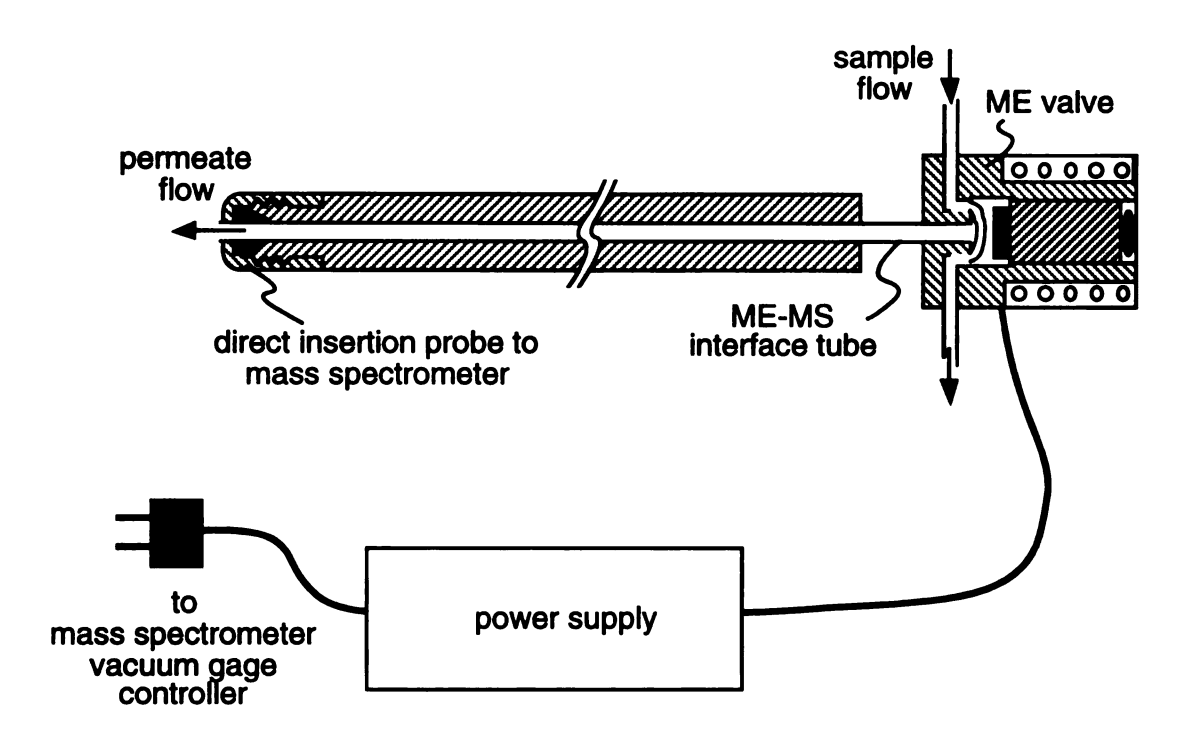


Figure 5.12. A membrane extraction valve coupled to a direct insertion probe.

- 3) The solenoid may be powered through the vacuum-protection circuit of the mass spectrometer so that in the event of a pressure surge due to a membrane rupture or seal failure, the mass spectrometer can be instantly isolated from the sample.
- 4) The device is constructed with a small void volume and surface area. Response times and carry-over are minimized relative to those of membrane extractor and valve in series. Although it may be desirable to minimize the distance between the membrane extractor and the mass spectrometer, this distance is not generally a transport-rate limiting parameter. The interface tube can be made very short and is typically heated independently of the ME valve.
- 5) The ME valve may be placed as close as possible to either the process or the analyzer, depending upon the requirements of the analysis. A variation of the ME valve described above may be used in cases where it is desirable to contact the membrane directly with a reactive or kinetic process. As shown in Figure 5.13, this variation involves expanding the lower section of the valve body so that the process actually occurs within the ME devices.
- 6) The ME valve may be useful in multiple stream sampling where each sample stream requires a separate ME device. If the membranes are housed inside of 3-way valves, then when one ME valve is not activated, the valve cavity may be evacuated through the divert port to an auxiliary vacuum pump to prevent accumulation of permeate.

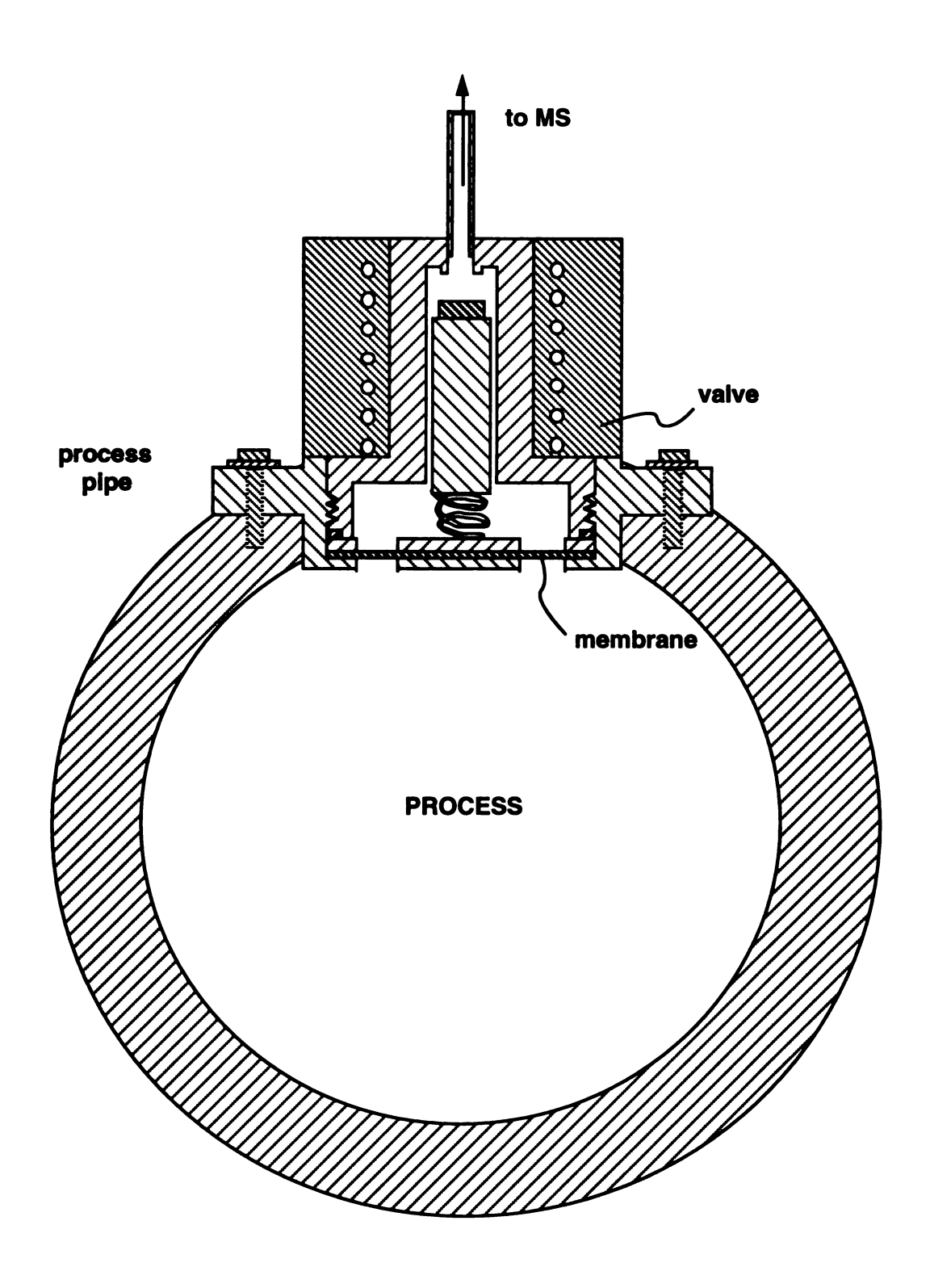


Figure 5.13. A configuration of ME valve where the lower section of the valve is expanded so that the process is carried out in direct contact with the membrane.

## REFERENCES

- (1) Westover, L. B.; Tou, J. C.; Mark, J. H. Anal. Chem. **1974**, 46, 568.
- (2) LaPack, M. A.; Tou, J. C.; Enke, C. G. Anal. Chem. 1990, 62, 1265.
- (3) Lipsky, S. R.; Horvath, C. G.; McMurray, W. J. Anal. Chem. 1966, 38, 1585.
- (4) Kallos, G. J.; Tou, J. C. Environ. Sci. Technol. 1977, 11, 1101.
- (5) Heinzle, E.; Reuss, M., eds. <u>Mass Spectrometry in</u>
  <u>Biotechnological Process Analysis and Control</u>; Plenum Press:
  New York, 1987.
- (6) Langvardt, P. W.; Brzak, K. A.; Kastl, P. E. 34th ASMS Conference on Mass Spectrometry and Allied Topics, 1986, Cincinnati, OH.
- (7) Pungor Jr., E.; Pecs, M.; Szigeti, L.; Nyeste, L. Anal. Chim. Acta 1984, 163, 185.
- (8) Llewellen, P. M.; Littlejohn, D. P. U.S. Patent 3,429,105, February, 1969.
- (9) Harland, B. J.; Nicholson, P. J. D.; Gillings, E. Wat. Res. **1987**, 21, 107.
- (10) Calvo, K. C.; Weisenberger, C. R.; Anderson, L. B.; Klapper, M. H. Anal. Chem. **1981**, 53, 981.
- (11) a) Bier, M. E.; Cooks, R. G.; Tou, J. C.; Westover, L. B. U.S. Patent 4,791,292, 1989.
  - b) Bier, M. E.; Cooks, R. G. Anal. Chem. 1987, 59, 597.

(12)

(13)

(14

(15

(16

(1.

(1

- (12) Bier, M. E.; Cooks, R. G.; Kotiaho, T. 37th ASMS Conference on Mass Spectrometry and Allied Topics, 1989, Miami Beach, FL.
- (13) Lauritsen, F. R. Int. J. Mass Spectrom. Ion Proc. 1990, 95, 259.
- (14) Bredeweg, R. A.; Langhorst, M. L.; Dittenhafer, D. R.; Strandjord, A. J.; Willis, R. S. 16th Annual Meeting of the Federation of Analytical Chemistry and Spectroscopy Societies, Chicago, IL, 1989.
- (15) Hwang, S.-T.; Kammermeyer, K. Membranes in Separations, Robert E. Krieger Publishing Co., Inc.; Malabar, FL, 1984.
- (16) Savickas, P. J.; LaPack, M. A.; Tou, J. C. Anal. Chem. 1989, 61, 2332.
- (17) Bier, M. E.; Kotiaho, T.; Cooks, R. G. Anal. Chim. Acta 1990, 231, 175.
- (18) Medical Materials Business Product Form No. 51-772B-89; Dow Corning Corp., Midland, MI.
- (19) Tojo, K.; Ghannam, M.; Sun, Y.; Chien, Y. W. *J. Cont. Release* **1985**, 1, 197.
- (20) Petropoulos, J. H.; Tsimboukis, D. G. *J. Membrane Sci.* **1986**, 27, 359.
- (21) Perry, R. H.; Green, D. <u>Perry's Chemical Engineer's Handbook</u>, 6th Ed.; Mcgraw-Hill Book Company: New York, NY; 1984.
- (22) Peters, T. L.; Stevens, T. S. U. S. Patent 4,684,470, 1987.
- (23) Stevens, T. S.; Jewett, G. L.; Bredeweg, R. A. Anal Chem. 1982, 54, 1206.

- (24) Weast, R. C.; Astle, M. J.; Beyer, W. H.; eds. <u>Handbook of Chemistry and Physics</u>,64th Ed.; CRC Press, Inc.: Baco Raton, FL; 1983; curve fitted from density data, p. F-5 and viscosity data, p. F-38.
- (25) Crank. J. <u>The Mathematics of Diffusion</u>, 2nd Ed.; Oxford University Press: New York, NY; 1971.
- (26) Korsmeyer, R. W.; Lustig, S. R.; Peppas, N. A. J. Polym. Sci. Polym. Phys. Ed. 1986, 24, 395.
- (27) Everett, D. H. In <u>The Solid-Gas Interface</u>, Vol. 2, Flood, E. A., ed.; Marcel Dekker, Inc.: New York, NY; 1967.
- (28) Lee, G. L.; Stern, S. A.; Mark, J. E.; Hoffman, E. <u>Investigation of Structure-Permeability Relationships of Silicone Polymer Membranes</u>; Final Report October 1982 September 1986; Gas Research Institute: Chicago, IL.
- (29) Brodbelt, J. S.; Cooks, R. G.; Tou, J. C.; Kallos, G. J.; Dryzga, M. D. Anal. Chem. 1987, 59, 454.

## CHAPTER 6

## The Application of Membrane Extraction Mass Spectrometry to the Analysis of Gas and Liquid Process Streams

The efficiency of chemical processes is becoming an increasingly important issue with the growing push toward waste reduction and minimizing organic emissions in air and water. Analytical chemistry can play a vital role in achieving and maintaining optimum process operating conditions. As opposed to off-line analysis, on-line analysis can provide more efficient use of information about a process in terms of the amount of data, the quality of data, and the ability to respond to changes in the process as exhibited by the data (1). As a simple example, the continuos temperature measurements obtained with a thermocouple device can provide a more statistically useful data set and more precise indications of changes in the process temperature than intermittent manual measurements with a thermometer. The same is true for other traditionally measured process parameters such as pressure and pH, as well as the more sophisticated measurements of the process composition. Currently, on-line process composition measurements are often obtained from chromatographic (2), spectroscopic (3, 4), or solid state chemical sensor (5) techniques, as dictated by the nature of the analyte and the process matrix. Although the speed, sensitivity, and selectivity of mass spectrometry make the

technique attractive, on-line analysis by mass spectrometry has until recently been limited to clean, well-defined gas phase streams.

Sampling is generally the most difficult problem associated with the on-line analysis of process streams, regardless of the analytical technique (6). Many gas and liquid process streams are chemically and physically complex and require pretreatment prior to analysis. This has been especially true for mass spectrometry, which has generally utilized a capillary or orifice sample introduction system that is limited to filtered gases. Many sampling problems can be circumvented utilizing membrane extraction techniques. Advantages of sampling with the silicone hollow fiber membranes include the simplicity of the membrane extractor device, the high sample surface area-to-volume ratio in the hollow fiber, the capability to obtain high linear flows at relatively low volume flows, and the ability of the membrane to provide efficient extractions of organic compounds from both air and water. In addition, the inertness of the silicone membrane material makes it suitable for use in many biological and chemically reactive systems. The headspace gases in reactors have been successfully monitored by ME-MS (7-10) as have liquid streams (11-14). However, the simultaneous on-line analysis of the influent and effluent gas and liquid streams of a reactor have not been previously reported.

While previous work focused on the measurement of compounds in either the effluent gas or the effluent liquid, all streams must be considered for complete process characterization. Assumptions made about the quantity of a compound in the influent stream can yield significant errors in the mass balance determinations. As will be demonstrated in this chapter, the measurement of the influent as well as the effluent streams minimizes these errors. A generic process that has liquid influent and effluent streams and gas influent and effluent streams is illustrated in Figure 6.1. This chapter describes the development of an on-line multi-gas/liquid-stream monitoring technique and its application to the simultaneous trace analysis of complex and dirty streams in three wastewater treatment reactors.

### **EXPERIMENTAL SECTION**

### Chemicals

The compounds used in this study were obtained from Fisher Scientific (Fair Lawn, New Jersey) and Aldrich Chemical Company (Milwaukee, Wisconsin). These compounds were generally non polar and relatively insoluble in water, so they were prepared in acetone to facilitate dissolution when spiked into the influent wastewater stream.

Water standards were prepared in a 1-L glass jar of deionized water with the same solutions used to spike the influent water stream. Air standards were prepared in a 100-L Saran<sup>TM</sup> (The Dow Chemical Company, Midland, Michigan) bag filled with air by injecting known volumes of 1:1 mixtures of the two compounds being studied. The standards were analyzed following each reaction analysis.

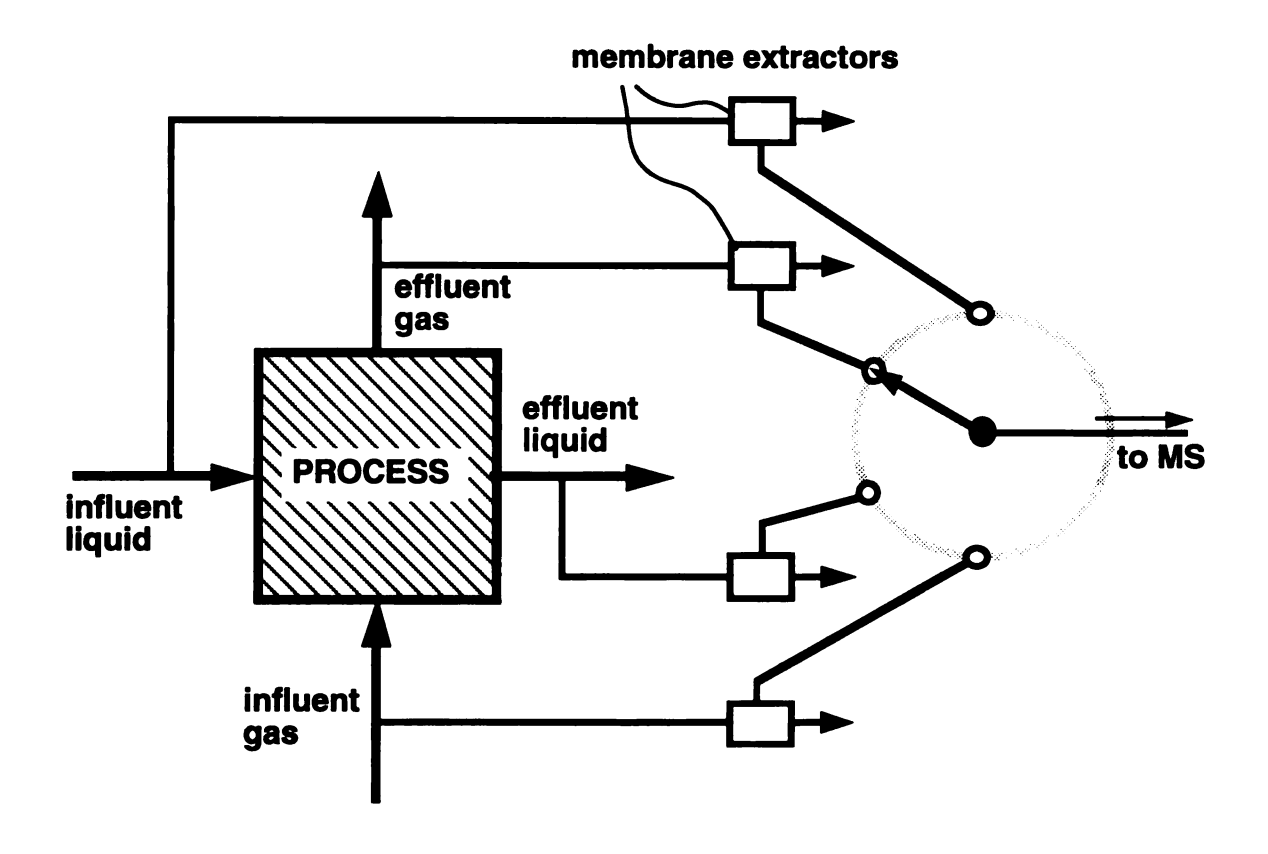


Figure 6.1. A configuration for the influent and effluent analysis by ME-MS of a multi-stream, multi-phase process.

## Analyzer

A Balzers QMG 511 quadrupole mass spectrometer was used in this study. The mass spectrometer, sampling valve, and data acquisition were controlled by in-house written software on a PDP 11-73 computer from Digital Equipment Corporation (Maynard,

Massachusetts). The instrumental conditions were as follows:

Mass range: 60-200 daltons

Scan rate: 30 msec/dalton, 10 scans averaged

Secondary electron multiplier voltage: 1900 V for water streams, 2000

V for air streams.

Analyzer pressure: 1 X 10<sup>-5</sup> torr for water streams, 3 X 10<sup>-6</sup> torr for air streams.

The combination of 10 averaged relatively slow scans was selected because these instrumental conditions provided very good sensitivity for full scans in less than one minute. To the limit where ion transmissions decay at high scan rates, the use of slow scan rates with a quadrupole mass analyzer will provide signal-to-noise ratios comparable to those obtained from averaging several fast scans over the same duration of time.

## Membrane and sampling system

The process streams were pumped from the reactors through the membrane extractors via 6-meter long, 1/8-inch (0.32-cm) o.d. stainless steel tubes. The silicone hollow fiber membranes used in this study were constructed by sealing 2.5-cm lengths of Dow Corning (Midland, Michigan) Silastic<sup>TM</sup> medical grade tubing into 1/8-inch stainless steel tubing tees, as shown in Figure 5.2. The two ends of

the hollow fiber membrane are sealed into stainless steel ferrules with Dow Corning Silastic silicone sealant. For sampling the effluent air streams, 0.0305-cm i.d., 0.0635-cm o.d. hollow fiber membranes were used. The effluent air was pumped through the membrane extractors at the rate of 60 cm<sup>3</sup>/minute with an air pump from Metal Bellows Corp. (Sharon, Massachusetts). Aqueous samples were drawn through 0.147-cm i.d., 0.196-cm o.d. hollow fiber membranes at the rate of 10 cm<sup>3</sup>/minute with fluid pumps from Fluid Metering Corp. (Oyster Bay, New York).

A 1/8 inch SC-12-HT hastelloy-C rotary switching valve from Valco Instruments Co., Inc. (Houston, Texas) was used to interface the membranes to the mass spectrometer. This valve was computeractuated so that a different stream was sampled every 5 minutes. The analyzer side of all inlets, when not selected for sampling to the mass spectrometer, was continuously evacuated by a vacuum pump to prevent accumulation of permeating species. The membranes and valve assembly were mounted in an oven and maintained at 30 °C. The permeation process is temperature dependent, as discussed in Chapter 2, therefore the inlet was maintained slightly above the process and maximum ambient temperatures. The analyzer vacuum chamber and transfer line between the valve and the mass spectrometer were heated to 100 °C.

## Wastewater treatment apparatus

To demonstrate the utility of ME-MS for on-line reaction monitoring of multiple streams, this study was performed with

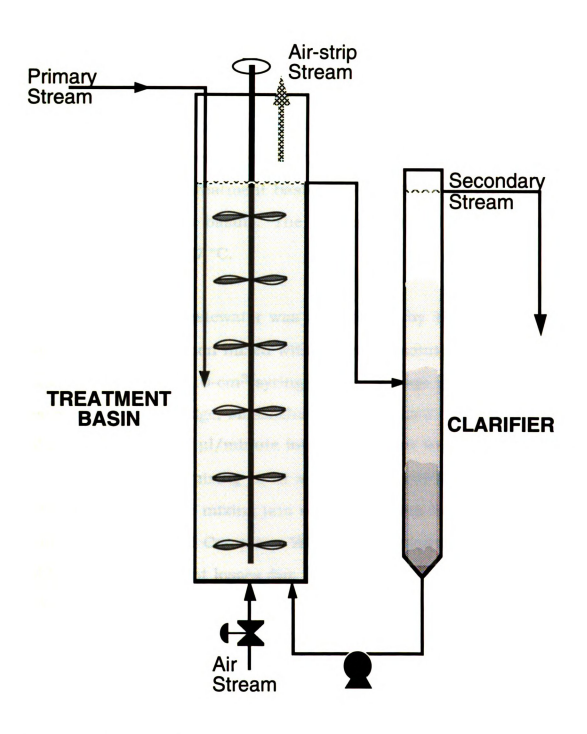
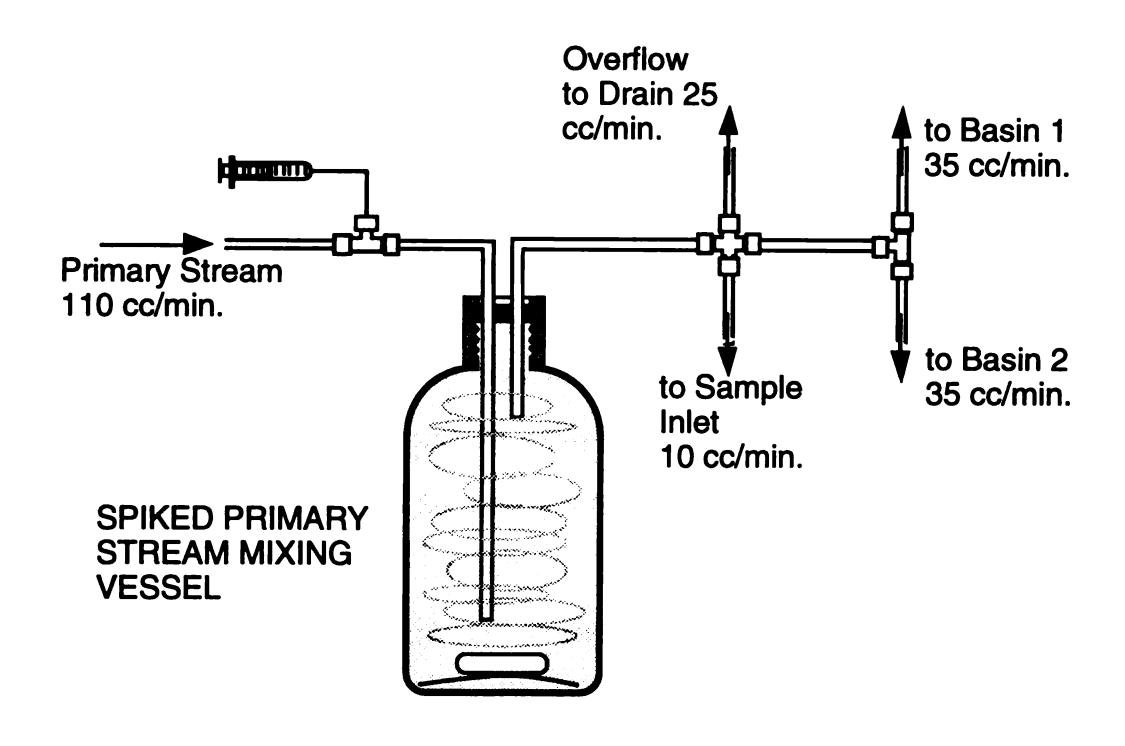


Figure 6.2. A diagram of the wastewater treatment bioreactor.

bioreactors in a wastewater treatment pilot plant at the Dow Chemical Company in Midland, Michigan. The pilot plant consists of three 75-L reactors, depicted in Figure 6.2, that were designed to simulate a large scale treatment process and were stocked with biomass from a general wastewater treatment plant. The flow-through reactors were composed of stirred treatment basins and clarifiers for recycling the biomass back into the basins. The temperature of the reactors was maintained at about 27 °C.

The influent wastewater was first filtered by 100-µm and 50-µm canister filters and then mixed with the spike solution in stirred 1-L glass mixing jars. A 10-cm<sup>3</sup> syringe with a syringe pump from Sage Instruments (Cambridge, Massachusetts) was used to inject the spike solution at a rate of 5  $\mu$ l/minute into the influent wastewater, which was flowing into the mixing jar at a rate of 110 cm<sup>3</sup>/minute (Figure 6.3). The caps of the mixing jars were fitted with Teflon<sup>TM</sup>-(E.I. du Pont de Nemours and Company, Wilmington Delaware) coated silicone rubber seals to prevent losses due to evaporation. The bioreactor influent streams, flowing at a rate of 35 cm<sup>3</sup>/minute, were drawn from the wastewater stream flowing from the mixing jar. A second mixing jar provided an unspiked wastewater stream to a bioreactor used to generate baseline data. The wastewater flows were driven by Masterflex<sup>TM</sup> peristaltic pumps from Cole Parmer Instrument Company (Chicago, Illinois). The influent air continuously flowed at a rate of 900 cm<sup>3</sup>/minute into the bottom of each basin. The tops of the reactors were covered with polyethylene sheeting tight enough to reduce the dilution of the effluent air stream due to air currents in the



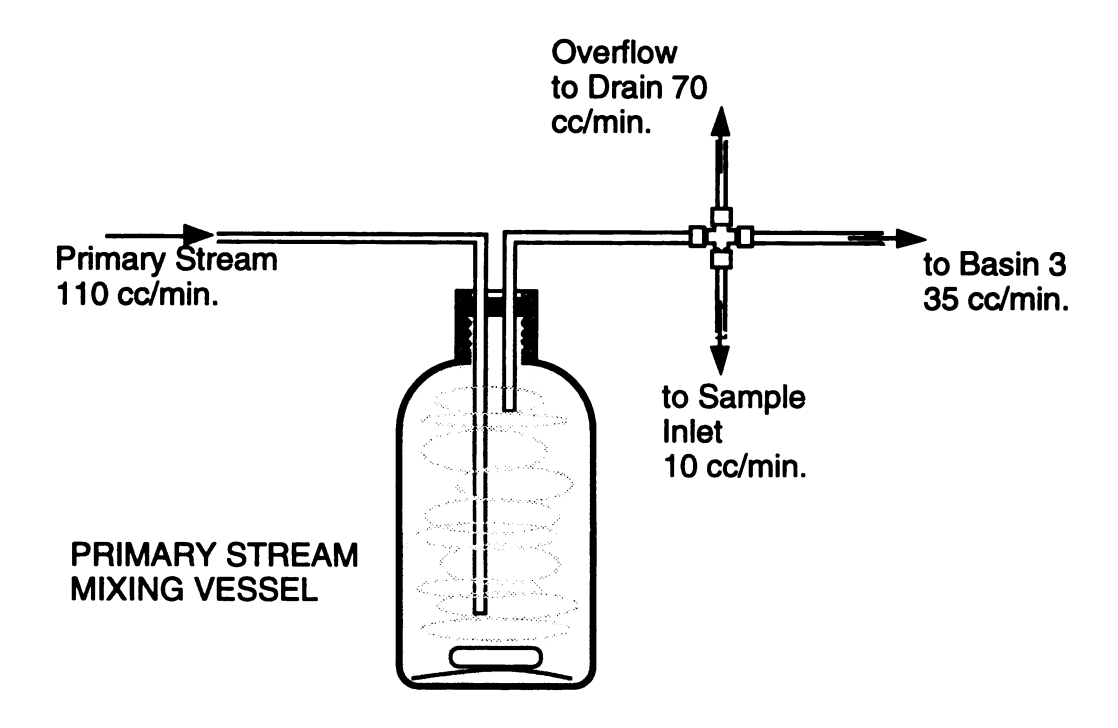


Figure 6.3. The syringe and mixing jar configuration for spiking organic compounds into liquid streams.

room, but not so tight as to cause a positive pressure in the reactor headspace.

#### **RESULTS AND DISCUSSION**

The system developed has been tested and evaluated in the context of process analysis. In many processes, both influent and effluent streams need to be analyzed for complete characterization of the process and to minimize errors due to impurities or inaccurate assumptions about the influent composition. Results of the technology development, performance tests, and an application of the technique to real processes are described below.

## Multi-gas/liquid-stream analysis

By analyzing the streams influent and effluent to a process, as illustrated in Figure 6.1, mass balance determinations can be performed and a more complete picture of a process can be obtained. For a given component entering the process under non-reactive conditions, the steady state mass balance equation is

$$m_{il} + m_{ig} = m_{el} + m_{eg}$$
 (6.1)

and under reactive conditions is

$$m_{il} + m_{ig} = m_{el} + m_{eg} + m_{p}$$
 (6.2)

where m is the mass flow rate for the component in the stream designated by the subscript, and where the subscripts i, e, l, and g designate the influent, effluent, liquid, and gas streams, respectively. The mass flow rate due to uptake of the compound by the process is designated  $m_p$ . The values for  $m_{il}$ ,  $m_{ig}$ ,  $m_{el}$ , and  $m_{eg}$  are determined from the on-line extraction and analysis of the streams and  $m_p$  is calculated from Equation 6.2.

The mass flow rates for a component in the different process streams are calculated by multiplying the process stream concentration (mg/L) by the process stream flow rate (L/minute). For example, the mass flow rate for a component in the influent liquid stream is determined mass spectrometrically from the following equation:

$$m_{il} = F_{il} \circ C_{il} = F_{il} \circ r.f._{std.l} \circ I_{il}$$
(6.3)

where  $C_{il}$  is the concentration of the component in the process stream,  $K_{std}$  is the analytical response factor for the compound obtained from analyzing the liquid standards, and  $I_{il}$  is the response for the compound in the process stream. This equation applies in the determination of both liquid and gas phase mass flow rates after substituting in the appropriate parameters.

It is useful to present the mass balance determinations in Equations 6.1 and 6.2 as percent recovery or percent conversion, defined as follows:

$$%Rec = 100% \cdot (m_{el} + m_{eg})/(m_{il} + m_{ig})$$
 (6.4)

$$%Con = 100\% \cdot m_p / (m_{il} + m_{ig}) = 100\% - %Rec.$$
 (6.5)

Furthermore, the fate of unreacted materials in the process is determined by calculating the percent recovery for the compound in each effluent stream. For example, the unreacted percent recovery for the compound in the liquid effluent stream is calculated as follows:

$$\Re \text{Rec}_{el} = 100\% \cdot m_{el} / (m_{il} + m_{ig})$$
 (6.6)

The capacity to monitor multiple streams and even multiple processes provides the ability to not only make mass balance determinations, but also to analyze reference baseline streams (no added reactants) to make these determinations more accurate. The percent recovery for process A is obtained from Equation 6.7, where the analytical results from process A are background corrected with the results from the baseline process B.

$$\Re \text{RecA} = 100\% \cdot [(m_{el}A - m_{el}B) + (m_{eg}A - m_{eg}B)] 
/[(m_{il}A - m_{il}B) + (m_{ig}A - m_{ig}B)]$$
(6.7)

More accurate results are obtained from determining percent recoveries for each sampling cycle rather than calculating the recoveries from time-weighted averages of each stream, since the background levels and the baseline signals may not be constant over time.

To demonstrate the utility of the ME-MS technique and the importance of analyzing process influent streams, two aqueous streams - one of which was continuously spiked with non polar organic compounds - were analyzed. The streams were a complex matrix of chemical wastewater containing solids and trace level organic contaminants. The diagram in Figure 6.3 shows the syringe and mixing jar configuration for spiking the aqueous stream with the organic compounds. These compounds, their concentration in the acetone dispersant, the mass/charge ratios (m/z) of the ions used for quantitation, and their mg/L-based response factors are listed in Table 6.1. Each spike set contained two of the compounds of interest. The second wastewater stream, which was not spiked, was analyzed in the same manner to obtain a baseline for calculating the spike contribution. An advantage of using hollow fiber membranes for the direct analysis of such complex samples is that fouling of the membrane by solids is inhibited by the high linear sample flows which continuously sweep the membrane surface.

Difficulty was encountered in spiking the aqueous stream - a problem that underscores the importance of analyzing the process influent streams. The measurements of some of the spiked compounds in the stream exiting the mixing jar were initially as low as 5% of the calculated levels. The aromatic compounds in particular showed very poor dissolution into the aqueous stream. Apparently, as the spike solution approached the exit tip of the 1/16-inch stainless steel syringe tubing, the acetone dissolved in the water stream, and the more insoluble organic compounds either precipitated in the

Table 6.1. Spike sets with volume % in acetone, monitored ions, and standard response factors. Baseline response was 0.0005.

		% in		respons	se/mg/L
spike sets		<u>acetone</u>	m/z	<u>in air</u>	in water
1	toluene	7.6	91	8.8	0.088
	dichloromethane	5.0	84	0.6	0.016
2	benzene	7.5	78	9.0	0.10
	carbon tetrachloride	4.2	117	2.5	0.034
3	ethylbenzene	7.6	106	7.6	0.055
	chloroform	4.4	83	2.1	0.060
4	styrene	12.0	104	10.3	0.092
	1,1,2-trichloroethane	7.6	97	2.5	0.030
5	chlorobenzene	6.0	112	1.4	0.018
	tetrachloroethene	4.0	129	0.9	0.006
6	bromoform	3.8	173	0.8	0.007
	1,1,1-trichloroethane	8.2	97	0.3	0.015

bottom of the mixing jar or dissolved back into the acetone solution in the syringe. This problem was not observed when preparing standards by quickly injecting 20 µl aliquots of the spike solutions into a 1-L jar of water. These results suggest that if the linear velocity of the spike solution was increased sufficiently, more complete mixing of the spiked organic liquids into the aqueous phase would occur. The syringe was modified such that a 4-cm length of 50-µm i.d. fused silica tubing was sealed with epoxy into the tip of the syringe needle, through which the spike solution flowed into the influent stream. The modified syringe provided a calculated 400-fold increase in linear velocity for the spiked solution and the spiking efficiency, for the most part, improved dramatically.

The calculated concentrations based upon the amount of compound spiked and the actual measured concentrations of the compounds in the wastewater are listed in Table 6.2. In spite of the improvements in the spiking technique, ethylbenzene continued to exhibit poor spiking efficiencies, possibly due to a combination of the low solubility for ethylbenzene in water (lowest among the compounds studied) and the high affinity of ethylbenzene for solids as noted by Hanna and co-workers (15). During the study of the wastewater treatment process discussed below, the water exiting the mixing jars was used as the liquid influent streams for the bioreactors. The measured influent values - not the calculated values - were used in the bioreactor mass balance determinations, thus minimizing the errors that may result from the false assumption that the spikes were 100% efficient.

Table 6.2. Spike concentrations (mg/L) in the influent wastewater.

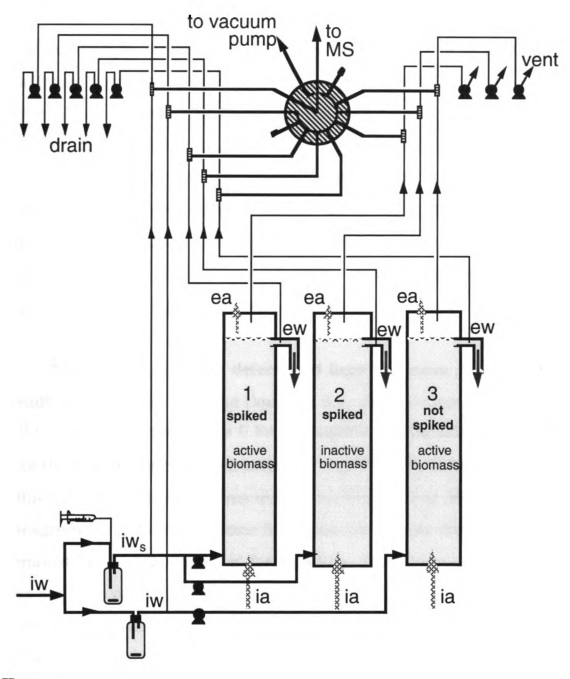
<u>calculated</u>	measured
3.57	2.35
3.57	3.40
3.47	0.49
3.47	2.66
3.54	3.71
3.61	3.61
5.78	5.39
5.81	5.81
3.43	4.69
3.36	3.75
5.95	2.98
5.95	3.78
	3.57 3.57 3.47 3.47 3.54 3.61 5.78 5.81 3.43 3.36 5.95

Application to a biological wastewater treatment process

The analyses of volatile organic compounds in wastewater and air are most commonly performed off-line after first extracting and concentrating the organic compounds from the matrix (16, 17). These procedures are often laborious, time-consuming, and require sample manipulation. With ME-MS, the on-line extraction, concentration, and analysis of the influent liquid and the effluent liquid and gas streams from the process shown in Figure 6.2 were performed nearly simultaneously. The influent air streams were analyzed for purity by ME-MS prior to the on-line analyses, but were not continuously monitored.

The process for the removal of volatile organic compounds from the wastewater mainly occurs via two mechanisms in a bioreactor: biodegradation and air-stripping. In many cases, these appear to be rate-competitive processes such that biodegradation of many compounds is improved when their residence time in the "biomass" is increased, i.e., when air-stripping is reduced. However, for aerobic biodegradation, aeration of the biomass is required, implying that some air-stripping is inevitable. The process shown in Figure 6.2 was studied by performing mass balance determinations for the organic priority pollutants listed in Table 6.1. With the multi-gas/liquid-stream analysis capability, process mass flow rates were determined for three different reactors. As shown in Figure 6.4, each reactor was prepared differently: In reactors 1 and 2, the influent wastewater was continuously spiked to 3-6 mg/L with the target compounds. Reactor 3, serving as the analytical blank or reference, was not spiked. Reactor 2, the analytical test sample, was spiked, but its biomass was rendered non-reactive by maintaining the contents at pH less than 2.

The aqueous streams were analyzed with the flow-through silicone hollow fiber membrane extractor with a 0.147-cm i.d., 0.196-cm o.d. hollow fiber membrane. A Reynolds number value of approximately 160 was achieved for the 10 cm<sup>3</sup>/minute sample flows from the wastewater influent and effluent streams. By minimizing the effects of boundary layers, Reynolds numbers approaching 800 have been shown to improve the membrane extraction efficiency for many compounds as discussed in Chapter 5. Reynolds number values of 800 were achieved with a 10 cm<sup>3</sup>/minute wastewater flow by utilizing a 0.0305 cm i.d. hollow fiber membrane, but plugging with solids and sludge resulted. A sample flow of 50 cm<sup>3</sup>/minute in the larger hollow



#### Key:

iw = influent wastewater stream
iw<sub>s</sub> = spiked influent wastewater stream
ia = influent air stream
ew = effluent water stream
ea = effluent air stream.

Figure 6.4. A process flow diagram illustrating the spiking and online sampling of three wastewater treatment bioreactors.

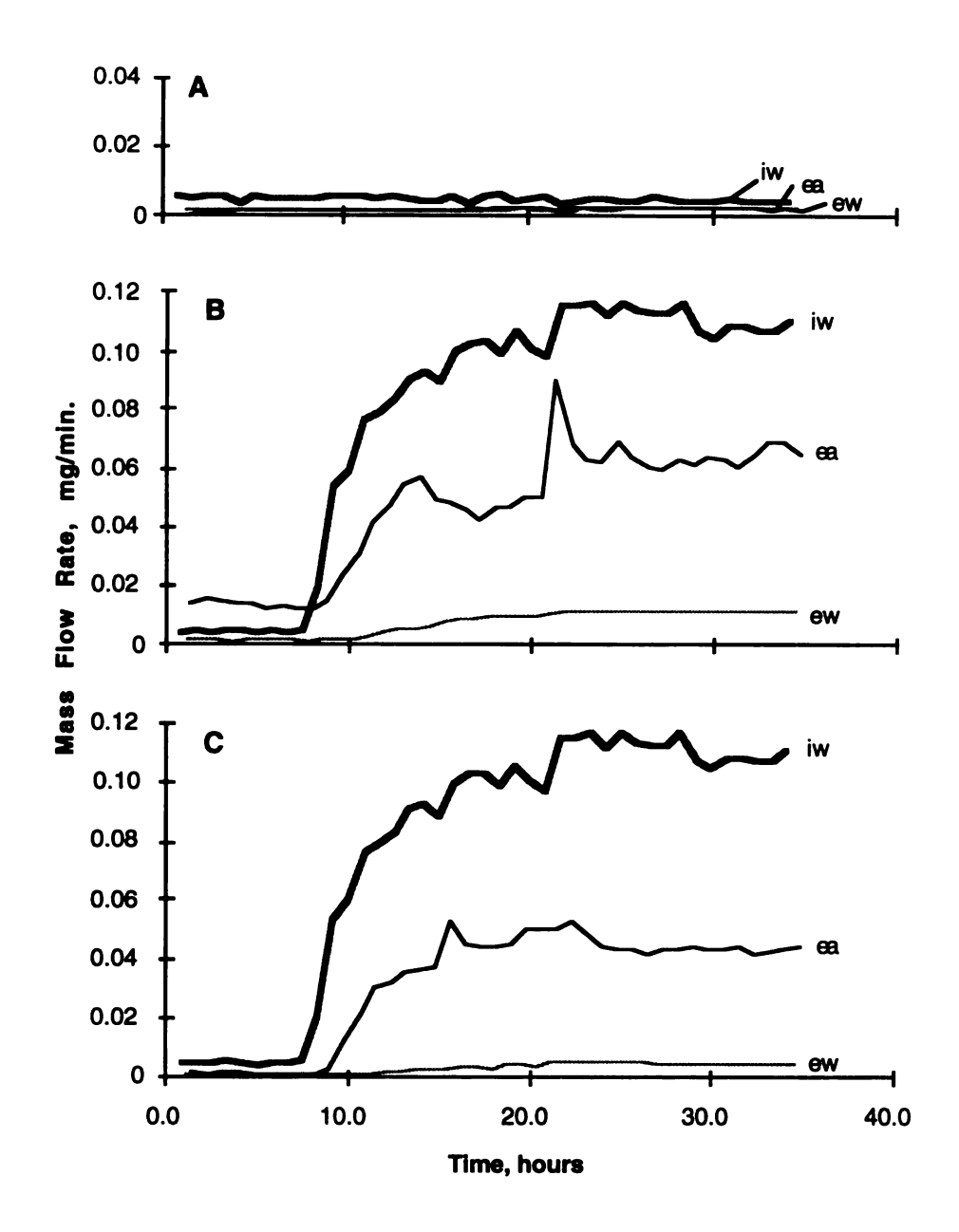
fiber would be required to attain these Reynolds numbers, but due to limits on sample consumption, 10 cm<sup>3</sup>/minute was chosen as the maximum flow rate. Zero sample consumption could have been achieved by recycling the sample streams back into the process, however, this was not done in this study. In any case, the sensitivities were sufficient with the larger diameter membrane. The effluent air samples were pumped through the 0.0305-cm i.d. hollow fiber at a rate of 60 cm<sup>3</sup>/minute. Convective mixing of the air streams is not as important because the diffusion of organic vapors in air is much more rapid than permeation through the membrane.

Mass flow rates were determined from the mass spectrometric steady state process data and Equation 6.4. Pure air was used for the influent gas, therefore  $m_{ig}$  = 0 for the organic compounds. Table 6.3 lists the steady state concentrations in mg/L for the compounds in the effluent water and air streams in the reactive process (with the background signal from reactor 3 subtracted). These data demonstrate the capability of the technique to provide sensitive online analyses of the physically and chemically complex multi-phase process. Mass flow rate vs. time plots are displayed in Figures 6.5 and 6.6 for carbon tetrachloride and benzene, respectively, from the three reactors. Carbon tetrachloride was observed to be much more inert to the action of the biodegradation process than was benzene, as discussed in more detail below. As demonstrated by these plots, mass flow rate determinations can be more meaningful than concentration values when defining a chemical process.

Table 6.3. Concentrations (mg/L) detected in the effluent water and the air streams in the reactive process. Styrene and chlorobenzene are not detected (N.D.) above the baseline in the effluent water.

compound	effluent water	<u>effluent air</u>
dichloromethane	0.41	0.003
chloroform	0.32	0.044
carbon tetrachloride	0.07	0.046
1,1,1 trichloroethane	0.30	0.073
1,1,2 trichloroethane	2.09	0.076
tetrachloroethene	0.15	0.065
bromoform	1.58	0.026
benzene	0.07	0.005
toluene	0.31	0.012
ethylbenzene	0.01	0.005
styrene	N.D.	0.003
chlorobenzene	N.D.	0.003

The percent recoveries for reactor 1 were calculated from Equation 6.7 with reactor 3 providing the background values. The percent recoveries from reactor 2 were calculated from the steady state mass flow rates using Equation 6.4. A fourth reactor, not spiked and containing non-reactive biomass, would provide baseline data for reactor 2, but was not available for this study. For these calculations, it was assumed that the signal was due entirely to the compound of interest. The percent recoveries for each compound in reactors 1 and 2 are summarized in Table 6.4. Had the amount of spiked compound added to the reactor influent been assumed to be correct and not measured, serious errors in the mass balance determinations would have resulted. The data in Table 6.4 demonstrate the capacity of the



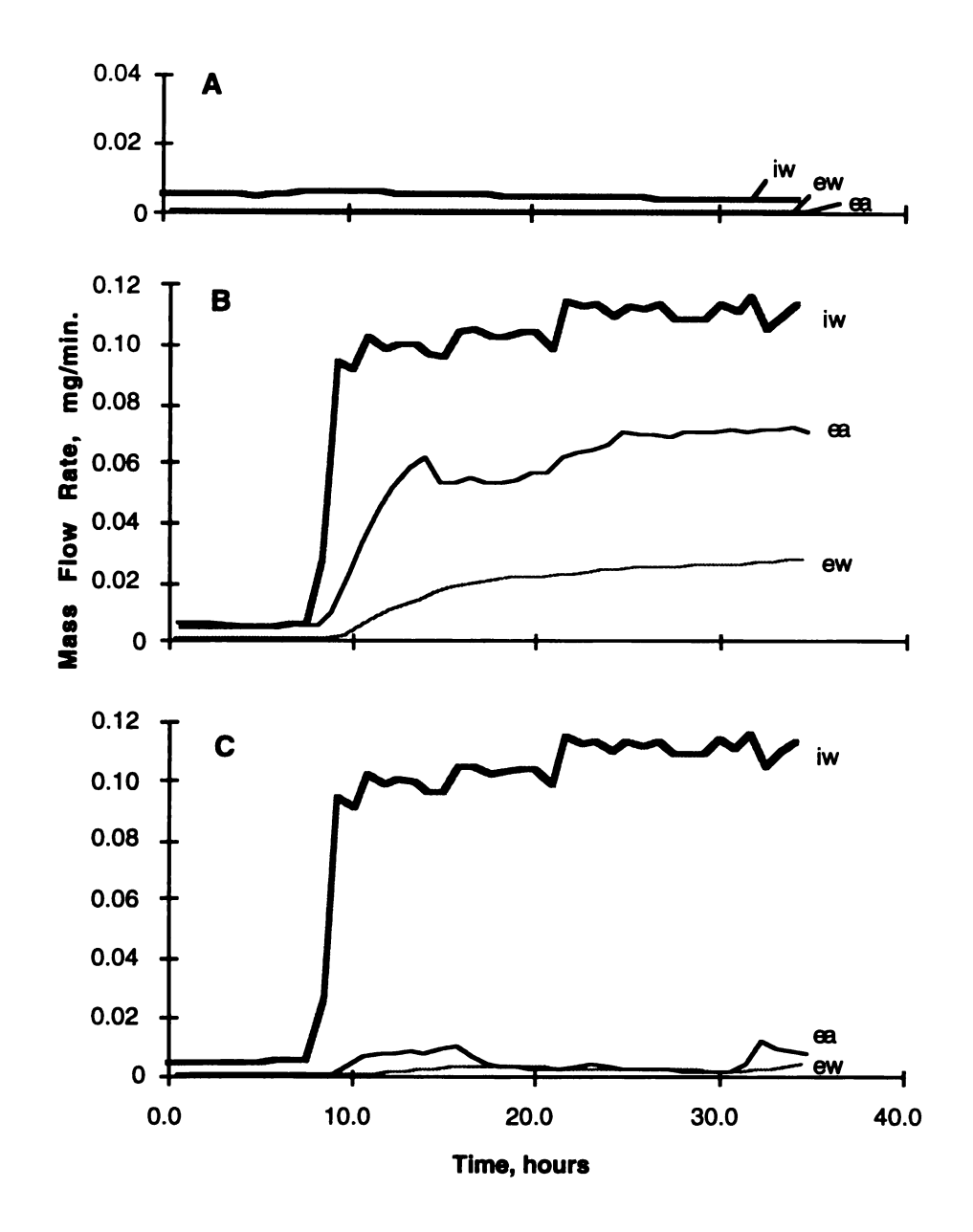
## Key:

iw = influent wastewater stream

ew = the effluent water stream,

ea = effluent air stream

Figure 6.5. Mass flow rate plots for carbon tetrachloride in A, reactor 3 (reactive, not spiked), B, reactor 2 (non-reactive, spiked), and C, reactor 1 (reactive, spiked). The spike was begun at the 8-hour mark.



### Kev:

iw = influent wastewater stream

ew = the effluent water stream,

ea = effluent air stream

Figure 6.6. Mass flow rate plots for benzene in A, reactor 3 (reactive, not spiked), B, reactor 2 (non-reactive, spiked), and C, reactor 1 (reactive, spiked). The spike was begun at the 8-hour mark.

on-line analytical system to determine the relative inertness of different organic materials to a reactive process, where the substances exhibiting higher percent recoveries are more inert to the process.

Table 6.4. Percent recoveries and standard deviations for the spiked organic compounds.

compound	reactive process	non-reactive process
dichloromethane	15; 1	100; 4
chloroform	64; 3	92; 5
carbon tetrachloride	42; 1	<b>72</b> ; 3
1,1,1 trichloroethane	69; 4	85; 6
1,1,2 trichloroethane	77; 7	87; 8
tetrachloroethene	59; 7	103; 4
bromoform	80; 14	105; 12
benzene	6; 4	88; 4
toluene	29; 2	100; 6
ethylbenzene	34; 33	113; 20
styrene	2; 1	75; 6
chlorobenzene	2; 1	96; 3

The capacity to determine the relative air-stripping process efficiencies for the different compounds is also demonstrated. The fractions of the organic compounds remaining in the effluent water and removed from the water by the air-stripping process were calculated using Equation 6.6 and are given in Tables 6.5 and 6.6, respectively. Again, the results for reactor 1 are baseline-corrected.

Table 6.5. Percent recoveries and standard deviations in the effluent water streams.

compound	reactive process	non-reactive process
dichloromethane	12; 1	30; 2
chloroform	12; 2	18; 1
carbon tetrachloride	2; 1	11; 1
1,1,1 trichloroethane	8; 2	10; 1
1,1,2 trichloroethane	36; 4	41; 4
tetrachloroethene	4; 1	9; 1
bromoform	53; 11	74; 11
benzene	2; 1	24; 1
toluene	13; 1	21; 2
ethylbenzene	1; 1	19; 1
styrene	0; 1	18; 1
chlorobenzene	0; 1	17; 1

Table 6.6. Percent recoveries and standard deviations in the effluent air streams.

compound	reactive process	non-reactive process
dichloromethane	3; 1	70; 2
chloroform	<b>52</b> ; 3	75; 4
carbon tetrachloride	40; 1	61; 3
1,1,1 trichloroethane	61;4	<b>75</b> ; <b>5</b>
1,1,2 trichloroethane	41; 3	46; 4
tetrachloroethene	55; 7	94; 4
bromoform	27; 3	31; 3
benzene	4; 3	<b>64</b> ; <b>2</b>
toluene	16; 1	79; 5
ethylbenzene	33; 33	94; 20
styrene	2; 1	58; 5
chlorobenzene	2; 1	79; 3

The background-corrected fraction of organic material removed due to uptake by the biomass in reactor 1 was calculated from Equation 6.5. This bio-uptake term represents the unrecovered fraction of material and may be a combination of biological fermentation and absorption. The actual percent removal due to the biomass may be affected by other factors. Deviations from 100% recoveries in the non-reactive process in reactor 2 are presumed to be due to experimental error as well as the presence of solids. These deviations are assumed to be consistent for the three reactors. Therefore, given the capacity to monitor all of the reactors, the recoveries from reactor 2 could be used as correction factors in calculating corrected bio-uptake values:

$$\%$$
Bio-uptake<sub>1</sub>(corrected) =  $100\%$ •[1 - ( $\%$ Rec<sub>1</sub>/ $\%$ Rec<sub>2</sub>)] (6.8)

Both the uncorrected and corrected (given in parentheses) values for the bio-uptake are listed in Table 6.7, along with values reported in the literature from off-line analyses (18-23). The capability to demonstrate the relative reactivity of the different compounds in biological wastewater treatment processes is provided by these analyses.

In most cases, the percent bio-uptake results from this study are consistent with the percent biodegradation values reported in the literature. The greatest disparity is observed for 1,1,1-trichloroethane and tetrachloroethene, where essentially no biodegradation was reported in one literature reference (18), although bio-uptake of 19%

Table 6.7. Percent bio-uptake and standard deviations.

Experimental values corrected for the recoveries in the analytical test reactor (reactor 2) are given in parentheses.

compound	experimental		literature
dichloromethane	85; 1	(85; 1)	50-95 <sup>b</sup> , 100 <sup>d</sup> , 96 <sup>e</sup>
chloroform	37; 3	(31; 4)	50-95 <sup>b</sup> , 0 <sup>a</sup>
carbon tetrachloride	58; 1	(41; 4)	50-95 <sup>b</sup>
1,1,1 trichloroethane	31; 4	(19; 4)	5b, 0a
1,1,2 trichloroethane	23; 7	(12; 2)	
tetrachloroethene	41; 7	(42; 7)	Oa
bromoform	20; 14	(24; 7)	
benzene	94; 4	(94; 4)	50-95 <sup>b</sup> , 85-88 <sup>f</sup>
toluene	71; 2	(71; 1)	50-95 <sup>b</sup> , 84-88 <sup>f</sup> , 40-79 <sup>c</sup>
ethylbenzene	66; 33	(70; 28)	50-95 <sup>b</sup> , 85-97 <sup>f</sup> ,
styrene	98; 1	(97; 1)	
chlorobenzene	98;1	(98;1)	91 <sup>a</sup> , 79-93 <sup>c</sup>

## Key:

a = Reference 18

b = Reference 19

c = Reference 20

d = Reference 21

e = Reference 22

f = Reference 23.

and 42%, respectively, were observed in this study. As with any process, biodegradation is highly dependent upon the reaction conditions. The age and species of biomass, organic influent concentration, mineral nutrient content, process flow rate (retention time), oxygen concentration, temperature, pH, and other factors influence the biodegradation process. As is apparent from the comparison of literature values, the results can vary widely depending upon these process conditions. For example, one study (18) showed no biodegradation of chloroform (as well as 1,1,1-trichloroethene and tetrachloroethene), while another (19) reported the biodegradation of chloroform to be in a range of 50-95%. A corrected value of 31% biouptake for chloroform was observed in this study.

In spite of the use of filters, the flow of sludges and small particulates was constantly observed in the influent wastewater. The concentration of solids was not constant and could not be predicted. The influent water was sometimes clear one day and turbid with solids the next day. These solids apparently were road dirt (earth moving vehicles were working in the area), tars, and sludge from aggregated biomass. Extracting the organic compounds from this physically complex wastewater matrix was a crucial step in these experiments, because sample matrix effects can lead to large errors in trace analyses (24). Even small errors in a stream analysis may result in large errors in the mass balance determinations.

Frequently, the presence of solids affected the process when the solid levels became particularly high in the influent wastewater,

causing the recoveries to become significantly depressed. For example, when high turbidity was observed during one process analysis, mass balance determinations for dichloromethane and toluene around the non-reactive process (reactor 2) showed recoveries of only 39% and 32%, respectively. Large differences were still observed between the reactive and non-reactive processes for this experiment, where mass balance determinations around the reactive process (reactor 1) showed recoveries of only 1.6% for dichloromethane and 1.0% for toluene.

These results demonstrate the capacity of the analytical system to monitor the effects of solids on the emissions of organic vapors from wastewater. However, the absorption of the organic compounds into the solids represented another process, thus introducing another uptake variable into the mass balance equation. This second uptake variable was difficult to separate from the bio-uptake variable and it was not within the scope of this study to do so. Therefore, when poor recoveries were observed from reactor 2, the experiment was repeated after the influent water became less turbid. As a result, the recoveries were sufficient for reactor 2 (mean percent recovery = 93,  $\sigma$  = 12) considering the complexity and the concentration levels of the process streams. Relatively large standard deviations in the recoveries exhibited for ethylbenzene are likely due to its low influent concentration (0.49 mg/L) which enhances the effects of random error and process baseline changes. Again, these results demonstrate the importance of analyzing the influent stream rather than relying on the calculated spike values.

When the process flows were interrupted for some reason (e.g., pump failure or plugging of the stainless steel sampling tubes) and solids dried on the membranes, the permeation characteristics changed. This happened occasionally and simply required replacement of the membranes. Following each study (every 3-4 days), the sample tubes and membranes for sampling the wastewater streams were flushed with clean tap water and allowed to sit for several hours to prevent the growth of anaerobic bacteria on the inside of the tubing. The membranes that were used to sample the gas streams showed no observable change in properties throughout these experiments.

#### CONCLUSIONS

It has been demonstrated that, with little or no sample preparation, membranes can be used as an effective interface between complex and dirty matrices (gas and liquid) and a mass spectrometer. The use of a single technique and a single analyzer for a multi-phase and multi-stream process minimizes experimental errors and simplifies calibration. The analytical system can be used to study, optimize, and potentially to help control and automate processes. In addition to the determination of the fate of organic compounds in waste treatment processes, other applications include the on-line study of fermentation, distillation, absorption, devolatilization, stripping, degassing, and membrane separation processes. The reliability of the continuous analysis of such processes depends upon a) the general reliability of the analyzer, b) the reliability of the sampling

system, and c) the reliability of the process itself. Mass spectrometers for process monitoring are commercially available and have demonstrated reliability for specific applications. However, as stated at the beginning of this chapter, sampling the process is generally the limiting factor such that the analyzer is only as good as the sample introduction system. Ultimately, the analysis depends upon routine maintenance and the continuous operation of the process at the range of conditions for which it - and the sampling system - was designed.

#### REFERENCES

- (1) Callis, J. B.; Illman, D. L.; Kowalski, B. R. Anal. Chem. **1987**, 59, 624A.
- (2) Manka, D.P. <u>Automated Stream Analysis for Process Control</u>, Vol. 1; Academic Press: New York, NY; 1982.
- (3) Eckstein, R. J.; Owens, G. D.; Baim, M. A.; Hudson, D. A. *Anal. Chem.* **1986**, 58, 2316.
- (4) Seitz, W. R. Anal. Chem. 1984, 56, 16A.
- (5) Schuetzle, D.; Hammerle, R. <u>Fundamentals and Applications</u> of <u>Chemical Sensors</u>, ACS Symposium Series 309; American Chemical Society: Washington, DC; 1986.
- (6) Blaser, W. W.; Ruhl, H. D.; Bredeweg, R. A. *Amer. Lab.* January **1989**, 69.
- (7) Tou, J. C.; Westover, L. B. J. Phys. Chem. **1974**, 78, 1096.
- (8) Kallos, G. J.; Tou, J. C. Environ. Sci. Technol. 1977, 11, 1101.
- (9) Savickas, P. J.; LaPack, M. A.; Tou, J. C. Anal. Chem. 1989, 61, 2332.
- (10) Van Nugteren-Osinga, I. C.; Bos, M.; Van Der Linden, W. E. Anal. Chim. Acta 1989, 226, 171.
- (11) Pungor Jr., E.; Pecs, M.; Szigeti, L.; Nyeste, L. Anal. Chim. Acta 1984, 163, 185.
- (12) Heinzle, E.; Reuss, M. <u>Mass Spectrometry in</u>
  <u>Biotechnological Process Analysis and Control</u>; Plenum Press:
  New York, NY; 1987.

- (13) Bier, M. E.; Kotiaho, T.; Cooks, R. G. Anal. Chim. Acta 1990, 231, 175.
- (14) Hayward, M. J.; Kotiaho, T.; Lister, A. K.; Cooks, R. G.; Austin, G. D.; Narayan, R.; Tsao, G. T. *Anal. Chem.* **1990**, 62, 1798.
- (15) Hanna, S. A.; Austern, B. M.; Eralp, A. E.; Wise, R. H. *J. Water Pollut. Control Fed.* **1986**, 58, 27.
- (16) EPA Test Methods for Evaluating Solid Waste, Volume 1B; Methods 8240 and 8270; U.S. EPA Office of Solid Waste and Emergency Response: Washington, D.C.; 1986.
- (17) NIOSH Mannual of Analytical Methods, 3rd Ed.; Methods 1003 and 1501; P. M. Eller, ed.; U.S. DHHS (NIOSH) Publication No. 84-100; U.S. Government Printing Office: Washington D.C.
- (18) Bouwer, E. J.; McCarty, P. L. Environ. Sci. Technol. **1982**, 16, 836.
- (19) Eckenfelder Jr., W. W.; Patoczka, J.; Watkin, A. T. *Chem. Eng.* **1985**, 60.
- (20) Kirsch, E. J.; Wukasch, R. F. Report to Municipal Environmental Research Laboratory; Office of Research and Development, U.S. Environmental Protection Agency: Cincinnati, Ohio, 45268.
- (21) Klecka, G. M. App. and Environ. Microbiology 1982, 44, 701.
- (22) Rittmann, B. E.; McCarty, P. L. App. and Environ. Microbiology **1980**, 39, 1225.
- (23) Kincannon, D. F.; Fazel, A. 41st Annual Purdue Industrial Waste Conference, Purdue University, West Lafayette, Indiana, 1986.
- (24) U.S. EPA Method 1624 and 1625; Federal Registry, 49(209); 1984.

## **APPENDIX**

# **Permeation Measurements**

The direct measurement of permeation parameters is commonly made by exposing the feed side of the membrane to a pure substance at a known pressure while measuring either the increasing pressure at the permeate side of the membrane with a pressure gauge (1) or the permeate flow with a flow meter (2, 3) or a simple detector such as a thermal conductivity detector (4, 5). Other methods include measuring the weight gain of the polymer in the presence of the gas of interest (6, 7). These techniques only allow for the analysis of a single component at any time and may suffer from interferences if the substance being tested is not pure or if the chamber leaks on either side of the membrane. In addition, contacting silicone with most pure organic solvents results in swelling of the polymer, yielding non-Fickian behavior. The sensitivity and specificity of a mass spectrometer provides for permeation rate measurements at low concentrations and independent of other components (8-10).

The response of the mass spectrometer to a gaseous substance flowing into the ion source, either by permeation through a membrane or by effusion through an orifice, is ideally given by Equation 2.8. The mass spectral response factor,  $Q_i$ , is not easily measured with a membrane, but may be obtained by analyzing gas standards from a

large reservoir through an orifice in a thin metal foil (11). At sufficiently low pressures or small orifice size (i.e., orifice radius smaller than the mean free path for gases), the flow rate of a component through an orifice of area  $A_0$  into a vacuum is given by (12)

$$F_i = 0.225 \cdot A_0 \cdot p_i / (M_i \cdot RT)^{1/2}$$
 (A.1)

where  $p_i$  is the partial pressure of component i in the reservoir,  $M_i$  is the molecular weight of the component, R is the ideal gas constant, and T is the absolute temperature. Therefore,

$$Q_{i} = I_{i} (M_{i} \cdot RT)^{1/2} / (0.225 \cdot A_{o} \cdot p_{i})$$
(A.2)

where Ii is the analytical response for the component. With the determination of  $Q_i$ , the permeability may be determined by substituting Equation 2.8 into Equation 2.6 or Equation 2.7. For the sheet membrane.

$$P_{i} = D_{i,s} \cdot K_{i} = (rf_{i} \cdot d)/(Q_{i} \cdot A)$$
(A.3)

The value for  $D_{si}$  is determined from the permeation response curve and Equation 2.13, and  $K_i$  is calculated from the ratio

$$K_i = P_i/D_{i,s} \tag{A.4}$$

The components of the permeation response curve used to determine  $P_i$  and  $D_{i,s}$  are shown in Figure A.1.

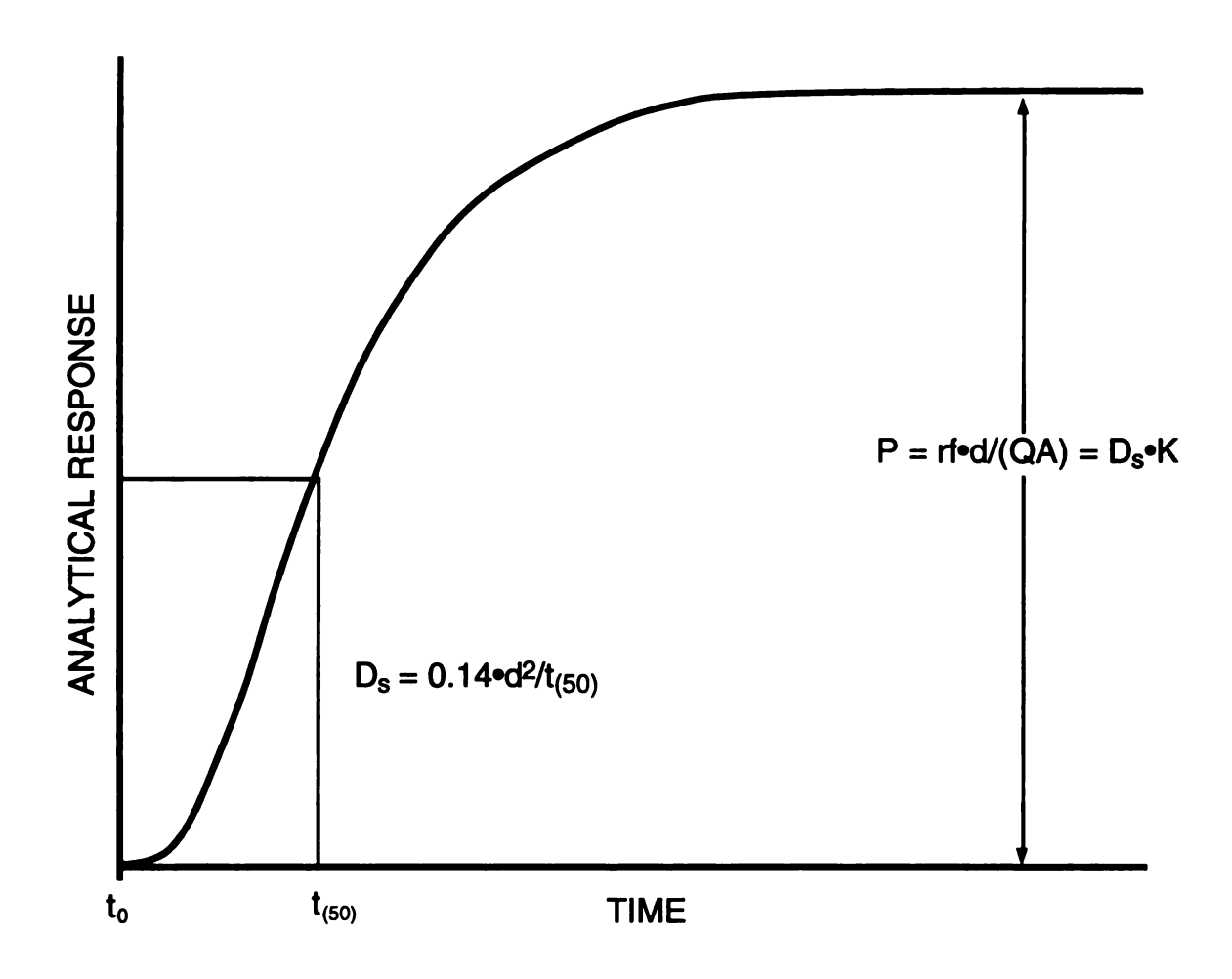


Figure A.1. Experimental determination of permeation parameters.

It is generally true that any quantitative analysis (i.e., the permeation rate measurement) should be performed soon before or after standardization of the analyzer (i.e., by the orifice technique). The number of compounds that can be studied in a reasonable time period is limited by the operations such as switching back and forth between the orifice and the membrane extractor. In addition, the permeation measurements may be time-consuming for larger organic molecules since they require not only the time to reach steady state permeation following a step change in the sample concentration, but time is also required to achieve a baseline following removal of the sample and prior to the next sample introduction. A more efficient approach to these measurements is to determine values for Q<sub>i</sub> for the compounds to be studied and normalize all of them to one of the compounds. These response factors, many of them relative to toluene, have been previously determined by a method developed by Caldecourt (11) for a large number of compounds and tabulated in a Dow Chemical Analytical Sciences mass spectral data base (13). A similar data base, with response factors relative to butane, has been generated by the Shell Oil Company (14). The relative response factor is defined here as follows:

$$q_i = (I_t/w_t)/(I_i/w_i)$$
(A.5)

where w is the weight of the substance injected into the reservoir and the subscript t indicates toluene, which is chosen to be the compound to which all others are normalized. Values for  $q_i$  for several compounds examined in this work are listed in Table A.1. For a given

Table A.1. Mass spectrometric response factors, relative to toluene, used to determine permeation parameters.

compound	m/z	relative response factor
nitrogen	28	0.39
oxygen	32	0.51
argon	40	0.33
carbon dioxide	44	0.49
methane	16	0.27
ethene	27	0.71
ethane	30	1.21
propane	44	1.96
butane	58	4.03
pentane	43	1.75
hexane	43	1.70
heptane	43	1.09
benzene	78	0.65
toluene	92	1.00
ethylbenzene	106	1.93
chlorobenzene	112	1.07
chloromethane	50	0.82
dichloromethane	49	1.41
carbon tetrachloride	117	3.90
chloroethene	62	1.10
1,1-dichloroethene	61	1.87
trichloroethene	95	2.81
tetrachloroethene	94	11.3
bromomethane	94	2.18
dibromomethane	93	3.15
bromoform	91	20.8
water	18	0.96
methanol	31	1.03
ethanol	31	1.29
1-propanol	31	0.67
2-propanol	45	0.74
1-butanol	56	1.53
acetone	43	0.93
2-butanone	43	0.73

mass spectrometer under proper operating conditions, the relative response factor is a constant. Day-to-day instrument drift resulting in variations in the response for one substance will result in proportional variations in response for the second substance. When a different mass spectrometer is used, additional errors are introduced. However, with proper tuning of the analyzer, these errors are minimized and the permeation parameters may be adequately estimated for several compounds in a relatively short period of time.

The weight of the standard added to the reservoir is related to the partial pressure by the ideal gas equation, where  $w_i = p_i \cdot M_i \cdot V/(R \cdot T)$ , which when substituted into Equation A.5 yields the following:

$$q_i = [(I_t/p_t)/(I_i/p_i)] \bullet [M_i/M_t]$$
(A.6)

The relationship between this relative response factor and the absolute response factor in Equation A.2 is given by

$$Q_t/Q_i = q_i \cdot (M_t/M_i)^{3/2}$$
 (A.7)

Applying Equation A.3 to this relationship yields the enrichment factor for compound i relative to toluene

$$\mathcal{E}_{i/t} = P_i/P_t = q_i \bullet (rf_i/rf_t) \bullet (M_t/M_i)^{3/2}$$
(A.8)

If  $P_t$  is measured by the technique described above, then the permeabilities for all of the components where  $q_i$  values are available can be easily estimated.

As stated previously, most of the permeation parameters for gases such as nitrogen are known for many membranes. It can easily be shown that the enrichment factors relative to nitrogen for the components where  $\mathbf{q}_i$  is known can be determined by the following equation:

$$\mathcal{E}_{1/N2} = P_1/P_{N2} = (rf_1/rf_{N2}) \cdot (q_1/q_{N2}) \cdot (M_{N2}/M_1)^{3/2}$$
(A.9)

The advantages to using this solution are 1) as stated above, the permeability parameters for nitrogen are well established for most membrane materials and 2) the nitrogen matrix, in which most standards are prepared, is much more representative of the air matrix most commonly encountered in true analytical applications. A similar equation is used to determine the enrichment factors relative to water.

#### **ERROR ANALYSIS**

Assuming that errors in the calculated permeation parameters are random, and that the sources of these errors can be identified and their magnitudes estimated, then the relative standard deviation for each parameter can be estimated. The relative variance for a measurement is given by the square of the relative standard deviation.

The relative standard deviation for the calculated permeation parameters is given by the square root of the sum of the variances for all of the sources of error (15). The equations used to calculate the permeation parameters and their corresponding relative standard deviation expressions are summarized as follows:

Enrichment factor (relative to nitrogen)

$$\mathcal{E}_{i/N2} = (I_i/I_{N2}) \cdot (c_{N2}/c_i) \cdot (q_i/q_{N2}) \cdot (M_{N2}/M_i)^{3/2}$$
(A.10)

$$\partial \mathcal{E}_{i/N2} / \mathcal{E}_{i/N2} = \{ (\partial I_i / I_i)^2 + (\partial I_{N2} / I_{N2})^2 + (\partial c_i / c_i)^2 + (\partial c_j / c_i)^2 + (\partial q_j / q_j)^2 \}^{1/2}$$

$$(A.11)$$

The relative response factors,  $q_i$  and  $q_{N2}$ , are assumed to be consistent from one mass spectrometer to another, as stated above. The molecular weights,  $M_i$  and  $M_{N2}$ , used in Equation A.10 are assumed to be accurate.

Permeability

$$P_{i} = P_{N2} \cdot \mathcal{E}_{i/N2} \tag{A.12}$$

$$\partial P_i/P_i = [P_{N2}/P_i] \bullet \partial \mathcal{E}_{i/N2} = \partial \mathcal{E}_{i/N2}/\mathcal{E}_{i/N2}$$
(A.13)

The value for the permeability of nitrogen,  $P_{N2}$ , used in Equation A.12 is assumed to be accurate.

Diffusivity

$$D_{i,s} = 0.14 \cdot d^2/(t_{50} - t_0)$$
 (A.14)

$$\partial D_{i,s}/D_{i,s} = \{(2 \cdot \partial d/d)^2 + ([\partial t_{50} - \partial t_0]/[t_{50} - t_0])^2\}^{1/2}$$
(A.15)

The error in the response time measurement is dependent upon the error in determining the time of initial contact of sample with the membrane,  $t_0$ , and in determining the time where one-half steady state permeation is achieved,  $t_{50}$ , as described in Chapter 2. The error in the time of initial contact is estimated to be approximately ;0.5 seconds. The error in the measurement of the time required for one-half steady state permeation is the difference in times between data points (;0.25 seconds) in the ion intensity vs. time permeation profile plot.

Distribution ratio

$$K_i = 76 \text{ cmHg} \cdot P_i / D_{i,s}$$
 (A.16)

$$\begin{split} \partial \mathbf{K_i} / \mathbf{K_i} &= \{ (\partial \mathbf{P_i} / \mathbf{P_i})^2 + (\partial \mathbf{D_{i,s}} / \mathbf{D_{i,s}})^2 \}^{1/2} \\ &= \{ (\partial \mathbf{\mathcal{E}_{i/N2}} / \mathbf{\mathcal{E}_{i/N2}})^2 + (\partial \mathbf{D_{i,s}} / \mathbf{D_{i,s}})^2 \}^{1/2} \end{split} \tag{A.17}$$

The total sample pressure,  $p_t = 76$  cmHg, used in Equation A.16 is assumed to be accurate.

Values estimated for the relative standard deviation for each known source of error are given, along with the relative standard deviations for the computed results for enrichment factors, permeabilities, diffusivities, and distribution ratios, in Table A.2. The relative standard deviations estimated for the analytical signals, I<sub>i</sub>, and the response times,  $(t_{50}-t_0)$ , are compound-dependent. Compounds that demonstrate poor analytical sensitivities and short response times exhibit the greatest relative variances. However, these sources of error are typically negligible when compared with the errors estimated for the relative response factors, qi, and the membrane thickness, d. The range of the relative standard deviations for the analytical responses does not affect the error analysis for the enrichment factors or the permeabilities. The range of the relative standard deviations for the response times only slightly affect the error analysis for the diffusivities and the distribution ratios. The tolerance reported for the membrane wall thickness (16),  $\partial d/d =$ 31%, is much larger than observed experimentally. In the current studies, relative standard deviation for the membrane thickness is more reasonably estimated to be less than 10%, in which case the range for the relative standard deviation for diffusivities is 20-24% and for the distribution ratios is 24-28%.

Table A.2. Relative standard deviation for each known source of error and for each computed permeation parameter.

	range of estimated	
known source of error	relative standard deviation	
$\partial I_i / I_i$	2.9X10 <sup>-2</sup> -1.7 %	
$\partial I_{N2}/I_{N2}$	6.0X10 <sup>-3</sup> %	
$\partial c_i/c_i$	1.0 %	
$\partial c_{N2}/c_{N2}$	1.0 %	
$\partial q_i/q_i$	10 %	
$\partial q_{N2}/q_{N2}$	10 %	
∂d/d	31 %	
$(\partial t_{50}$ - $\partial t_0)/(t_{50}$ - $t_0)$	0.21-14 %	
result		
$\partial \mathcal{E}_{i/N2}/\mathcal{E}_{i/N2}$	14 %	
$\partial P_i/P_i$	14 %	
$\partial D_{i,s}/D_{i,s}$	62-64 %	
$\partial K_i/K_i$	64-66 %	

#### REFERENCES

- (1) Barrer, R. M. Trans. Faraday Soc. 1939, 35, 628.
- (2) Brubaker, D. W.; Kammermeyer, K. Ind. Eng. Chem. 1952, 44, 1465.
- (3) Stancell, A. F. In <u>Polymer Science and Materials</u>, Tobosky, A. V.; Mark, H. F., Eds; Wiley-Interscience: New York, NY, 1971.
- (4) Pasternak, R. A.; Schimscheimer, J. F.; Heller, J. J. Polym. Sci. 1970, 8, 467.
- (5) Ziegel, K. D.; Frensdorff, H. K.; Blair, D. E. J. Polym. Sci. 1969, 7, 809.
- (6) Laatikainen, M.; Lindstrom, M. J. Membrane Sci. 1986, 29, 127.
- (7) Ho, J. S.-Y.; Schlecht, P. C. Am. Ind. Hyg. Assoc. J. 1981, 42, 70.
- (8) Eustache, H.; Histi, G. J. Polymer Sci. 1981, 8, 105
- (9) Harland, B. J.; Nicholson, J. D.; Gillings, E. Wat.Res. 1987, 21, 107.
- (10) Tou, J. C.; Rulf, D. C.; DeLassus, P. T. Anal. Chem. 1990, 62, 592.
- (11) Caldecourt, V. Anal. Chem. 1955, 27, 1670.
- (12) Barrow, G. M. Physical Chemistry, 4th Ed.; McGraw-Hill: New York, NY; 1979.
- (13) Analytical Sciences Mass Spectral Data Base, internal communication, The Dow Chemical Co., Midland, MI.

- (14) Caldecourt, V., personal communication.
- (15) Laitinen, H. A.; Harris, W. E. <u>Chemical Analysis</u>, 2nd Ed.; McGraw Hill: New York, NY; 1975, Chapter 26.
- (16) Medical Materials Business Product Form No. 51-769A; Dow Corning Corp., Midland, MI.

